Czech Technical University in Prague

Faculty of Electrical Engineering
Department of Electric Drives and Traction

Optimal Control Strategy of Hybrid Electric Vehicle

Doctoral Thesis

Tomáš Haubert

Prague, August 2017

Ph.D Programme: Electrical Engineering and Information Technology
Branch of study: Electric Machines, Apparatus and Drives

Supervisor: doc. Ing. Pavel Mindl, CSc.

Ph.D. Thesis

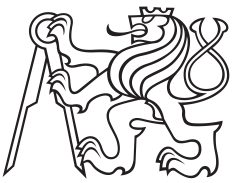

Czech Technical University in Prague

F3

Faculty of Electrical Engineering
Department of Electric Drives and Traction

Optimal Control Strategy of Hybrid Electric Vehicle

Tomáš Haubert
Electrical Engineering and Information Technology - Electric Machines, Apparatus and Drives

August 2017
Supervisor: doc. Ing. Pavel Mindl, CSc.

Acknowledgement / Declaration

I would like to thank to my supervisor doc. Ing. Pavel Mindl, CSc. for his support during my PhD. study. The other thank is for the team members of the research group, namely prof. Ing. Zdeněk Čeřovský, DrSc. and Ing. Pavel Mňuk, CSc. Many other thanks is to my colleagues from the department for creation of creative atmosphere, namely Ing. Jan Bauer, PhD., Ing. Vít Hlinovský, CSc. and Ing. Jan Bradna. I also thank to Škoda auto a.s. for the providing of the Škoda Rapid EV for the testing. The last but very important thanks is to my wife Michaela and to my son Tomáš. My life without them would be empty.

This thesis is result of my doctoral study at CTU Prague, Faculty of Electrical Engineering, Department of Electric Drives and Traction. The work was partly supported by internal student grants of the CTU in Prague and also was supported by the Technological Agency, Czech Republic, programme Centers of Competence, project TE01020020 Josef Božek Competence Centre for Automotive Industry. This support is gratefully acknowledged.

This doctoral thesis is submitted in partial fulfillment of the requirements for the degree of doctor (PhD.). The work submitted in this dissertation is the result of my own investigations, except where otherwise stated. I declare that I worked out this thesis independently and I quoted all used sources of information in accord with Methodical instructions about ethnical principles for writing academic theseses.

.....

Abstrakt / Abstract

Tato práce se zabývá velmi progresivní oblastí automobilového průmyslu, hybridními a elektrickými vozidly. S ohledem na konfiguraci používají hybridní a elektrická vozidla elektrický motor pro konverzi elektrické energie na mechanickou energii, která je použita pro pohyb vozidla. Hlavním omezením těchto vozidel, speciálně čistě elektrických vozidel, je jejich omezený dojezd. Jedna možnost jak zvýšit dojezd je přidat další bateriové články, které ale zvýší cenu vozidla, nebo použít optimalizační metody v součinnosti s pokročilými asistenčními systémy. Návrh optimalizační metody je hlavním cílem této práce. Výsledky optimalizační metody jsou porovnány s reálným jízdním cyklem provedeným pomocí Škody Rapid EV poskytnutým firmou Škoda auto a.s. Tato práce se také zabývá návrhem řídicí části DC/DC měniče výkonu pro superkondenzátor. Superkondenzátory mohou být užity v hybridních a elektrických vozidlech jako dočasné úložiště elektrické energie, pokud je vyžadována rekuperace.

Klíčová slova: Hybridní vozidla, elektrická vozidla, optimalizaci jízdního cyklu, řízení nabíjení a vybíjení superkondenzátoru

This thesis deals with the very progressive branch of the automotive industry, hybrid and electric vehicles. Based on the configuration the hybrid and electric vehicles are using an electric motor for the converting of the electrical energy into the mechanical energy, which is used for the vehicle moving. The main limit of these vehicles especially pure electric vehicles is limited range. One way how to extend the range is to add other battery cells, which increases the price of the vehicle, or to use optimization methods in cooperation with advanced driver assistance systems. The proposal of the optimization method is the main goal of this thesis. The results of the optimization method are compared with the real driving cycle made by Škoda Rapid EV provided by Škoda auto a.s. This thesis also deals with design of control part of DC/DC power converter for super-capacitor. Super-capacitors can be used in the hybrid and electric vehicles as a temporary storage of the electrical energy if a recuperation is needed.

Keywords: Hybrid Vehicle, Electric Vehicle, Driving Cycle Optimization, Super-capacitor Charging and Discharging Control

Contents /

Tables / Figures

Chapter 1
Introduction

Increasing of living standards increased needs for people transport. Gas emissions and fossil fuel consumption are actual problems for global environment quality on the Earth. Gas emission of car internal combustion engines (ICE) brings many ecological problems in big cities specially. One way how to reduce gas emissions in big cities is to use electric vehicles. Nowadays it is planning in big cities (Paris, London) to limit an access to the cities for all vehicles with a combustion engine. The development of the electric vehicles is faster in recent years and now it is very progressive branch of industry. The most significant problems of recent electric vehicles are high purchase price and short driving distance. The driving distance depends on the capacity of the battery pack where all energy is stored in electrochemical cells. During the drive the energy flows from the battery to the powertrain where is converted into the mechanical energy. The capacity of the battery, efficiency of the powertrain and the driver's style determines maximum length of the driving distance.

1.1 Motivation

The area of the vehicles for personal transport is very wide. There is a lot of options and power source combinations. The vehicles can have only one source of energy or two or more sources of energy (hybrid vehicles). The area of vehicles was from the childhood for me very interesting. In my bachelor and diploma thesis I worked on the linear combustion engine and the possibility to use this engine as a range extender for electric vehicles. After finishing of my master thesis I focused more on the electric drives and their control and modelling. This was the reason to start PhD. study on the Department of Electric Drives and Traction and to build up a new laboratory with modern equipment for electric drive development and testing.

1.2 Current State of Art

The optimization in the hybrid and electric vehicle area is a quite new. In the 1990s started a development of algorithms for efficiency optimization using different methods. For example fuzzy logic [1] or neural network [2]. At the end of 90s is possible to find other publications which deal with the optimal multivariable control of hybrid electric vehicles [3], [4]. On begin of the 21st century was created a lot of publications in the optimization in the hybrid and electric vehicle area [5], [6], [7], [8], [9], [10] or [11]. An article [12] from 2007 brings a good overview in the optimal energy management strategies area for hybrid electric vehicles. Until 2010s was published approx. up to 100 articles per year and from 2010 the number of articles is increasing up to approx. 1000 articles in the 2016. An article [13] from 2010 brings an overview of methods for loss minimization in induction machines. In the last 7 years the articles deals more with the charging of hybrid and electric vehicles and with the impact of the charging on the grid [14], [15], [16] or [17].

Nowadays there is a lot of approaches to the optimization of energy consumption for hybrid and electric vehicles, for example Model Predictive Control (MPC) [18]. The article [19] presents a trip-oriented energy management for plug-in hybrid electric vehicle. The control strategy provides an optimization to improve real-word fuel economy. An overview of the power management control algorithms are in [20]. There are:

- Model Predictive Control (MPC)
- Dynamic Programming (DP)
- Pontryagin's Minimum Principle and ECMS

The most used method is dynamic programming (DP). The control strategy based on the DP method for HEV is described in [21] or in [22] or for electric vehicles in [23]. The other method (Pontryagin's Minimum Principle) for hybrid and electric vehicles is explained in [24], [25] or in [26].

1.2.1 History and Current State of Art on CTU Prague

Since 2000 started a development and building of an experimental stand for hybrid electric vehicle with an electric power splitter. The experimental stand is introduced in the chapter 2. The first thesis [27] (2006) about this stand is from Vladek Pavelka, where a first version of the control strategy is introduced. The other thesis [28] (2009) about a control strategy is from Dobri Cundev. In this thesis is presented HEV-SCADA concept for the experimental stand. I started on this project in 2010. My target was DC/DC power converter for super-capacitor and optimization during charging/discharging. The first version of the new control system was developed in 2012 with my student Jakub Kucka [29]. In 2012 and 2013 I made an advanced control system for super-capacitor which is described in [30]. In 2012 started a new project in Roztoky (see the chapter 5) focused mainly on the electric vehicles. Since 2014 I started to work on this project where the target is to reduce CO_2 emissions and energy consumption in transport. During this project a laboratory with dynamometer test bench was built up in cooperation with Škoda auto a.s.

1.3 Goal of the Doctoral Thesis

The main goal of this thesis is to develop a method for design of the optimal speed profile and verifying on the test bench. The list of the goals:

- Design of control algorithm for DC/DC power converter for super-capacitor based on the optimal controller design methods
- Integration of the proposed control strategy of the DC/DC power converter into digital signal processor and verifying the functionality and comparing with the mathematical model of DC/DC power converter
- Design of control system concept for automated driving cycle measurement in the laboratory in VTP Roztoky
- Design of optimization algorithm for optimal speed profile design
- Verification of optimization algorithm results on the test bench in VTP Roztoky and its comparing with the logged data from real vehicle

Chapter 2
Hybrid and Electric Vehicles

2.1 History

Electric vehicles (EVs) have been around since the 1800s. They were very popular and number of EVs increased until about 1918. In this time approximately 38 % of vehicles were electric, 22 % gasoline and 40 % steam powered. Since this time the number of EVs were decreasing and were replaced by the gasoline engines. Gasoline was low-cost, the internal combustion engines got an electric starter and the interest in EVs was completely declined [31].

EV development activity was pushed to the forefront during the Arab oil embargo (1973 - 1974) but when the prices of gasoline fell during the late 1970s, the EV development activity was again declined. At the begin 1990s the development of EVs started again and GM developed a pure electric vehicle called EV1. The EV1 was a battery-operated EV based on lead acid batteries with an asynchronous induction motor. It was offered for lease in 1996 and was the first mass-produced EV from a major automotive company. From the reason of limited range, the lead acid batteries were replaced in 1999 by nickel metal hydride (NiMH) batteries that offered a longer range but a much higher cost. During 1990s, other automotive companies ware also developing EVs. For example Toyota developed a pure electric version of RAV4 and hybrid vehicle Prius.

Figure 2.1. Toyota Prius (2008)

In 2003, Tesla Motors announced the development of pure EVs. The Tesla Roadster is a battery EV produced between 2008 and 2012. The Tesla Roadster was the first production vehicle which used Li-Ion battery and the first production vehicle with the range more than 200 miles (320 km). Today, a few other EVs such as Tesla Model S, BMW i3, VW e-Golf, Nissan Leaf, Mitsubishi i-MiEV and so on are commercially available. In the last twenty years, plug-in hybrid electric vehicles (PHEVs) are attracting increasing interest in North America, Japan and Europe. A plug-in hybrid is a series or parallel hybrid with a battery restored to full charge by connecting to the electric network via a charger. PHEVs have a range in EV mode about 50 km. The most popular PHEV is Toyota Prius. The other PHEVs are also Chevrolet Volt, Opel Ampera, VW Passat GTE, etc. The battery capacity is approximately 5 – 15 kWh. PHEVs are compromise between a cost (a battery with limited capacity) and a range (availability of an internal combustion engine).

2.2 Types of HEVs Powertrain

Hybrid electric vehicles are vehicles which have more than one source of energy for the vehicle moving. The main sources are an internal combustion engine (ICE) and an electric motor (EM). Based on the connection of the ICE and the EM is possible to divide the types by design into:

- Parallel hybrid
- Series hybrid
- Power-split hybrid

Based on the combination of impact of the electric motor on the vehicle movement is possible to divide the types by degree of hybridization into:

- Mild hybrid
- Full hybrid
- Plug-in hybrid

2.2.1 HEV Types by Design

Parallel hybrid has a parallel connection of an ICE and EM to the transmission. The both motors can be used for the vehicle movement independently. In the most cases the ICE is dominant and runs continously. The EM supports the ICE during acceleration and braking. This category is known as mild hybrids. In 2017 the company Continental developed a mild hybrid system with 48 V supply network. The first vehicle with this system will be Renault Scenic. The main scheme of parallel hybrid is depicted in the Fig. 2.2.

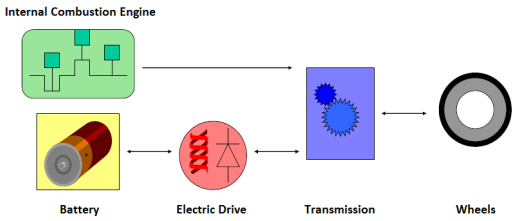

Figure 2.2. Parallel hybrid

Series hybrid is a type where an EM is the main source of the energy for the movement. The EM has to be designed to the higher power then EM in parallel hybrids. Series hybrid are sometimes reffered to range-extended electric vehicles. The biggest advantage of this concept is that the ICE can operate in the highest efficiency state and charge the battery via an electric generator. The basic configuration is depicted in the Fig. 2.3. This configuration can be extended via capacitor with own DC/DC converter and connected parallel to battery.

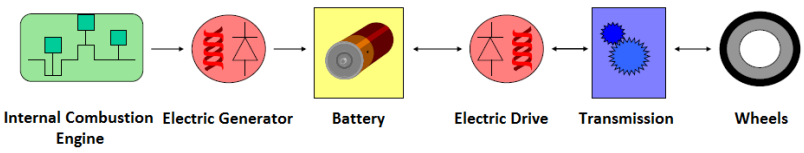

Figure 2.3. Series hybrid

Power-split hybrid (also known as series-parallel hybrid) is a parallel hybrid with a power-split device. The power-split device can be mechanical (for example planetary

gearbox) or electrical (for example electric power splitter). A planetary gearbox is used for example in Toyota Prius or Lexus RX400h. The both companies are part of the Toyota concern. The configuration of this hybrid is similar with the parallel hybrid (Fig. 2.2). An electric power splitter (EPS) is an electric machine which has a rotor with permanent magnets and a stator with 3-phase winding which is also rotating (basically, it is a second rotor). A cross section of EPS is depicted in the Fig. 2.4. The EPS is a part of an experimental stand of hybrid drive at Czech Technical University in Prage. More information is possible to find in chapter 3.

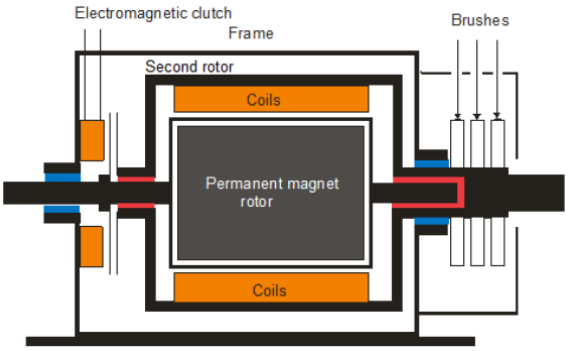

Figure 2.4. Electric power splitter - cross section

2.2.2 HEV Types by Degree of Hybridization

Mild hybrids are conventional vehicles with limited hybrid functionality. ICE is used as a primary source for the vehicle movement and an EM supports the ICE during accelerating. EM can be mounted between ICE and transmission and can be used also for the ICE starting. The new 48 V mild hybrid system from Continental (developed in 2017) has an EM connected instead of alternator and connected with a shaft of ICE via belt. This mild hybrid system has a separate Li-Ion battery which is charged during regenerative braking. The main parts of this system are in the Fig. 2.5. For example Volvo wants to use the 48 V mild hybrid system in all vehicles from 2019.

Figure 2.5. Mild hybrid concept (Continental 2017)

Full hybrids are vehicles where the vehicle movement is provided only by ICE or only by EM or their combination. These vehicles need an advanced decision algorithm which will decide which motor will be used. For example Toyota Prius can operate in this five regimes [32]:

- Electric Vehicle Mode: The ICE is off and the battery powers the EM (or charges during regenerative braking). Battery SOC (State Of Charge) must be high.
- Cruise Mode: The vehicle is cruising (speed is constant) and the power from ICE is split between the mechanical path and the generator if battery SOC is low.
- Overdrive Mode: A portion of the rotational energy produces electricity, because the ICE's full power is not needed.

- Battery Charge Mode: Can be use in idle mode, the ICE charges the battery if the battery SOC is low.
- Power Boost Mode: If there is a requirement to the maximum power, then the ICE and EM power the vehicle during accelerating.

Plug-in hybrid electric vehicle (PHEV) is a vehicle that uses batteries or another energy storage that can be recharged by plugging it to an external source of electric power. PHEVs are a compromise between pure gasoline and pure electric vehicles.

2.3 Electric Drives in EVs and HEVs

An electric drive is a connection of an electric machine and a power converter. An electric machine is a converter for conversion of electrical energy into the mechanical energy. A power converter is needed for the torque or speed control of electric machine. The torque control of electric machine is used in vehicles and the input is a driver's pedal position. The speed controller can be a driver or a cruise control (CC) system in vehicle. The CCs can be passive for the control to constant speed or adaptive with a radar which controls a distance between vehicle and other objects in front of vehicle. The system is called adaptive cruise control (ACC) and it is available approximately 80% of new vehicles in market.

Nowadays, the two types of electric machines are used in vehicles:

- Asynchronous induction machine
- Permanent magnet synchronous machine

Asynchronous induction motor (IM) is an AC electric motor with the 3 phase stator winding and the rotor with squirrel-cage type. The rotor can be also wound type but this type is not used in vehicles. The torque is produced by an electromagnetic induction from the stator winding's magnetic field. The efficiency of the IM is about $80 - 97\%$ [33]. The power losses can be divided into joule losses caused by stator or rotor resistances, iron losses and into indirect losses caused by friction and ventilation.

Permanent magnet synchronous motor (PMSM) is an AC electric motor with 3 phase stator winding and the rotor with permanent magnets. Permanent magnets produce a constant magnetic field. The stator produce a rotating magnetic field. At synchronous speed the rotor poles lock to the rotating magnetic field.

In the past when the power electronic was not in the same level as nowadays, used the electric vehicles also **DC motor** in series connection. Series connection means a connection of the armature and excitation windings in series with a common DC power source. This connection provides very high starting torque. This motor was used in vehicles in 1990s as Citroen Saxo or Peugeot Partner.

The table 2.1 includes a comparing of the IM, PMSM and DC motor. For the using in EVs and HEVs are the best solution IM and PMSM. For example Tesla is using IM and VW is using PMSM. IM is not too sensitive to overcurrent and the temperature. Magnets in PMSM has the maximum operating temperature about $150°C$. The magnets loose magnetic field if the temperature is more than the maximum operating temperature.

Power electronic consists of power switching devices, power converter topology with its switching strategy and the closed-loop control system. The main requirements on the power electronic are:

Machine	IM	PMSM	DC
Torque density	+/-	++	-
Efficiency	+/-	++	-
Weight	+	++	-
Machine cost	+/-	+/-	–
Drive cost	+/-	+/-	+/-
Production	+	-	-

Table 2.1. Comparing of different machine types

- High efficiency
- Small size
- Low cost

All current HEVs and EVs use the 3-phase bridge converter topology with the DC supply from battery and 3-phase connection with an AC motor. This topology enables to connect more types of electric machines. The first types of power converters used MOSFET transistors connected in parallel. The next generation is using IGBT modules. This technology will be in the near future replaced by the silicon carbide (SiC) and gallium nitride (GaN) devices [34]. Advanced features of SiC devices are high temperature operating capacity, high power efficiency and flexibility to be used as substrate. GaN devices are projected to have higher performance over silicon-based devices and much better performance than SiC devices, because of the material properties such as high electron mobility, high breakdown field and high electron velocity. The cost is higher than silicon but always cost less than SiC because GaN is compatible with silicon substrates. The power electronic has to monitor the condition of electric machine and detect any failures such as bearing, rotor and stator faults. By diagnosing of the electric machine faults as early possible, the life time of the electric machine can be prolonged by performing maintenance before a catastrophic failure occurs.

2.4 Market overview

This subchapter covers the current situation on market with HEVs and EVs. List contains vehicles only currently produced by the selected major carmaker companies. Not all information about each car is publicly available and information about power electronics is usually nowhere to be found so the following list does not contain it.

2.4.1 BMW

BMW is a German luxury vehicle manufacturing company founded in 1916. In EVs and HEVs area offers BMW i sub-brand. BMW i founded in 2011 to design and manufacure plug-in hybrid and electric vehicles. BMW i offers two vehicles BMW i3 (pure electric vehicle) and BMW i8 (plug-in hybrid vehicle). BMW also offers plug-in hybrid variants of standard classes as 2, 3, 5, 7 and SUVs X5 and X6.

BMW i3 is a five door urban electric vehicle. The concept vehicle was unveiled at the 2011 and the production was started in July 2013 with the 22 kWh battery. In July 2016, BMW released the 2017 model year with an improved 33 kWh battery pack. BMW is offering also a version with range extender powered by 647 ccm two-cylinder gasoline engine. This motor with a generator produces additional electrical energy and extends the range to 160 km under EPA test cycle.

Figure 2.6. BMW i3

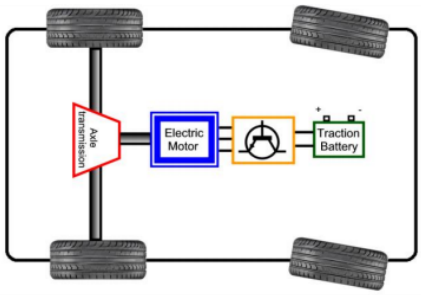

Figure 2.7. BMW i3: Structure of Powertrain

Technical data	
Top speed	150 km/h
Acceleration 0 - 100 km/h	7.2 s
Official range	183 km (EPA)
Electric Motor	
Type of EM	BMW manufactured PMSM (AC)
Maximal power	125 kW
Maximal torque	250 Nm
Maximal speed	11400 rpm
Battery Pack	
Capacity	33 kWh
Nominal voltage	350 V

Table 2.2. BMW i3: Technical data

2.4.2 Volkswagen

Volkswagen is a German company founded in 1937 and headquartered in Wolfsburg. The first diesel hybrid vehicle from Volkswagen was XL1. The XL1 has a diesel combustion engine (800 ccm TDI two-cylinder common rail) and electric motor. Volkswagen offers also hybrid variants of standard models. These hybrid models are marked as GTE (Passat GTE, Golf GTE and Jetta GTE). GTE version has standard 1.4 litre 100 kW petrol engine and 75 kW electric motor. The electric motor is included between a combustion engine and a transmission. The total power is approx. 150 kW. For example Golf GTE has in EV mode the range about 50 km. Volkswagen has also full electric variant of Golf and Up called Volkswagen e-Golf and e-Up. This technology will be in the future also used in other car brands of Volkswagen concern like Skoda, Seat, etc.

Volkswagen e-Golf is a result of a development which already started in 2008 with Golf Variant Twin Drive HEV. In 2011 a massive field testing started with 500 units in Europe and then also in the U.S. with a small group of vehicles. Testing in U.S. showed that the high temperatures did not affect the battery performance so there was no need to use a liquid cooling system in the packs. Sales are satisfying as the customers appreciate its similarity to the classic VW Golf.

Figure 2.8. Volkswagen e-Golf

Technical data	
Top speed	140 km/h
Acceleration 0 - 100 km/h	10.4 s
Official range	150 km (NEDC)
Electric Motor	
Type of EM	VW manufactured PMSM (AC)
Maximal power	85 kW
Maximal torque	270 Nm
Maximal speed	12000 rpm
Battery Pack	
Capacity	24.2 kWh
Nominal voltage	250 V - 430 V

Table 2.3. Volkswagen e-Golf: Technical data

Volkswagen e-UP is the electric version of VW Up and is equipped with front-wheel drive. It is the first fully electric car made by the biggest German automotive company. While the main usage of this EV should be focused on urban driving its top speed makes suitable for driving on the highways too even though for a short period of time. It is one of the most successful city EVs on the market right now.

Figure 2.9. Volkswagen e-UP

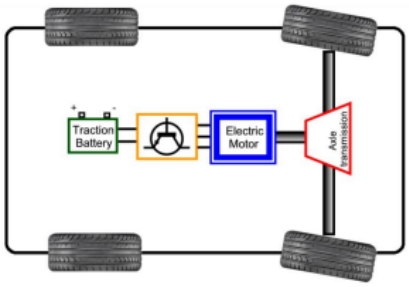

Figure 2.10. Volkswagen e-Golf and e-UP: Structure of Powertrain

Technical data	
Top speed	130 km/h
Acceleration 0 - 100 km/h	12.4 s
Official range	150 km (NEDC)
Electric Motor	
Type of EM	VW manufactured PMSM (AC)
Maximal power	60 kW
Maximal torque	210 Nm
Maximal speed	12000 rpm
Battery Pack	
Capacity	18.7 kWh
Nominal voltage	296 V - 418 V

Table 2.4. Volkswagen e-UP: Technical data

2.4.3 Tesla

Tesla in an American company founded in 2003. The company specializes in electric vehicles, lithium-ion battery energy storage and solar panels production. The first model was Tesla Roadster with the start of the production in February 2008. The company's second vehicle is Tesla Model S. Model S is an electric sedan with the start of the production in June 2012. The third model is Tesla Model X, a full-size crossover with the start of production in September 2015. The newest model is Tesla Model 3. The limited production of the Model 3 began in July 2017. This model will be the cheapest Tesla with the expected price approx. 35 000 USD. Tesla is using in all models own developed asynchronous induction machines and own developed baterry pack with battery cells from Panasonic.

Tesla Model S is at this moment the most important model of Tesla. The Model S has two variants: RWD (rear wheel drive) and AWD (all wheel drive). The capacity of the battery pack was 60 kWh in the first versions and it is 85 kWh now. Not only this vehicle belongs to high class limousines but it beats its competitors by the best range of the currently worldwide sold EVs. Tesla managed to develop a vehicle with great power and energy storage ratio so the vehicle still remains fast and agile while the weight of the vehicle suffers from the large battery pack (around 500 kg). Another cause of the great success of Model S is the wide network of the superchargers currently built in the U.S. and Europe. In 2014 Tesla revealed the all-wheel drive version of the Model S. There are two versions both with 85 kWh battery pack but with electric motors of different

specs. The weaker model 85D has two identical motors 140kW/245Nm on both axles. In April 2015 also a version with 70 kWh battery pack and total power of 245 kW has been revealed and the 60 kWh RWD version got discontinued. Tesla claimed that this all-wheel drive solution should be the preparation for the following Tesla Model X. It provides excellent all-weather driving abilities and superb acceleration.

Figure 2.11. Tesla Model S

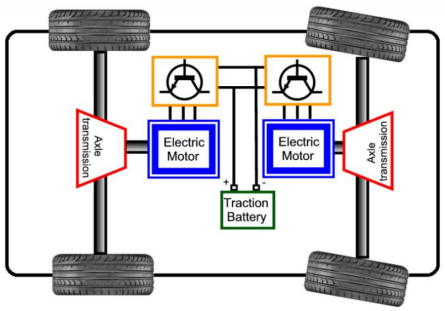

Figure 2.12. Tesla Model S P85D: Structure of Powertrain

Technical data	
Top speed	249 km/h
Acceleration 0 - 100 km/h	3.4 s
Official range	407 km (EPA)
Electric Motor	
Type of EM	Tesla manufactured ASM (induction)
Maximal power	165/350 kW (front/rear)
Maximal torque	330/600 Nm (front/rear)
Maximal speed	16000 rpm
Battery Pack	
Capacity	85 kWh
Nominal voltage	402 V

Table 2.5. Tesla Model S P85D: Technical data

Tesla Model X is a full-sized, crossover SUV that used falcon wing doors for access to the second and third row seats. Model X was developed from the Model S platform and shares about 60 % of part. The production started in September 2015 and in December 2016, global deliveries totaled more than 25 000 units. The Model X has a choice of five Li-Ion battery packs (60, 70, 75, 90 or 100 kWh). The highest performance version P100D has acceleration 0 - 100 km/h in 2.9 seconds.

Chapter 3
DC/DC Power Converter for Super-capacitor

This chapter deals with the DC/DC converter for super-capacitor and design of an optimal control. The optimal control reduces switching losses of IGBT transistors and therefore increases efficiency. For the design of optimal control is needed an analysis of switching losses and creation of a mathematical model. More information is in [30].

3.1 Experimental Stand of Hybrid Drive

The experimental stand of hybrid drive has been created at Czech Technical University on Department of Electric Drives and Traction. This stand simulates combined hybrid drive with electric power splitter. The diagram of this stand is shown in Fig. 3.1. The parts of this drive are two identical induction motors. The first motor simulates a combustion engine (ICE). The traction load (BRAKE) is simulated by the second motor.

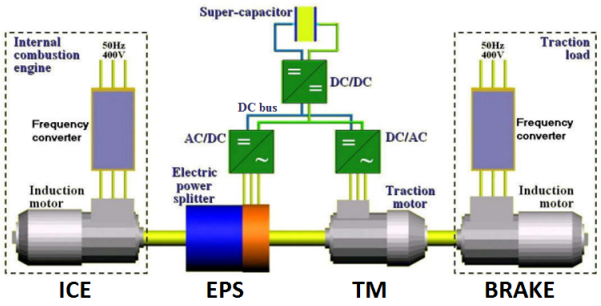

Figure 3.1. Structure of Experimental Stand of Hybrid Drive

The electric power splitter (EPS) is a synchronous machine, which has two rotating parts - two rotors. On the first rotor are mounted permanent magnets. This rotor is driven by ICE. The second rotor is provided with three-phase winding, which is connected by brushes to the input of AC/DC converter (AFE). The output DC voltage that supplies the DC bus is controlled by PWM in range 0 - 500 V (typically 200 V). The DC bus is connected to the DC/DC converter for charging/discharging the super-capacitor and to the DC/AC frequency converter which supplies the traction motor (TM). More information about experimental stand of hybrid drive are presented in [35] and [36].

3.2 Mathematical Model of DC/DC Converter

The DC/DC converter for super-capacitor is used for charging and discharging. It is needed to transfer energy from high voltage side to the low voltage side and vice versa. Therefore converter must be bi-directional.

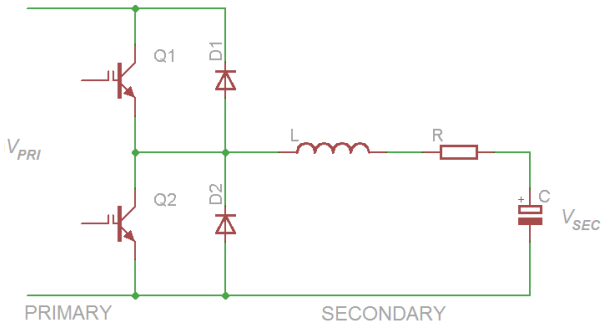

Figure 3.2. Diagram of bi-directional DC/DC converter

The converter is able to transfer the energy from higher voltage level V_{PRI} to lower voltage level V_{SEC} and the other way round. The diagram is shown in Fig. 3.2. To transfer the energy from higher voltage level to lower voltage level, the DC/DC converter is operating in buck mode and to transfer from lower voltage level to higher voltage level, the DC/DC converter is operating in boost mode.

3.2.1 Buck Mode

Buck mode is the operational mode of DC/DC converter during which the energy is being stored from the higher voltage level source to super/capacitor with lower voltage. The diagram is described in Fig. 3.3.

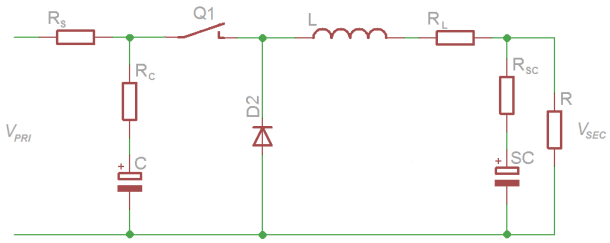

Figure 3.3. Diagram of DC/DC converter operating in buck mode

The transistor Q1 has two states: $u = 1$, when transistor is switched ON and $u = 0$, when transistor is switched OFF. For ideal assumptions:

- ideal switch $R_{ON} = 0$
- ideal capacitor $R_{SC} = 0$
- ideal inductor $R_L = 0$

the buck converter can be described using ordinary differentiation equations as follows:

$$\begin{aligned} SC\frac{dv_{SC}}{dt} &= i_L - \frac{v_{SC}}{R} \\ L\frac{di_L}{dt} &= u \cdot v_C - v_{SC} \\ C\frac{dv_C}{dt} &= \frac{v_{PRI} - v_C}{R_s} - i_L \end{aligned} \tag{3.1}$$

With respect non-zero resistance of inductor $R_L \neq 0$ and nonzero Equivalent Series Resistor (ESR) of the super-capacitor $R_{SC} \neq 0$, the equations (3.1) can be described as follows:

$$\begin{aligned} SC\frac{dv_{SC}}{dt} &= i_L - \frac{v_{SEC}}{R} \\ v_{SEC} &= v_{SC} + R_{SC}SC\frac{dv_{SC}}{dt} \\ L\frac{di_L}{dt} &= u \cdot v_C - v_{SEC} - R_L i_L \\ C\frac{dv_C}{dt} &= \frac{v_{PRI} - v_C}{R_s} - i_L \end{aligned} \tag{3.2}$$

Inserting the second equation from (3.2) into the first from (3.1) leads to:

$$\begin{aligned} SC\frac{dv_{SC}}{dt} &= i_L - \frac{v_{SC}}{R} - \frac{R_{SC}}{R}SC\frac{dv_{SC}}{dt} \\ SC(1 + \frac{R_{SC}}{R})\frac{dv_{SC}}{dt} &= i_L - \frac{v_{SC}}{R} \end{aligned} \tag{3.3}$$

Hence,

$$v_{SEC} = v_{SC}\frac{R}{R + R_{SC}} + i_L\frac{RR_{SC}}{R + R_{SC}} \tag{3.4}$$

The overall model is

$$\begin{aligned} SC\frac{dv_{SC}}{dt} &= \frac{R}{R + R_{SC}}(i_L - \frac{v_{SC}}{R}) \\ L\frac{di_L}{dt} &= u \cdot v_C - v_{SEC} - R_L i_L \\ C\frac{dv_C}{dt} &= \frac{R_s}{R_C + R_s}(\frac{v_{PRI} - v_C}{R_s} - i_L) \\ u_{SEC} &= u_{SC}\frac{R}{R + R_{SC}} + i_L\frac{RR_{SC}}{R + R_{SC}} \end{aligned} \tag{3.5}$$

The mathematical model has been created using equations (3.5) in MATLAB/Simulink. The diagram of this model is shown in Fig. 3.4. The integrator of i_L has limited output in range (0; 1). In real buck converter is negative current limited by diode (see diode D2 in Fig. 3.4).

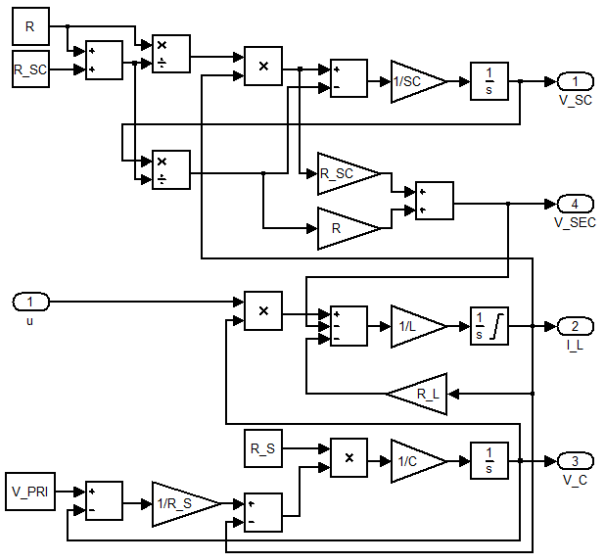

Figure 3.4. Diagram of buck converter in MATLAB/Simulink

3.2.2 Boost Mode

Boost mode is the operational mode of DC/DC converter during which the energy is being restored to the higher voltage level source from super-capacitor with lower voltage level. The diagram is described in Fig. 3.5.

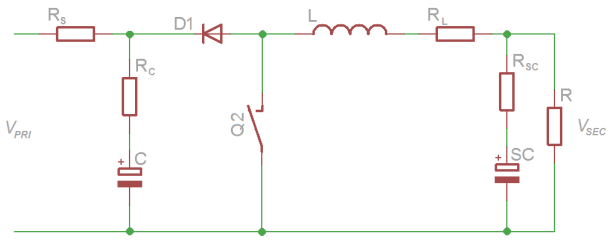

Figure 3.5. Diagram of DC/DC converter operating in boost mode

The transistor Q2 has two states: $u = 1$, when transistor is switched ON and $u = 0$, when transistor is switched OFF. The voltage is generated on inductor L and the energy is transferred through diode D1 to the higher voltage source (primary side). The inductance of inductor should be high enough, so that the voltage generated on it is higher than the source voltage. For ideal assumptions:

- ideal switch $R_{ON} = 0$
- ideal capacitor $R_{SC} = 0$
- ideal inductor $R_L = 0$

the boost converter can be described using ordinary differentiation equations as follows:

$$\begin{aligned} -SC\frac{dv_{SC}}{dt} &= i_L + \frac{v_{SC}}{R} \\ L\frac{di_L}{dt} &= v_{SC} - (1-u)v_C \\ C\frac{dv_C}{dt} &= (1-u)i_L - \frac{v_{PRI} - v_C}{R_s} \end{aligned} \tag{3.6}$$

With respect non-zero resistance of inductor R_L and non-zero equivalent series resistor (ESR) of the super-capacitor R_{SC}, the equations (3.6) can be described as follows:

$$\begin{aligned} -SC\frac{dv_{SC}}{dt} &= i_L + \frac{v_{SEC}}{R} \\ v_{SEC} &= v_{SC} + R_{SC}SC\frac{dv_{SC}}{dt} \\ L\frac{di_L}{dt} &= v_{SEC} - (1-u)v_C - R_L i_L \\ C\frac{dv_C}{dt} &= (1-u)i_L - \frac{v_{PRI} - v_C}{R_s} \end{aligned} \tag{3.7}$$

Inserting the second equation from (3.7) into the first from (3.6) leads to:

$$\begin{aligned} -SC\frac{dv_{SC}}{dt} &= i_L + \frac{v_{SC}}{R} + \frac{R_{SC}}{R}SC\frac{dv_{SC}}{dt} \\ -SC(1 + \frac{R_{SC}}{R})\frac{dv_{SC}}{dt} &= i_L + \frac{v_{SC}}{R} \end{aligned} \tag{3.8}$$

Hence,

$$v_{SEC} = v_{SC}\frac{R}{R+R_{SC}} - i_L\frac{R_{SC}R}{R+R_{SC}} \tag{3.9}$$

The overall model is

$$\begin{aligned} -SC\frac{dv_{SC}}{dt} &= -\frac{R}{R+R_{SC}}(i_L + \frac{v_{SC}}{R}) \\ L\frac{di_L}{dt} &= v_{SEC} - (1-u)v_C - R_L i_L \\ C\frac{dv_C}{dt} &= (1-u)i_L - \frac{v_{PRI} - v_C}{R_s} \\ v_{SEC} &= v_{SC}\frac{R}{R+R_{SC}} - i_L\frac{R_{SC}R}{R+R_{SC}} \end{aligned} \tag{3.10}$$

The mathematical model of boost converter has been created using equations (3.10) in MATLAB/Simulink. The schema of this model is shown in Fig. 3.6. The integrator of i_L has limited output in range (0; 1). In real buck converter is negative current to limit by diode (see diode D1 in Fig. 3.6). The integrator of v_{SC} has limited output in range (0; 1) and it is necessary to set initial condition, because for boost converter is super-capacitor voltage source.

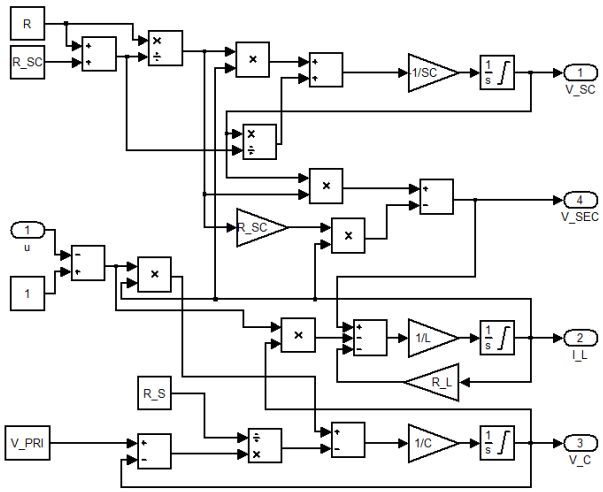

Figure 3.6. Diagram of boost converter in MATLAB/Simulink

3.3 Switching Losses of IGBT

The instantaneous power dissipation $p(t)$ had been determined by multiplication of instantaneous current i_d and voltage u_d values. The integral of $p(t)$ reflects the total IGBT losses over whole period.

$$W_{LOSS}(t) = \frac{1}{T}\int_0^T u_d(t)\cdot i_d(t)dt \tag{3.11}$$

The typical waveform for the IGBT transistor during turn ON is shown in the Fig. 3.7. There are shown the waveforms for current through IGBT and voltage between collector and emitter. The total power is calculated by multiplication of current and voltage (as shown in the equation (3.11)). It is clear from Fig. 3.7 and from equation (3.11) that the switching losses increasing proportionally to the frequency.

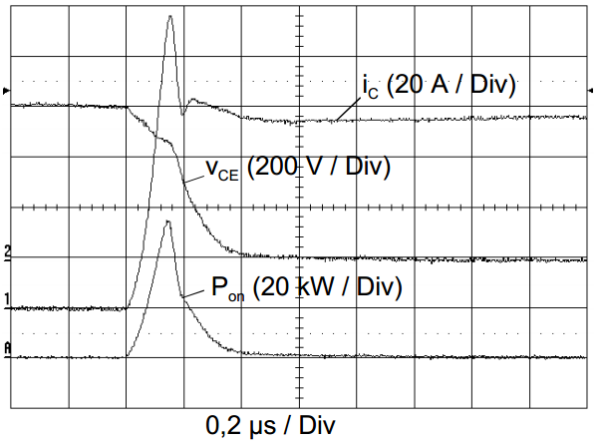

Figure 3.7. The waveform for IGBT turn ON

3.4 Switching Frequency Analysis

3.4.1 Buck Mode

By switching the transistor Q1, we are able to regulate the mean value of voltage on secondary side. The mean value of voltage depends linearly on the time when transistor is switched on (3.12).

$$V_{SEC} = V_{PRI} \cdot duty = \frac{V_{PRI} \cdot t_{ON}}{t_{ON} + t_{OFF}} \tag{3.12}$$

The mean value of voltage on secondary side is a function of source for current through inductor L and resistor R. This current is charging the super-capacitor. The main function of inductor is to keep the uninterrupted value of charging current through diode D2 during the transistor is switched off. The value of inductor has to be high enough to keep it. In general to choose a right inductor is a compromise between inductance, maximal current, price and weight. Another way how to keep the uninterrupted current would be the high switching frequency, but we are limited by the abilities of transistors.

3.4.2 Boost Mode

For switching frequency optimization in boost mode an analysis is needed, if optimal energy amount is stored in the inductor before the transistor is switched off. The circuit, when the transistor Q2 is switched on, can be described by following equations (we are setting the resistor $R = 0$):

$$\begin{aligned} v_{SC}(t) &= \frac{\partial i_L(t)}{\partial t} \cdot L \\ -i_L(t) &= \frac{\partial v_{SC}(t)}{\partial t} \cdot SC \end{aligned} \tag{3.13}$$

And setting the conditions at the time t=0:

$$v_{SC}(0) = V_0, i_L(0) = 0 \tag{3.14}$$

The result of this equations are the equations for current through inductor i_L and the voltage on super-capacitor v_{SC}.

$$i_L(t) = \frac{\sqrt{SC} \cdot V_0 \cdot \sin\left(\frac{t}{\sqrt{SC \cdot L}}\right)}{\sqrt{L}} \tag{3.15}$$

$$v_{SC}(t) = V_0 \cdot \cos\left(\frac{t}{\sqrt{SC \cdot L}}\right) \tag{3.16}$$

From equations (3.15) and (3.16) we are able to calculate the power which describes how energy is being transferred into inductor.

$$p(t) = v_{SC}(t) \cdot i_L(t) = \frac{\sqrt{C} \cdot V_0^2 \cdot \cos\left(\frac{t}{\sqrt{SC \cdot L}}\right) \cdot \sin\left(\frac{t}{\sqrt{SC \cdot L}}\right)}{\sqrt{L}} \tag{3.17}$$

The next step is to enumerate the function of mean value of power with dependence on time during the transistor is switched on t_{ON}.

$$P_{MEAN}(t_{ON}) = \int_0^{t_{ON}} \frac{p(t)}{t_{ON}} dt \tag{3.18}$$

$$P_{MEAN}(t_{ON}) = \frac{SC \cdot V_0^2 \cdot \sin^2\left(\frac{t_{ON}}{\sqrt{SC \cdot L}}\right)}{2 \cdot t_{ON}} \tag{3.19}$$

The result is plotted in the Fig. 3.8 ($L = 4mH, SC = 100F, V_0 = 50V$).

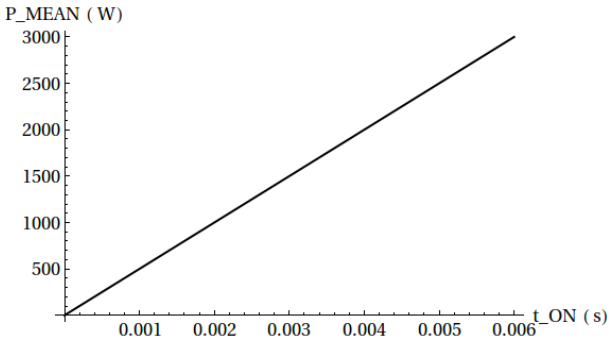

Figure 3.8. Graph of power mean value as function t_{ON}

It is clear from the figure, that the maximal mean power depends linearly on the maximal time t_{ON}. This is valid only for small t_{ON}, because the equation (3.19) is not linear. For example: for the time $t_{ON} = 0.005s$ the mean power is about $P_{MEAN}(t_{ON}) = 2.5kW$ and the switching frequency should be 100 Hz with the respect $t_{ON} = t_{OFF}$ for controller operating range. For this frequency we have made a graph of maximal mean value of power depending on voltage on super-capacitor (Fig. 3.9). From this graph we have decided that the working voltage on super-capacitor will be 25 - 50 V with the respect the range of P_{MEAN} which is from 550 to 2500 W.

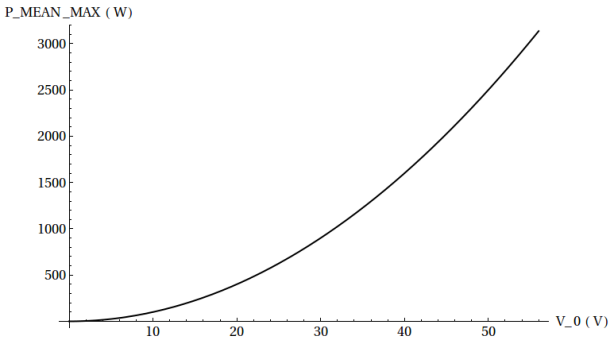

Figure 3.9. Graph of maximal mean value of power

3.5 Design of Control for DC/DC Converter

Possible control strategies are discussed in [37], [38] and [39]. This section deals with the design of LQR (Linear Quadratic Regulator) controller for DC/DC converter and with the switching frequency optimization. Designed controller will optimize the switching frequency with these criteria:

- Minimal switching losses
- Maximal transferred electrical power
- Minimal current ripple

The maximal current ripple is 20% for buck converter. The maximal difference between input and super-capacitor voltage is 180V , the inductor has the inductance $L = 4mH$. The minimal time t_{ON} is about $50us$, if the $t_{ON} = t_{OFF}$, the switching frequency is about $10kHz$ for all transferred electrical power with respect to minimal switching losses. The time t_{ON} for boost converter depends on the transferred electrical power and it is calculated using (3.19). In accordance with the Minimal current ripple criterium we need to calculate the time t_{ON} for every using of boost mode. The switching frequency for this mode is from $50Hz$ to $500Hz$.

3.5.1 LQR Controller

The mathematical model is linear time-invariant system of 3rd order and the state-variable equations are given by:

$$\dot{x} = Ax + Bu. \tag{3.20}$$

where x is 3×1 state vector and u is 1×1 input vector. Matrix A is the system matrix, B is the input matrix, C is the output matrix and D is the direct feed matrix.

The states variables are:

- v_{SC}: voltage on super-capacitor
- i_L: current through inductor
- v_C: voltage on capacitor

We consider this performance index:

$$J(u) = \int_0^\infty (x^T Q x + u^T R u + 2x^T u) dt \tag{3.21}$$

where Q and R is given 3×3 and 1×1 real symmetry weight matrix, respectively Q is semi-positive definite and R positive definite. When (A, B) is controllable and (A, C) is observable, the optimal state-feedback law is $u = -Kx$ such that J is minimized.

The design procedure for finding the state-feedback K is:

- Select parameters of Q and R matrices
- Solve the algebraic Riccati equation for P: $A^T P + PA + Q - PBR^{-1}B^T P = 0$
- Find the state-feedback $K = R^{-1}B^T P$
- Verify the design. If not suitable, go to first step and design different matrices Q and R.

3.5.2 Design of LQR Controller

The design of LQR controller is based on the mathematical model. For the complete mathematical model are needed these parameters:

- $SC = 100F$
- $C = 100mF$
- $L = 4mH$
- $R = 1000\Omega$
- $R_{SC} = 0.05\Omega$
- $R_C = 0.001\Omega$
- $R_L = 0.03\Omega$
- $R_S = 0\Omega$

The state-space matrices for the buck converter (where u=1) are:

$$A = \begin{pmatrix} -9.9995 \cdot 10^{-6} & 0.01 & 0 \\ -249.9875 & -19.9994 & 250 \\ 0 & 0 & -10000 \end{pmatrix}$$

$$B = \begin{pmatrix} 0 \\ 0 \\ 10000 \end{pmatrix}$$

$$C = \begin{pmatrix} 1 & 0 & 0 \\ 0 & 1 & 0 \\ 0 & 0 & 1 \end{pmatrix}$$

$$D = \begin{pmatrix} 0 \\ 0 \\ 0 \end{pmatrix}$$

The state-space system based on these matrices is fully controllable (the controllability matrix has full rank). For the design of LQR controller are needed the matrixes Q and R. The designed controller is used for the inductor current control. The state i_L is in the second row in matrix A. The first and third row of matrix Q are zeros. The maximal current of the transfer function depends on the value of second row. The physical limit of DC/DC converter is 50A - for this value the matrices are:

$$Q = \begin{pmatrix} 0 & 0 & 0 \\ 0 & 0.2 & 0 \\ 0 & 0 & 0 \end{pmatrix}$$

$$R = (\,0.5\,)$$

The main design of LQR controller is in MATLAB. The state-feedback K is solved using lqr function.

$$K = (\,-0.0144\ 0.5564\ 0.0138\,)$$

The design for the boost converter is similar. The output from controller is connected on PWM (Pulse-Width Modulation) generator input, which generates pulses for IGBT switching transistor in accordance with the frequency switching optimization using (3.19). The reference signals are voltage on super-capacitor and charging/discharging current. The inductor has an inductance 5 mH, super-capacitor has a capacity 100

F and maximal voltage 56 V. Those parts are used for building prototype of DC/DC converter and comparing of simulated and measured signals.

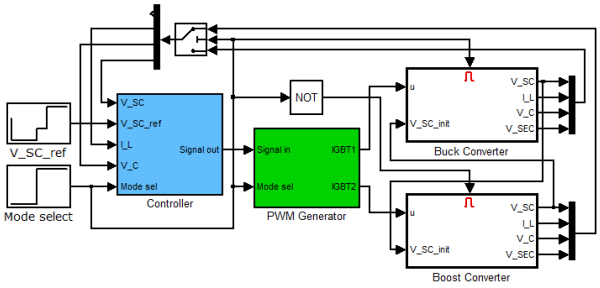

Figure 3.10. Model of DC/DC converter in MATLAB/Simulink

The MATLAB/Simulink model is shown in Fig. 3.10. The model has three main parts. First is a part with mathematical models of buck and boost converter. Second part is a PWM generator. The PWM generator transfers reference signal to PWM signal for IGBT transistors. Third part is controller, where are included both controllers. The output from this block is signal for PWM generator.

3.6 Prototype of DC/DC Converter for HEV

The prototype of DC/DC converter was developed for validation of simulation results. The control algorithm is programmed in Digital Signal Processor from Freescale using a processor board of Freescale TOWER System. Freescale TOWER System is modular development platform, where it is possible to combine different processor platforms and different peripheral modules. The TOWER System used for control of DC/DC converter is shown in the fig. 3.11. The processor board (blue board) has included processor 56F8257 type and it was designed by Freescale. The peripheral board was designed especially for this converter. The board has included 2 CANNON connectors: 1st for PWM signals and 2nd for measuring of current and voltage.

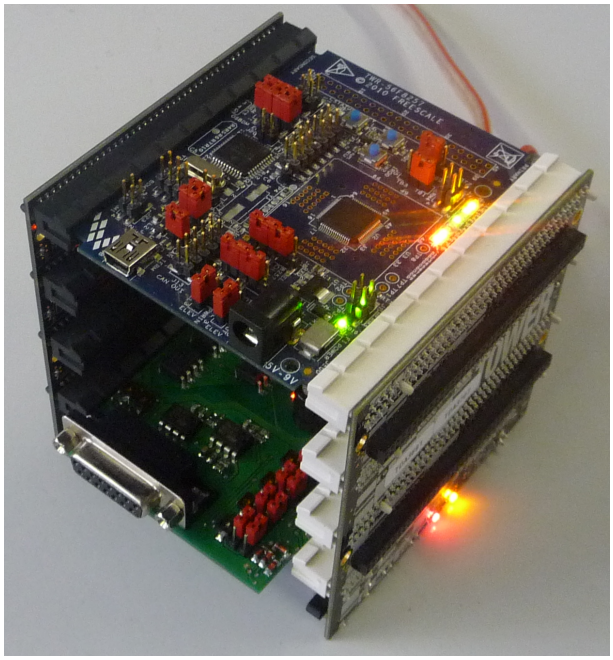

Figure 3.11. Control part of DC/DC converter

Chapter 4
Vehicle Dynamics, Track and Powertrain Modelling

This chapter deals with the modelling of vehicle dynamics, energy model, model of the track and powertrain. The models described in this thesis are based on the models created by my diploma students Tomáš Hlinovský, Jan Kacetl and Tomáš Kacetl.

4.1 Track

Track can be understood as a smooth continuous function describing the trajectory of vehicle motion, or the motion of the mass point in a 3 dimensional space as a variable of:

- time t, then it is possible define the position in ortogonal space with axes x, y, z as $P(x, y, z) = f(t)$
- traveled distance d, then it is possible can define the position in ortogonal space with axes x, y, z as $P(x, y, z) = f(d)$

For the purpose of optimization, the description of track is used where the trajectory is considered only in a 2-dimensional space with the axes z which refers to altitude h and x as a function of the traveled distance d. The position of the mass point is then:

$$P(x, h) = f(d) \tag{4.1}$$

I will adopt this simplification due to the vehicle dynamics description in the next section which ignores the lateral force applied on the vehicle in motion as these forces are a minor source of energy dissipation compared to the complicated calculation which would make the optimization algorithm almost infinite. However, the curvature of the track is not ignored at all inasmuch. The track is further divided into small sections of constant length d and constant angle of inclination α. This fact causes no big inaccuracy while using appropriate small section length, apparent in figure 4.1 [40].

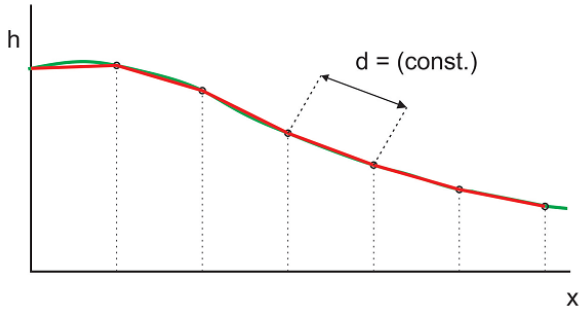

Figure 4.1. Track discretization [40]

I have chosen this type of description along the previously mentioned reasons bearing in mind possible sources of data. There is no way the track can be described by mathematical function, and the description of real track is, therefore, always given as a series of sampled points with discrete values. The most common description is GPS coordinates, which consist of altitude, longitude and latitude. Almost every device designed for measuring GPS coordinates provides information about the traveled distance, which gives us all the data necessary for the track description.

For the purpose of obtaining data before taking a drive, it is possible to use one of many web services 'APIs', which provides GPS coordinates of the designed track in user interface. Furthermore, the advantage of using web services APIs is that they provide a lot of useful information about traffic situation, speed limit, and the character of the road. The most significant APIs are Google maps and OpenStreetMaps. When compared, the Google maps provide more accurate information with easy scripting as there are a lot of examples on the official support pages, however, for information about speed limit and traffic situation, Google charges large amount of money (approx. 5000 EUR/year for noncommercial using). In the case of OpenStreetMap, everything is absolutely for free, nevertheless, the consistency of data differs between city road and countryside and also depends on the country of usage. Another trable is missing documentation and the minimal number of examples (year 2015) which makes using OpenStreetMaps very uncomfortable and difficult.

4.1.1 Speed limits

As mentioned at the end of previous section, there is no satisfactory source of speed limit. However, maximum speed is not given only by traffic signs, but also by the curvature of the chosen road as well. Motion of vehicle in curves is described in physics as the movement of mass point along the circumference of a circle, called circular motion. During a circular motion, there is a force applied on the vehicle and passengers called centrifugal force $\vec{F}_{cen}$.

$$\vec{F}_{cen} = m \cdot \frac{\vec{v}^2 \cdot \vec{n}_v}{R_v} \tag{4.2}$$

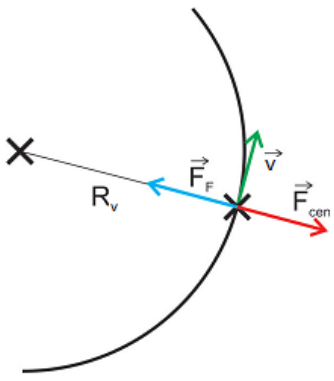

Figure 4.2. Centrifugal force applied on mass point in curve

As we can see in equation (4.2), the magnitude of the force is quadraticaly proportional to the magnitude of the velocity $|\vec{v}|$ of the vehicle and inversely proportional to the radius of the curvature R_v. The centrifugal force vector has the normal direction of velocity vector $\vec{n}_v$, which is apparent in figure 4.2. The radius of the curvature is

calculated from the GPS coordinates, but first it is necessary to transform the altitude, latitude and longitude coordinates to the cartesian coordinate system. Relation between these systems is apparent in figure 4.3. GPS coordinates are understood as spherical coordinates described by latitude φ and longitude λ corresponding to the azimutal and polar angle and altitude, which by adding Earth radius ($R = 6378km$) corresponds to the radial distance. Transformation equations are then as follows:

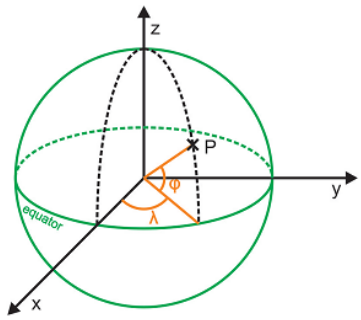

Figure 4.3. Spherical and cartesian coordinates [40]

$$r = R + altitude \tag{4.3}$$

$$x = r \cdot \cos(\phi) \cdot \cos(\lambda) \tag{4.4}$$

$$y = r \cdot \cos(\phi) \cdot \sin(\lambda) \tag{4.5}$$

$$z = r \cdot \sin(\phi) \tag{4.6}$$

However, the radius of curvature is calculated in x and y axes, and recalculation of these axes in respect to the axes z has to be done.

4.1.2 Geometrical Circle Approximation

As a circle is defined by minimum of three points, the calculation is made for each triplet of consecutive points labeled $P_1(x_1, y_1), P_2(x_2, y_2), P_3(x_3, y_3)$. Geometrically, it is known that the center of a circle $M(x_m, y_m)$ lies on lines that pass through the midpoints of chords $\bar{P}_1\bar{P}_2$ and $\bar{P}_2\bar{P}_3$ and are perpendicular to each chord. Equations of the cord lines are:

$$m_{12} = \frac{y_2 - y_1}{x_2 - x_1} \tag{4.7}$$

$$m_{23} = \frac{y_3 - y_2}{x_3 - x_2} \tag{4.8}$$

$$y_{12} = m_{12} \cdot (x - x_1) + y_1 \tag{4.9}$$

$$y_{23} = m_{23} \cdot (x - x_2) + y_2 \tag{4.10}$$

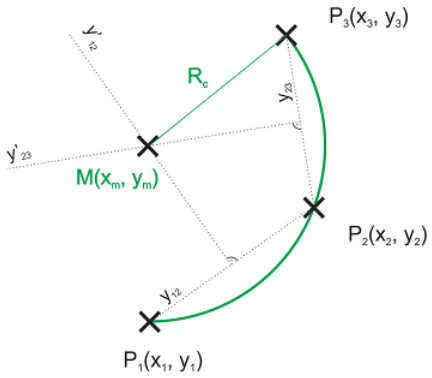

Figure 4.4. Geometrical construction of the circle [40]

Equation of the perpendicular lines are:

$$y'_{12} = -\frac{1}{m_{12}} \cdot (x - \frac{x_1 + x_2}{2}) + \frac{y_1 + y_2}{2} \tag{4.11}$$

$$y'_{23} = -\frac{1}{m_{23}} \cdot (x - \frac{x_2 + x_3}{2}) + \frac{y_2 + y_3}{2} \tag{4.12}$$

Both of these lines pass through the midpoint of the circle which is identical to their point of intersection. The geometrical construction is clear from figure 4.4. Coordinate x_m is found by equation:

$$x_m = \frac{m_{12} \cdot m_{23} \cdot (y_3 - y_1) + m_{12} \cdot (x_2 + x3) - m_{23} \cdot (x_1 + x_2)}{2 \cdot (m_{12} - m_{23}} \tag{4.13}$$

Coordinate y is easily calculated by substituting x into the equation of one of lines y'_{12} or y'_{23}. Finally the radius of the curvature is the distance between midpoint and any point of taken triplet.

$$R_c = \sqrt{(x_1 - x_m)^2 + (y_1 - y_m)^2} \tag{4.14}$$

Geometrical approximation of every triplet of consecutive points is possible only in the case of extremely accurate set of data. However, GPS coordinates of Google maps API are precise within meters, which is comparable to the desired sampling and, thus, the result of geometrical approximation is nonsense. For this purpose, it is by far better to calculate the curvature of cornering by algebraic approximation using multiple consecutive points.

4.1.3 Taubin-Raphson Approximation

In general, algebraic methods use larger sets of data than the previous method and minimize the sum of squares of algebraic distances between each point of given set and fitted circle and, thus, this method is one of Least-Squares fitting methods [41]. This fact can be written as follows:

$$F_1(a, b, R) = \sum_{k=1}^{n} [(x_k - a)^2 + (y_k - b)^2 - R^2]^2 \tag{4.15}$$

Where F_1 is the object of minimization, variables a and b are coordinates of center, and R is radius of fitted circle. Generally speaking, the problem of fitting is described as polynomial function $P(x_i, y_i)$ and function F_1 can be rewritten as:

$$F_1 = \sum_{k=1}^{n} [P(x_i, y_i)]^2 \tag{4.16}$$

Improved methods called the gradient weighted algebraic fit are based on minimizing (4.17)

$$F_2 = \sum_{k=1}^{n} \frac{[P(x_i, y_i)]^2}{\|\nabla P(x_i, y_i)\|^2} \tag{4.17}$$

where $\nabla P(x_i, y_i)$ is the gradient of the function $P(x_i, y_i)$ in (4.16). The function F_2 works better than F_1, because using the Taylor expansion we have

$$\frac{[P(x_i, y_i)]}{\|\nabla P(x_i, y_i)\|} = d_i + O(d_i^2) \tag{4.18}$$

where d_i is the geometric distance of the point (x_i, y_i) to the curve $P(x_i, y_i)$. The function F_2 is therefore a linear approximation to the function F_1. For a circle we can write

$$P(x_i, y_i) = (x_i^2 + y_i^2) - 2 \cdot a \cdot x_i - 2 \cdot b \cdot x_i + a^2 + b^2 - R^2 \tag{4.19}$$

$$\nabla P(x_i, y_i) = (2x_i - 2a, 2y_i - 2b) \tag{4.20}$$

$$\|\nabla P(x_i, y_i)\| = 4(x_i^2 + y_i^2) - 8ax_i - 8by_i + 4a^2 + 4b^2 \tag{4.21}$$

The minimization objective function is then

$$F_2 = \sum_{k=1}^{n} \frac{(x_i^2 + y_i^2) - 2ax_i - 2bx_i + a^2 + b^2 - R^2}{4(x_i^2 + y_i^2) - 8ax_i - 8by_i + 4a^2 + 4b^2} \tag{4.22}$$

This is a nonlinear problem that can be solved iteratively, hence, it is possible approximation which allows us to use simpler solution. Taubin's approximation averages the variables in the denominator. When we will substitute $(x_i^2 + y_i^2) = z_i$, we get to the function:

$$F_2 = \sum_{k=1}^{n} \frac{[z_i - 2ax_i - 2bx_i + a^2 + b^2 - R^2]^2}{4y_i - 8ax_i - 8by_i + 4a^2 + 4b^2} \tag{4.23}$$

Now we can switch to the algebraic circle parameters A, B, C, D by following substitutions:

$$\begin{aligned} a &= -\frac{B}{2A} \\ b &= -\frac{C}{2A} \\ R^2 &= -\frac{B^2 + C^2 - 4AD}{4A^2} \end{aligned} \tag{4.24}$$

and we obtain function F_3 as:

$$F_3(A, B, C, D) = \sum_{k=1}^{n} \frac{[Az_i + Bx_i + Cy_i + D]^2}{4A^2 y_i + ABx_i + ACy_i + B^2 + C^2} \tag{4.25}$$

The minimization of function (4.25) is equivalent to the minimization of function F_4 in (4.26)

$$F_4(A, B, C, D) = \sum_{k=1}^{n} [Az_i + Bx_i + Cy_i + D^2]^2 \tag{4.26}$$

with this constraint

$$4A^2 z_i + ABx_i + ACy_i + B^2 + C^2 = 1 \tag{4.27}$$

4.1.4 Taubin-Raphson Implementation

First, it is necessary eliminate the parameter D by centering the data set considering $x_i = y_i = 0$ and using $D = -A\bar{z}$ we get the function [42]:

$$F_5(A, B, C, D) = \sum_{k=1}^{n} [A(z_i - \bar{z}) + Bx_i + Cy_i]^2 \tag{4.28}$$

and constraint

$$4A^2 \bar{z} + B^2 + C^2 = 1 \tag{4.29}$$

It is convenient to introduce parameter A_0 as

$$A_0 = 2\sqrt{\bar{z}}A \tag{4.30}$$

Now it is necessary minimize function F_6 with the constraint as folllows:

$$F_6(A_0, B, C) = \sum_{k=1}^{n} [A_0 \frac{z_i - \bar{z}}{2\sqrt{\bar{z}} + Bx_i + Cy_i}]^2 \tag{4.31}$$

$$A_0^2 + B^2 + C^2 = 1 \tag{4.32}$$

Secondly, we make reduction to eigenvalue problem by rewriting the function (4.31) in a matrix form:

$$F_6 = \|\mathbf{X_0}\mathbf{A_0}\|^2 = \mathbf{A_0^T}(\mathbf{X_0^T}\mathbf{X_0})\mathbf{A_0} \tag{4.33}$$

where $\mathbf{X_0}$ and $\mathbf{A_0}$ can be written as:

$$\mathbf{A_0} = (A_0, B, C)^T \tag{4.34}$$

$$\mathbf{X_0} = \begin{bmatrix} \frac{z_1 - \bar{z}}{2\sqrt{\bar{z}}} & x_1 & y_1 \\ \vdots & \vdots & \vdots \\ \frac{z_n - \bar{z}}{2\sqrt{\bar{z}}} & x_n & y_n \end{bmatrix} \tag{4.35}$$

The minimum of F_6 is attained on the unit eigenvector of the matrix $\mathbf{X_0^T X_0}$ corresponding to its smallest eigenvalue. This matrix is symmetrical and positive-semidefinitive, thus, all its eigenvalues are real and non-negative. Furthermore, this matrix is non-singular, positivedefinitive, unless the data points lie of a circle or a line. For a faster solution, the eigenvalue λ of the matrix $\mathbf{X_0^T X_0}$ is found by solving its characteristic equation:

$$det(\mathbf{X_0^T X_0} - \lambda \mathbf{I}) = 0 \tag{4.36}$$

Equation (4.36) is rewritten into polynomial form of the 3rd degree in λ:

$$P(\lambda) = c_3\lambda^3 + c_2\lambda^2 + c_1\lambda + c_0 = 0 \tag{4.37}$$

Coefficients c_0, c_1, c_2, c_3 are as follows:

$$\begin{aligned} c_3 &= 4\bar{z} \\ c_2 &= -\bar{z}\bar{z} - 3\bar{z}^2 \\ c_1 &= \bar{z}(\bar{z}\bar{z} - \bar{z}^2) + 4\bar{z}(\bar{x}\bar{x}\bar{y}\bar{y} - \bar{x}\bar{y}^2) - \bar{x}\bar{z}^2 - \bar{y}\bar{z}^2 \\ c_0 &= \bar{x}\bar{z}^2\bar{y}\bar{y} + \bar{y}\bar{z}^2\bar{x}\bar{x} - 2\bar{x}\bar{x}\bar{y}\bar{z}\bar{x}\bar{y} - (\bar{x}\bar{x}\bar{y}\bar{y} - \bar{x}\bar{y}^2)(\bar{z}\bar{z} - \bar{z}^2) \end{aligned} \tag{4.38}$$

As the eigenvalues of $\mathbf{X_0^T X_0}$ are real and non-negative, the characteristic polynomial equation (4.37) always has three non-negative real roots and $P(0) \leqq 0$. In the non-singular case, the $P(0) < 0$, and then $P''(\lambda) < 0$ in the interval between 0 and the smallest root. Newton-Raphson method with initial guess $\lambda = 0$, hence, always converges to the smallest desired root. Parameters of the fitted circle are calculated as:

$$a = \frac{2(\bar{x}\bar{z}\bar{y} - \lambda\bar{x}\bar{z} - \bar{y}\bar{z} - \bar{y}\bar{z}\bar{x}\bar{y})}{\lambda^2 - \lambda\bar{z} + \bar{x}\bar{y} - \bar{x}\bar{y}\bar{x}\bar{y}} + x_0 \tag{4.39}$$

$$b = \frac{2(\bar{x}\bar{z}\bar{x} - \lambda\bar{x}\bar{z} - \bar{y}\bar{z} - \bar{y}\bar{z}\bar{x}\bar{y})}{\lambda^2 - \lambda\bar{z} + \bar{x}\bar{y} - \bar{x}\bar{y}\bar{x}\bar{y}} + y_0 \tag{4.40}$$

$$R = \sqrt{a^2 + b^2} \tag{4.41}$$

4.1.5 Velocity Calculation

Maximum velocity in a curve can be calculated by limiting centrifugal acceleration applied on the vehicle and passengers inside. For the vehicle, the centrifugal force $\vec{F}_{cen}$ causes skid of the vehicle. Magnitude of the centrifugal force is directly proportional to the mass of the vehicle m, square of the vehicle speed $\vec{v}$, and inversely proportional to the radius of curvature R_v as described in (4.40).

$$\vec{F}_{cen} = m \cdot \frac{|\vec{v}|^2 \cdot \vec{n}_v}{R_v} \tag{4.42}$$

According to the priciple of action and reaction, there is a force which is applied on the vehicle in the opposite direction to the centrifugal force. This force is caused by the friction between tires and the road, and its maximum magnitude is calculated as:

$$\vec{F}_{FM} = \mu \cdot m \cdot |\vec{g}| \cdot (-\vec{n}_v) \tag{4.43}$$

Where m is the mass of the vehicle, $\vec{g}$ is gravitational acceleration and μ is the coefficient of friction between the vehicle tires and surface of the road. The coeffient of friction depends on the surface of the road and the typical values are in the table 4.1. For each of these coefficients, maximal magnitude of centrifugal acceleration $|\vec{a}_{cskid}|$ is calculated according to the equation (4.44) and its value is also in the table 4.1.

$$|\vec{a}_{cskid}| = \vec{g} \cdot \mu \tag{4.44}$$

Road type	μ	$\lvert\vec{a}_{cskid}\rvert$
Dry asphalt	0.9	8.83
Wet asphalt	0.6	5.89
Snow	0.2	1.96
Ice	0.05	0.49

Table 4.1. Frictions coeficients and maximum lateral acceleration [40]

Once the centrifugal force exceeds friction force maximum, the vehicle gets into skid, which is undesirable and can be a cause of traffic accident.

Another factor limiting centrifugal acceleration is the comfort of the passengers. For railway, the limit of the centrifugal acceleration [1] is $|\vec{a}_{cskid}| = 2\ m \cdot s^{-2}$. Taking to consideration dry or wet asphalt and snow, we are limited by the the comfortable lateral acceleration $|\vec{a}_{cskid}| = 2\ m \cdot s^{-2}$. Now it is possible to calculate the speed limit of each point of the track as follows:

$$v_{max} = \sqrt{R_v \cdot |\vec{a}_{cmax}|} \tag{4.45}$$

4.2 Vehicle Dynamics

The motion of a vehicle on a road is a complex system described by several differential equations. The model of ideal rigid vehicle is difficult enough for purpose of optimization. There are loads of forces which differ in their magnitude, direction and point of application. Therefore, some simplifications are introduced in order to create an optimization algorithm fitting present computing capability and keep satisfactory precision. For the above reasons, straight motion of an ideal rigid vehicle on an inclined road is considered including acceleration force, gravitation force, air friction and rolling resistance . Resultant force of each considered is applied in the center of gravity. The sum of these forces is the total resultant force applied on a vehicle in motion. This force has multiple variables, and the detailed description is the subject of the following sections, where each of these forces is examined separately [40].

4.2.1 Gravitation Force

Any two objects with a mass attract each other with a force called gravitation force. This force is directly proportional to the product of their masses and inversely proportional to the square of the distance. For our proposes when the distance between a vehicle and Earth is from the Earth size point of view constant, we will consider a gravitational field with gravitational constant. Gravitation force is then:

$$\vec{F}'_g = m \cdot \vec{g} \tag{4.46}$$

A road is not flat and it is necessary to consider a track profile where a track angle is still changing. The track angle is marked by a letter α and the gravitation force recalculate using sinus function. The result is then

$$\vec{F}_g = \vec{F}'_g \cdot \sin\alpha = m \cdot \vec{g} \cdot \sin\alpha \tag{4.47}$$

[1] The value $2\ m \cdot s^{-2}$ is a result of a measuring of comfort centrifugal acceleration in Škoda auto a.s. It is clear that for different persons are different values and the value $2\ m \cdot s^{-2}$ is a median.

4.2.2 Drag Force

Drag force is the resultant force of forces acting opposite to the relative motion of any object moving in respect to the surrounding fluid (between two fluid layers or a fluid and a solid surface). The drag force is directly proportional to velocity for laminar flow according to the Stokes law, and squared for turbulent flow according to the Newton's law. The flow depends on the shape of the moving object and on the Reynolds number:

$$R_e = \frac{v \cdot D}{\nu} \tag{4.48}$$

$$\nu = \frac{\mu}{\rho} \tag{4.49}$$

Where ν is kinematic viscosity of the fluid (viscosity μ divided by the density ρ of the fluid) and D is characteristic diameter. Calculation of the force applied on the vehicle in motion is computed in iterative steps to determine the type of flow and associated drag coefficient. Moreover, the flow type changes from the vehicle hood to the back of the vehicle. Precise examination of the flow along the vehicle is inappropriate for the purpose of real-time simulation and optimization. Hence, the Newton's resistance law based on conservation of energy is used. An object moving in a fluid pushes the originally still fluid. The force, which the vehicle exerts on the fluid, according to the principle of action and reaction, is equal to the drag force in the opposite direction. The work of this force is equal to the kinetic energy of the moving fluid, hence:

$$\vec{F}_d' = \frac{1}{2} \cdot \rho \cdot A \cdot \vec{v}^{\,2} \tag{4.50}$$

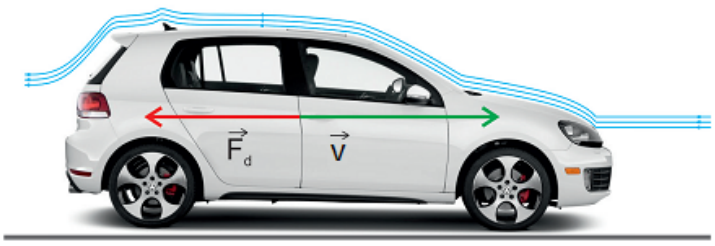

Figure 4.5. Drag between the fluid and the vehicle in motion [40]

However, this force does not respect the shape of the moving object and properties of the fluid. Therefore, the drag coefficient C_D is introduced and the Newton's resistance law equation is as follows:

$$\vec{F}_d' = \frac{1}{2} \cdot \rho \cdot C_D \cdot A \cdot \vec{v}^{\,2} \tag{4.51}$$

Where A is the area of the cross section. Drag force is the most significant of motion resistant forces [43].

4.2.3 Rolling Resistance

Rolling resistance F_r is generated by a turning tire on the road. Direction of the force is opposite to the direction of the motion and the magnitude is directly proportional to the normal component of the gravitation force.

$$\vec{F}_r = \mu_r \cdot \vec{F}_g n \tag{4.52}$$

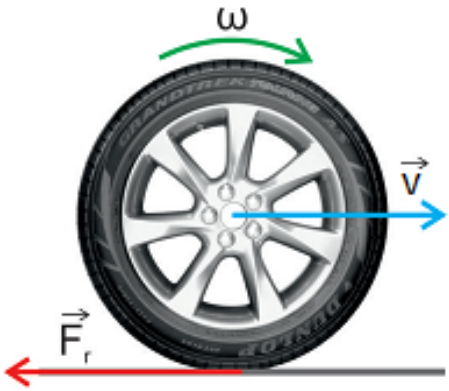

Figure 4.6. Resistance force applied on a rolling wheel [40]

The value of the friction coefficient μ_r depends on the tire velocity, inflation pressure, sideslip and camber angles and mechanical properties, wear, temperature, load, driving and braking force, and road conditions. It would put extreme demands on the simulation time to consider all the operating condition dependencies. In the case of velocity, the rolling friction coefficient increases with the square of the velocity. However, the part of the equation (4.53) with coefficient μ_1 is insignificant compared with the first part of the equation for values of velocity under $100m/s$ which highly exceed speed limits of any road [44].

$$\mu_r = \mu_0 + \mu_1 \cdot \vec{v}^{\,2} \tag{4.53}$$

Hence, it is possible to omit that part and for the simulation model we can consider the rolling friction as follows:

$$\vec{F}_r = \mu_0 \cdot |\vec{F}_g| \cdot \cos\alpha \tag{4.54}$$

4.2.4 Acceleration Force

Acceleration force is generated by the imbalance between load torque $\vec{M}_L$ and torque of the powertrain on wheels $\vec{M}_W$ according to the motion equation (4.55), where $\vec{M}_D$ is the dynamic torque. The acceleration torque is on the side of load because of the principle of action and reaction.

$$\vec{M}_W = \vec{M}_D + \vec{M}_L + \vec{M}_a \tag{4.55}$$

In a steady state when the vehicle is not accelerating ($\frac{dv}{dt} = 0$), the dynamic torque is equal to zero. In the case of torque surplus ($\vec{M}_W - \vec{M}_L > 0$) the vehicle is accelerating, in the case of torque lack ($\vec{M}_W - \vec{M}_L < 0$) the vehicle is deccelerating. The dynamic torque represents the moment increasing the angular velocity of rotating mass which is specified by the rotational inertia J.

$$\vec{M}_D = J \cdot \frac{d\vec{\omega}}{dt} \tag{4.56}$$

Acceleration torque can be separated from the equation as follows:

$$\vec{M}_a = \vec{M}_W - \vec{M}_L - \vec{M}_D \tag{4.57}$$

The acceleration force is then simply calculated as torque divided by the radius of wheels r_w, and $\vec{a}$ is the acceleration of the vehicle in the direction of the motion.

$$\vec{F}_a = \frac{\vec{M}_a}{r_w} = m \cdot \vec{a} \tag{4.58}$$

4.2.5 Forward Vehicle Model

In mathematical model, we substitute vehicle by mass point moving along the track with applied forces explained in the previous chapters. For the motion of a vehicle, we can use equation of force balance.

$$\vec{F}_W + \vec{F}_a + \vec{F}_g + \vec{F}_d + \vec{F}_r = 0 \tag{4.59}$$

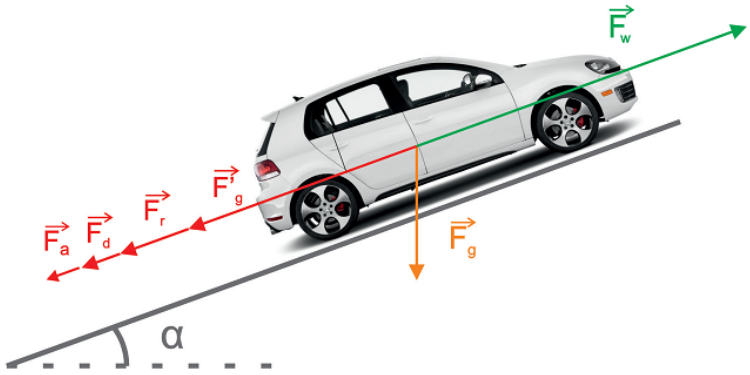

Figure 4.7. Forward vehicle model [40]

As we can see in the picture 4.7, we only consider forces in the same direction and opposite the direction of a motion which allows us to transfer vectors of forces to scalars with appropriate signs. Where minus sign indicates force direction opposite the motion and plus sign indicates force in the direction of motion. Then we can rewrite the equation (4.59) to the scalar form

$$F_M - F_a - F_g - F_d - F_r = 0 \tag{4.60}$$

We can also multiply the equation (4.60) by the radius of wheels r_w and add dynamic moment and get equation of motion in scalar form. Using equations of each force leads to the full form of equation (4.61) describing the motion of a vehicle.

$$M_W - m \cdot a - m \cdot g \cdot \sin\alpha - \frac{1}{2} \cdot \rho \cdot C_D \cdot A \cdot v^2 - \mu_0 \cdot m \cdot g \cdot \cos\alpha - J \cdot \frac{d\omega}{dt} = 0 \tag{4.61}$$

Using equation (4.62) and separating the acceleration $a = \frac{dv}{dt}$ from the equation (4.61) we get a equation (4.63) for the using in simulation.

$$\omega = \frac{v}{2 \cdot \pi \cdot r} \tag{4.62}$$

$$\frac{dv}{dt} = \left(\frac{J}{2 \cdot \pi \cdot r} + m\right) \cdot \left(M_W - m \cdot g \cdot \sin\alpha - \frac{1}{2} \cdot \rho \cdot C_D \cdot A \cdot v^2 - \mu_0 \cdot m \cdot g \cdot \cos\alpha\right) \tag{4.63}$$

4.3 Energy Model

Energy model is the essential simplification mentioned in the section 4.2. It is based on the division of the route into sections from the section 4.1. Generally speaking, it is necessary to decompose the drive into many drives by sections, which we can handle separatly.

4.3.1 Velocity od the Vehicle

The dynamic model in the previous section considers velocity as a continuous smooth function of traveled distance s:

$$v = f(s) \tag{4.64}$$

However, similar to the track characteristic values, we will also sample the function of velocity. Every section is characterized by start point and end point, where in each of these points velocity $v(k)$, altitude $h(k)$ and distance between these points d, which is designed as a constant, are defined. As in the case of altitude, the velocity is changing linearly from the start point to the end point of a section and the end point of a section is the start point of following section. This fact transforms the smooth velocity function to function (4.65) of discrete variable k, which refers to the index of the section.

$$v(s) = v(k) + \frac{v(k+1) - v(k)}{d} \cdot s \tag{4.65}$$

The set of all velocity values describing all sections gives velocity profile, which may be subject of optimization, apparent in figure 4.8.

4.3.2 Energy of Section

With all the so far made steps, there are no more difficulties to calculate the energy of every single section, which is generally given by altitude and velocity in every section. The energy of every section is calculated by integration of force over its distance. As well as forces, we can also examine kinetic energy $E_k(k)$, gravitational energy $E_g(k)$, drag energy dissipation $E_d(k)$ and roll energy dissipation $E_r(k)$ separately. The total energy of the section $E_T(k)$ is then the sum of these energy components (4.66)

$$E_T(k) = E_k(k) + E_g(k) + E_d(k) + E_r(k) \tag{4.66}$$

In the following text, we will derive formulas of each component of total energy.

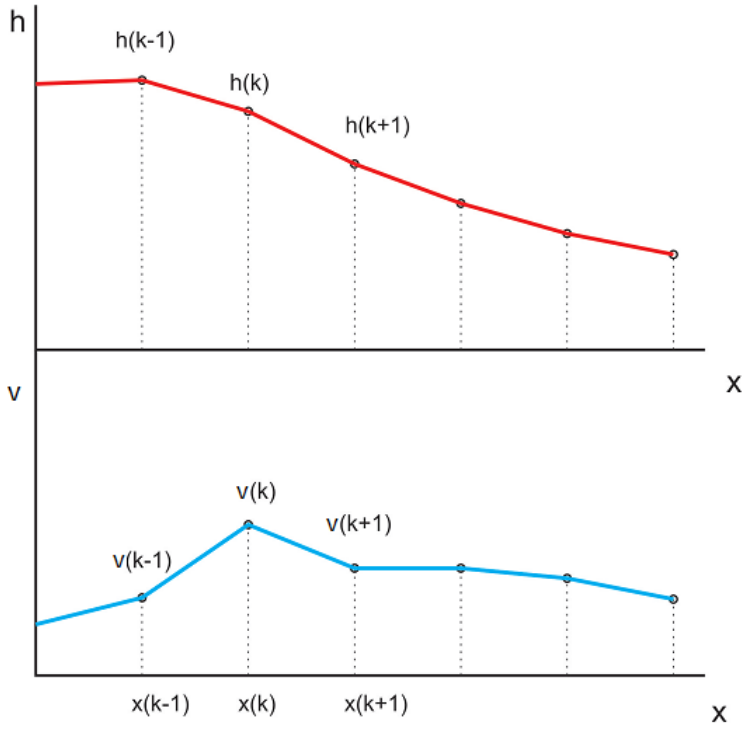

Figure 4.8. Speed profile introduction [40]

Kinetic energy

Kinetic energy of a vehicle is the energy that it possesses due to its motion. We can define it as the work needed to accelerate the vehicle of mass m from velocity of the start point $v(k-1)$ to the velocity of the end point $v(k)$ in equation (4.67).

$$E_k(k) = \frac{1}{2} \cdot m \cdot (v^2(k) - v^2(k-1)) \tag{4.67}$$

Gravitational energy

Gravitational force applied on the vehicle in the motion was examined in one of the previous subsections. When we multiply the force by element of track dh in its direction, we get an element of gravitational energy.

$$dE_p = m \cdot g \cdot dh \tag{4.68}$$

By integration of the energy element (4.68) over the section we get the gravitational energy (4.69).

$$E_p(k) = \int_{h(k-1)}^{h(k)} m \cdot g \cdot dh \tag{4.69}$$

As we can see, the energy depends simply on the altitude of start point and altitude of end point.

$$E_p(k) = m \cdot g \cdot (h(k) - h(k-1)) \tag{4.70}$$

Drag resistance energy

Element of drag resistance dissipation energy dE_d (4.71) is calculated from drag resistance force and element of track in the direction of motion ds.

$$E_d(k) = B \cdot v^2(s) \cdot ds \tag{4.71}$$

Total energy is given as integration over the track from start point to end point.

$$E_d(k) = \int_{d(k-1)}^{d(k)} B \cdot v^2(s) \cdot ds \tag{4.72}$$

We can substitute for the velocity $v(s)$ from equation (4.65).

$$E_d(k) = B \int_{d(k-1)}^{d(k)} (v(k+1) + \frac{v(k) - v(k-1)}{d} \cdot s)^2 \cdot ds \tag{4.73}$$

After integration we get the total energy:

$$E_d(k) = B \cdot (v^2(k-1) \cdot d + v(k-1) \cdot (v(k) - v(k-1)) \cdot d + \frac{1}{3} \cdot (v(k) - v(k-1))^2 \cdot d) \tag{4.74}$$

Roll resistance energy

Roll resistance dissipation energy is caused by roll resistance force. According to the similar procedure as in the case of drag resistance energy, we have equation for the element of the energy (4.75).

$$dE_r = \mu_0 \cdot m \cdot g \cdot \cos\alpha \cdot ds + \mu_1 \cdot m \cdot g \cdot v^2(s) \cdot \cos\alpha \cdot ds \tag{4.75}$$

The next step is to integrate dE_r over the track section of length d

$$E_r = \int_{d(k-1)}^{d(k)} \mu_0 \cdot m \cdot g \cdot \cos\alpha \cdot ds + \int_{d(k-1)}^{d(k)} \mu_1 \cdot m \cdot g \cdot v^2(s) \cdot \cos\alpha \cdot ds \tag{4.76}$$

The slope of the track $\cos\alpha$ is given as follows

$$\cos\alpha = \frac{d}{x(k-1) - x(k)} \tag{4.77}$$

and if we substitute from (4.65) we get

$$\begin{aligned} E_r = \frac{\mu_0 \cdot m \cdot g \cdot x}{d} \cdot \int_{d(k-1)}^{d(k)} ds + \frac{\mu_1 \cdot m \cdot g \cdot x}{d} \cdot \\ \int_{d(k-1)}^{d(k)} (v(k-1) + \frac{v(k) + v(k-1)}{d} \cdot s)^2 ds \end{aligned} \tag{4.78}$$

By integration and substitution of limits of integration we get the equation of total roll resistance energy of section

$$E_r(k) = \mu_0 \cdot m \cdot g \cdot x + \mu_1 \cdot m \cdot g \cdot x \cdot \frac{1}{3} \cdot (v^2(k) + v(k) \cdot v(k-1) + v^2(k-1)) \tag{4.79}$$

Total energy

Total energy consumed during drive on a given track is simply calculated as the sum of energy components over all section, where k is the index of section and n is the total count of section.

$$E_{total} = \sum_{k=1}^{n} E(k) \tag{4.80}$$

4.4 Time calculation

As I have chosen distance d as variable of function describing the vehicle motion, which brought about many simplifications, on the other hand the time calculation of the vehicle motion is quite complicated. However, time calculation is neccessary to determine the arrival time, which may be one of the conditions characterizing the drive. Total time, similar to the energy calculation, is given as the sum of times to pass each section. In the calculation, we can start with the definition of velocity

$$v(s) = \frac{ds}{dt} \tag{4.81}$$

We can separate element of time dt on the left side of equation

$$dt = \frac{1}{v(s)} \cdot ds \tag{4.82}$$

Time to pass a section can be obtained by integrating both sides of the equation

$$t(k) = \int_0^d (\frac{1}{v(s)})ds \tag{4.83}$$

The last step is to substitude for velocity from equation (4.65).

$$t(k) = \int_0^d (\frac{1}{v(k-1) + \frac{v(k)-v(k-1)}{d} \cdot s})ds \tag{4.84}$$

After integration we get the final expression of time to pass a section as follows:

$$t(k) = \frac{d}{v(k) - v(k-1)} \cdot ln(\frac{v(k)}{v(k-1)}) \tag{4.85}$$

Complication that are brought about by choosing distance domain may not be clear right now, but if we want to make inverse calculation to obtain velocity on the end of the section $v(k)$ as a function of time $t(k)$, there is no way to get the function $v(k) = f(t(k))$ by using elemental function as the variable $v(k)$ appears in the logarithm and also in the fraction in front of the logarithm. Hence, we must use the so called Lambert function $W(x)$, which is an inverse relation of the function:

$$f(x) = x \cdot e^x \tag{4.86}$$

$$x = f^{-1}(x \cdot e^x) = W(x \cdot e^x) \tag{4.87}$$

We can now find the inverse function to the original problem by using the Lambert function as:

$$v(k) = -\frac{d \cdot W(-\frac{v(k-1) \cdot t(k) \cdot e^{\frac{v(k-1) \cdot t(k)}{d}}}{d})}{t(k)} \tag{4.88}$$

The Lambert function is commonly implemented in almost all mathematical oriented programming languages or can be easily included by mathematical package if necessary. Nevetheless, the previously mentioned problem is not the only one. The energy model introduced in this chapter can partly substitute the dynamic model, however, sections cannot be examined completely separately. It is clear that change in velocity of a section

affects all parameters of following or previous section, depending whether we change $v(k)$ or $v(k-1)$ of the k-th section. Problem of time calculation is, therefore, far more complicated. Changing the original velocity $v(k)$ to new value $v_0(k)$ causes change of time of the k and $(k+1)$ section and, hence, the total time changes by value ΔT.

$$\Delta T = \frac{d}{v'(k) - v(k-1)} \cdot ln(\frac{v(k+1)}{v'(k)}) + \frac{d}{v(k+1) - v'(k)} \cdot ln(\frac{v(k+1)}{v'(k)}) - \\ - t(k) - t(k+1) \tag{4.89}$$

Where $t(k)$ and $t(k+1)$ are the original time associated to the original velocity $v(k)$. There is no possible way to get inverse function as $v(k) = f(\Delta T(k, k+1))$. For this purpose, we have to use numerical methods to obtain the value of inverse function.

4.4.1 Numerical Methods

Numerical analysis provides equation solving without an analytical solution or equation where analytical solution requires high computing performance. These methods are largely based on linear approxiamtion combined with iterative calculation to achieve minimal deviation. Taking into consideration the type of problematical equations and the simplicity of their derivations, we can choose Newton-Raphson method. The advantage of this method is that it provides very precise solution in a few iterative steps, which leads to a higher performance of optimization algorithm.

Newton-Raphson Method

As was mentioned earlier, most of the numerical methods use linear approximation. In the case of Newton-Raphson method, the approximation is a tangent of the observed function. The principle of this method is clear from the graph in the figure 4.9, where we start with the initial guess x_0 approximating the function by tangent $f'(x_0)$ to get the result of the first iteration x_1, which serves for further calculation as an initial guess.

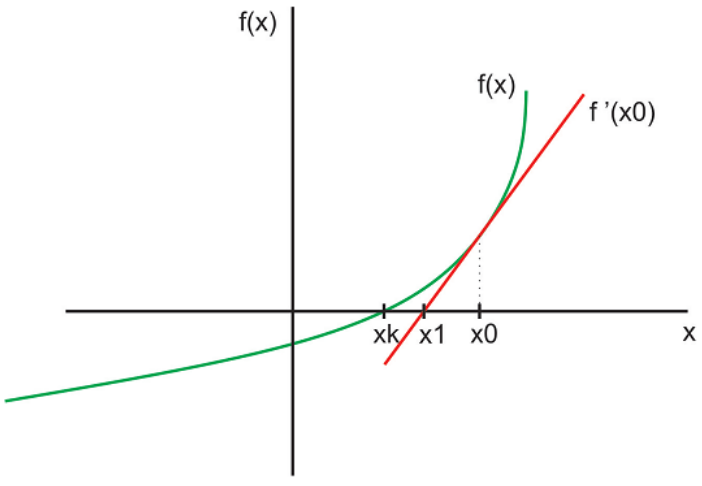

Figure 4.9. Newton-Raphson method principle [40]

The function in figure 4.9 has only one variable x, however, the method naturally works with a set of functions of multiple variables. Implementation of this method for a general function of n variables is hard to represent graphically, thus, we rather use mathematical representation. We form the matrix of equation as:

$$\mathbf{f}(\mathbf{x}) = \begin{bmatrix} f_1(x_1, x_2, \ldots, x_n \\ f_2(x_1, x_2, \ldots, x_n] \\ \vdots \\ f_n(x_1, x_2, \ldots, x_n \end{bmatrix} = \begin{bmatrix} y_1 \\ y_2 \\ \vdots \\ y_n \end{bmatrix} = \mathbf{y} \tag{4.90}$$

First of all, we must come up with some reasonable guess $\mathbf{X_0} = [x_{10}, x_{20}, \ldots, x_{n0}]$ as close to the solution as possible. In the second step, we calculate the value of the function for the guess established in the previous step.

$$\mathbf{f}(\mathbf{x_0}) = \mathbf{y_0} \tag{4.91}$$

Now we can calculate the deviation from the desired value as:

$$\mathbf{D} = \mathbf{y} - \mathbf{y_0} \tag{4.92}$$

In the third step, we calculate the Jacobian matrix which refers to the derivatives of all the functions and variables.

$$\mathbf{J} = \frac{d\mathbf{f}}{d\mathbf{x}} = \begin{bmatrix} \frac{df_1(x_1,x_2,\ldots x_n)}{dx_1} & \cdots & \frac{df_1(x_1,x_2,\ldots x_n)}{dx_n} \\ \vdots & \ddots & \vdots \\ \frac{df_n(x_1,x_2,\ldots x_n)}{dx_1} & \cdots & \frac{df_n(x_1,x_2,\ldots x_n)}{dx_n} \end{bmatrix} \tag{4.93}$$

In the last step, we calculate solution $\mathbf{x} = [x_1, x_2, \ldots, x_n]$

$$\mathbf{x} = \mathbf{x_0} - \mathbf{J} \cdot \mathbf{D} \tag{4.94}$$

If the precision is not sufficient, we can set $\mathbf{x_0} = \mathbf{x}$ and continue in the next iteration from the first step until the deviation $\mathbf{D}$ is in the desired band. Numerical calculations in this project are always solving one equation of one variable and thus we can use all the previously mentioned equations substituting the matrices by single variables [45].

4.5 Powertrain Model and Parameter Identification

This section describes the mathematical model of the EV powertrain. There are many possible powertrain configurations. In this thesis the powertrain model from a prototype of Škoda Rapid EV is used. This vehicle was built up in Škoda auto a.s. with cooperation of EVC GROUP s.r.o. company. The Škoda Rapid EV is a front whell drive electric vehicle and the powertrain includes:

- Battery pack (own developed and assembled)
- Power converter (SEVCON Gen4)
- Induction motor (TEM 112)
- Transmission (DSG automatic transmission - can operate in constant motor speed/ vehicle speed ratio)

The connection between these part is described in the Fig. 4.10.

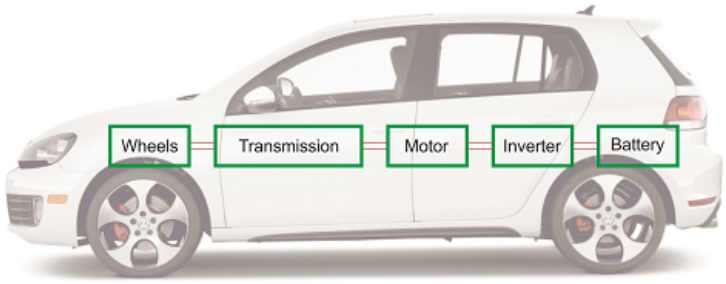

Figure 4.10. Electric vehicle powertrain composition [40]

4.5.1 Battery Pack

There are various kinds of mathematical models of battery cell which describe various properties and behaviour. In this system, we would like to observe the power flow when it is discharging (or charging) the cell by pulse current. In this context, transient response is needed to be taken into account [46]. An ideal solution with satisfying accuracy would be an equivalent circuit with 2 RC networks (see Fig. 4.11). A model of battery is necessary for the parametrization of the Battery Simulator in the laboratory in Roztoky as described later in chapter 5.

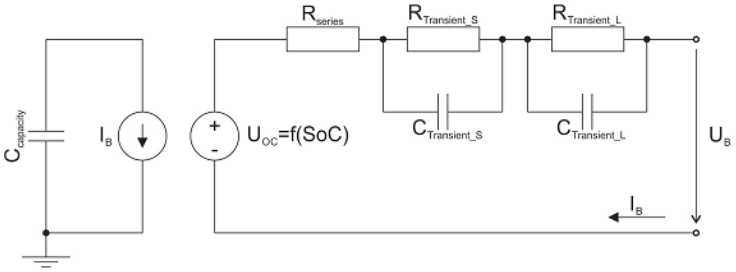

Figure 4.11. Battery cell equivalent circuit [47]

According to [48], an equivalent circuit with 2 RC networks is, in automotive applications, a suitable trade-off between complexity and accuracy and simultaneously predicts runtime, steady-state, and transient response accurately. The state equation for the equivalent circuit is shown in equation (4.95).

$$\begin{bmatrix} \dot{SoC} \\ \dot{u_{RCS}} \\ \dot{u_{RCL}} \end{bmatrix} = \begin{bmatrix} 0 & 0 & 0 \\ 0 & -\frac{1}{R_{TS}CTS} & 0 \\ 0 & 0 & -\frac{1}{R_{TL}CTL} \end{bmatrix} \begin{bmatrix} SoC \\ u_{RCS} \\ u_{RCL} \end{bmatrix} + \begin{bmatrix} \frac{1}{Q_R} \\ \frac{1}{C_{TS}} \\ \frac{1}{C_{TLL}} \end{bmatrix} \tag{4.95}$$

Capacitor $C_{capacity}$ and current controlled current source on the left side of the equivalent circuit (Fig. 4.11) represents battery runtime. The voltage controlled voltage source, series resistor and RC networks respond to the current-voltage characteristic of the battery cell (4.95).

Usable capacity represents the charge obtained from the battery cell when discharging from a fully charged state until the end of discharge voltage at cell terminal is reached. Usable capacity depends on the State of Life (SoL), discharge current, storage time (selfdischarging), depth of discharge (DoD) and temperature. The influence of some of these phenomenons is not taken into account in this mathematical model as we focus on the power flow between the battery cell and the load. The state of charge

is equal to 1 for fully charged state and is equal to 0 for fully discharged state. Self-discharging of the battery cell could be modelled by a resistor parallel to the capacitor $C_{Capacity}$. In our model, self-discharging is not taken into account [47].

Open circuit voltage drops while the battery cell is discharging. There is a non-linear relation between open circuit voltage and state of charge, which must be included in the model. This non-linear relation represents the function for output voltage of voltage source $U_{OC} = f(SoC)$ in Fig. 4.11. We can measure this function as a steady-state open circuit voltage for different states of charge.

Transient response of the battery cell consists of 3 parts.

- Instantaneous voltage drop across series resistor R_{Series}.
- Fast voltage drop across the R_{CTS}, which describes short time transient response
- Slow voltage drop across the R_{CTL}, which describes long time transient response

The inclusion of more RC networks makes model more accurate, however, increases complexity. As mentioned before, two RC networks are the best trade-off between accuracy and complexity. All these components are theoretical functions of SoC, SoL, discharge current and temperature [48].

In order to get appropriate voltage level in the DC link of the power inverter, it is necessary to configure the battery cells in series. The terminal voltage of the battery pack is calculated using equation (4.96).

$$U_{BP} = U_B \cdot n_s \tag{4.96}$$

Where U_{BP} is the terminal voltage of the battery pack, U_B is the terminal voltage of the battery cell and ns is the number of battery cells in series. To increase the capacity of the battery pack, the series branches are configured in parallel. As the impedance of the branches is the same, the current splits between these branches as shown in equation (4.98).

$$I_B = \frac{I_{BP}}{n_p} \tag{4.97}$$

Where I_{BP} is the battery pack terminal current, I_B is the current flowing through one branch and n_p is the number of the parallel branches. [1]

The values of the parameters of the equivalent circuit elements are obtained from the voltage transient response on the current discharge pulse. The transient response is measured for two different current pulses at different states of charge. The state of charge is established using equation (4.98).

$$SoC = \frac{1}{Q_c} \int i_{dis}(t)dt \tag{4.98}$$

Where Q_c is the capacity of the battery cell and $i_{dis}(t)$ is the discharge current. As the discharge current is constant, the SoC is calculated as shown in equation (4.99).

$$SoC = \frac{I_{dis}t}{Q_c} \tag{4.99}$$

[1] The real battery cells do not have the same parameters, so the particular cells are not stressed equally. This can lead to a difference in the aging of cells. Moreover, it can cause failure of the system. To avoid these issues, the charging and discharging is managed by battery management system (BMS). The battery cells in the mathematical model are considered as ideal so the battery management system is not modelled.

The measurement is done in three steps:

1. The battery is discharged until the required SoC is reached.
2. The battery is disconnected till terminal voltage is stabilized.
3. The battery is loaded by short current pulse.
4. The voltage transient response is measured.

Considering the current pulse short, we can continue in the measurement repeating these steps until the end of discharge voltage is reached (SoC = 0%). The parameters of the equivalent circuit are then calculated from the voltage transient response as shown in Fig. 4.12.

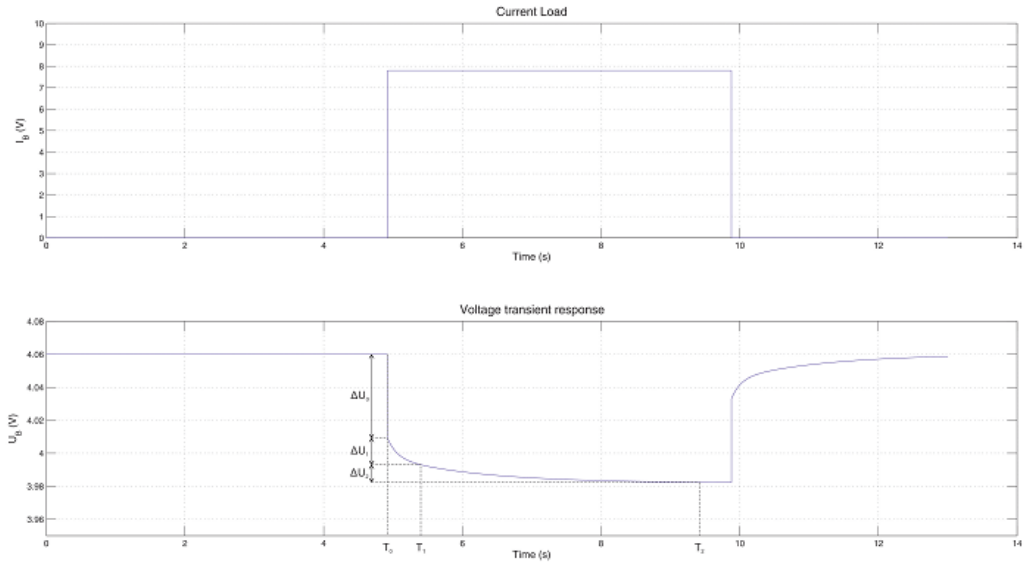

Figure 4.12. Parameters identification [47]

From figure 4.12, the series resistance is calculated from instantaneous voltage drop ΔU_0 at time T_0, as shown in equation (4.100).

$$R_{Series} = \frac{\Delta U_0}{I_{dis}} \tag{4.100}$$

The resistances of the RC networks are then calculated as shown in equations (4.101) and (4.102).

$$R_{TS} = \frac{\Delta U_1}{I_{dis}} \tag{4.101}$$

$$R_{TL} = \frac{\Delta U_2}{I_{dis}} \tag{4.102}$$

The RC network capacities are calculated from time constants ($\tau = RC$). Considering the transient finished after time $T = 3\tau$, the capacity values are calculated as (4.103) and (4.104).

$$C_{TS} = \frac{T_1 - T_0}{3R_{TS}} \tag{4.103}$$

$$C_{TL} = \frac{T_2 - T_0}{3R_{TL}} \tag{4.104}$$

This system identification method is applied on Li-ion battery cell KOKAM SLPB11043140H4. The parameters are calculated for 9 different states of charge and 2 different current pulses. The result of the measurement is displayed in the figures 4.13 - 4.18. These parameters are used in the Battery Simulator.

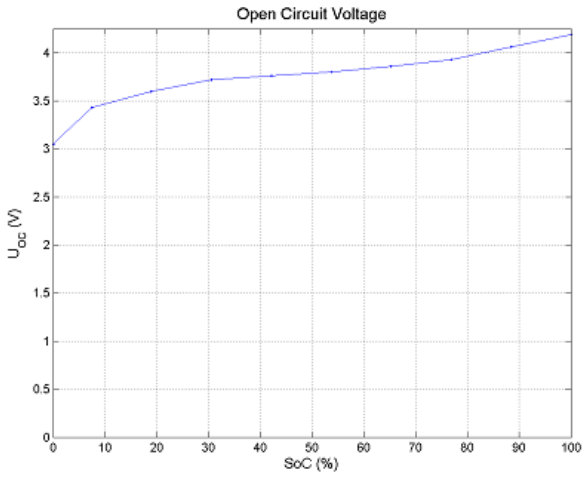

Figure 4.13. Open circuit voltage [47]

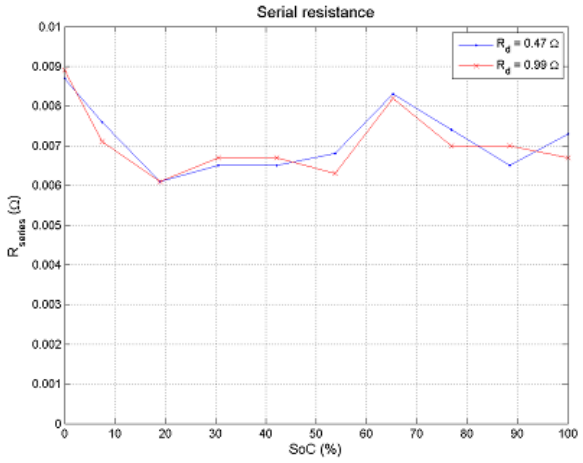

Figure 4.14. Series resistance [47]

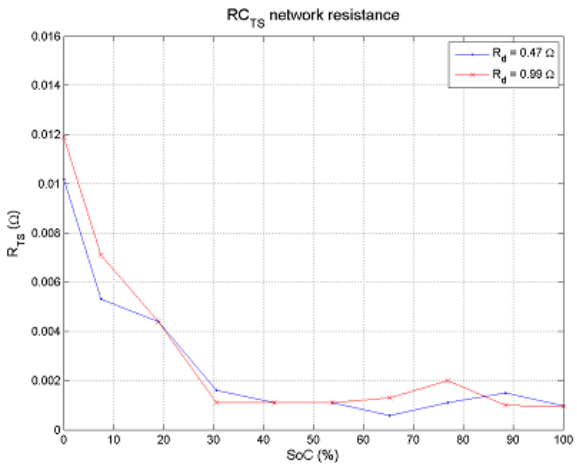

Figure 4.15. Resistance of RC_{TS} network [47]

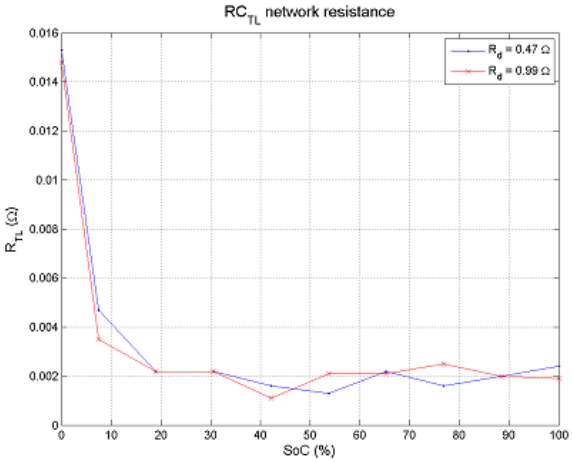

Figure 4.16. Resistance of RC_{TL} network [47]

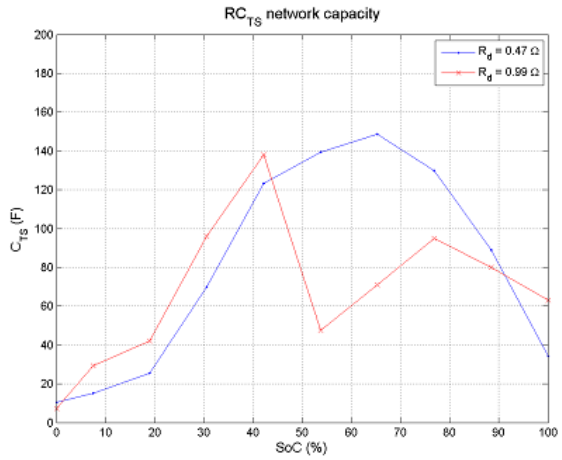

Figure 4.17. Capacitance of RC_{TS} network [47]

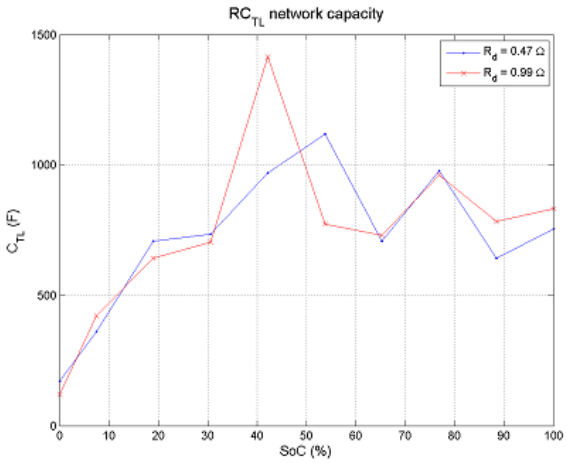

Figure 4.18. Capacitance of RC_{TL} network [47]

4.5.2 Induction Motor

The induction motor is an AC electric machine converting electrical power into mechanical power. Stator of the motor is made of electrical steel sheets to minimize hysteresis and eddy current losses. The stator windings are distributed sinusoidally around the stator and are placed in slots. The rotor is also made of electrical steel sheets. The rotor winding can be wounded or made as a squirrel-cage. The air gap between stator and rotor must be as small as possible to minimize leakage flux. The torque is produced by interaction between the magnetic flux produced by the stator windings and the current of the rotor windings. The rotor current is induced in the rotor winding by the rotating magnetic field in the air gap. Thus the induction motor is also known as a rotating transformer [47].

The construction of the three-phase induction motor with squirrel-cage is simple as mentioned in the introduction of this section. On the other hand, mathematical description of the system is quite complex. To simplify the mathematical description, the following conditions are defined:

- Symmetrical stator windings
- Symmetrical rotor windings
- Invariable air gap
- Sinusoidal distribution of windings
- Without core losses
- Magnetic materials are operated in their linear region and has infinite permeability

To describe a quantity in the three-phase system, a space vector is used. Unlike phasors, space vectors are also applicable under dynamic condition [49]. The space vector can easily describe the field quantities distributed sinusoidally in the air gap. The resultant voltage, current and flux linkage space vectors are calculated as sums of products of instantaneous phase values and the winding orientations of every single phase.

A space vector of a physical quantity in three-phase system, under condition of sinusoidal distribution of winding, is described by equation (4.105).

$$\vec{i}_s(t) = K(i_a(t) \cdot e^{0j} + i_b(t) \cdot e^{\frac{2\pi}{3}j} + i_c(t) \cdot e^{\frac{4\pi}{3}j}) \tag{4.105}$$

Equation (4.106) is valid for three-phase connected power system

$$\vec{i}_a(t) + \vec{i}_b(t) + \vec{i}_c(t) = 0 \tag{4.106}$$

Substituting equation (4.106) into equation (4.105) we get

$$\vec{i}_s(t) = K(\frac{3}{2} i_a(t) + j\frac{\sqrt{3}}{2}(i_a(t) + 2i_b(t))) \tag{4.107}$$

If we separate real and complex parts of equation (4.107) and rewrite this equation in a matrix form with an index α for the real part and β for the imaginary part we get equation (4.108). This transformation is called Clarke transformation, or α, β transformation. The transformation is shown in Fig. 4.19.

$$\begin{bmatrix} i_\alpha(t) \\ i_\beta(t) \end{bmatrix} = K \begin{bmatrix} \frac{3}{2} & 0 & 0 \\ \sqrt{3} & \frac{\sqrt{3}}{2} & 0 \end{bmatrix} \cdot \begin{bmatrix} i_a(t) \\ i_b(t) \\ i_c(t) \end{bmatrix} \tag{4.108}$$

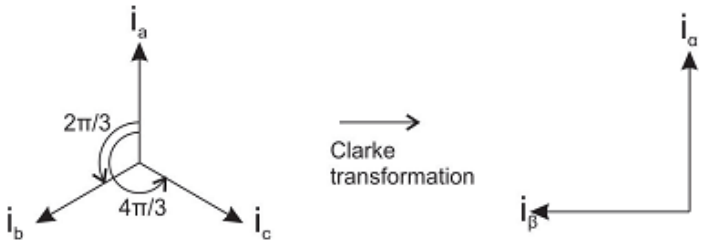

Figure 4.19. Clarke transformation [47]

The α, β is a reference frame fixed with the stator. In general, α, β reference frame can be transformed into rotating reference frame rotating by relative angular speed ω, as shown in Fig. 4.20.

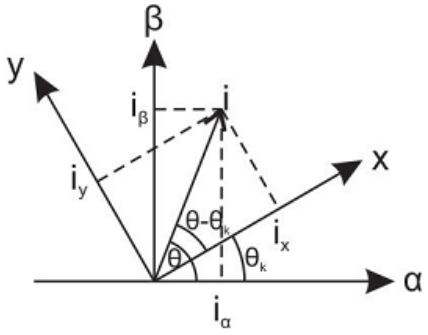

Figure 4.20. Park transformation [47]

The transformation from α, β reference frame into rotating reference frame is described by equation (4.109).

$$\begin{bmatrix} i_x(t) \\ i_y(t) \end{bmatrix} = \begin{bmatrix} \cos\Theta & \sin\Theta \\ -\sin\Theta & \cos\Theta \end{bmatrix} \cdot \begin{bmatrix} i_\alpha(t) \\ i_\beta(t) \end{bmatrix} \tag{4.109}$$

The relation between a space vector of a quantity $\vec{x}^k$ in the reference frame rotating by angular speed ω_k and space vector of the same quantity in the α, β reference frame $\vec{x}^s$ are expressed as follows in equation (4.110).

$$\vec{x}^k = \vec{x}^s \cdot e^{j\vartheta_k} \tag{4.110}$$

Using space vector, the circuit equations of stator and rotor circuits are described by equations (4.111) and (4.112) according to Kirchhoff's circuit law.

$$\vec{u}_s^k \cdot e^{j\vartheta_k} = R_s \cdot \vec{i}_s^k \cdot e^{j\vartheta_k} + \frac{d}{dt}(\vec{\psi}_s^k \cdot e^{j\vartheta_k}) \tag{4.111}$$

$$\vec{u}_r^k \cdot e^{j(\vartheta_k - \vartheta)} = R_r \cdot \vec{i}_r^k \cdot e^{j(\vartheta_k - \vartheta)} + \frac{d}{dt}(\vec{\psi}_r^k \cdot e^{j(\vartheta_k - \vartheta)}) \tag{4.112}$$

Where $\vec{u}_s^k$ is the space vector of stator voltage, R_s is the stator phase resistance, $\vec{i}_s^k$ is the space vector of stator current and $\vec{\psi}_s^k$ is the space vector of stator flux linkage. The same principle in equation (4.111) applies to the rotor equation (4.112). The index k denotes a general reference frame rotating by angular speed ω_k.

By differentiating the last elements in both equations we get equations (4.113) and (4.114).

$$\vec{u}_s^k = R_s \vec{i}_s^k + \frac{d\vec{\psi}_s^k}{dt} + j\omega_k \vec{\psi}_s^k \tag{4.113}$$

$$\vec{u}_r^k = R_r \vec{i}_r^k + \frac{d\vec{\psi}_r^k}{dt} + j(\omega_k - \omega)\vec{\psi}_r^k \tag{4.114}$$

The stator and rotor flux linkages are expressed by space vector equations (4.115) and (4.116).

$$\vec{\psi}_s^k = L_s \vec{i}_s^k + L_m \vec{i}_r^k \tag{4.115}$$

$$\vec{\psi}_r^k = L_m \vec{i}_s^k + L_r \vec{i}_r^k \tag{4.116}$$

These equations describe stator and rotor circuit in a general reference frame rotating by rotation speed ω_k. Some of the frequently used reference frames and their rotation speeds are listed in table 4.2.

Reference Frame	Marking	Rotation Speed
Reference frame fixed with stator	α, β	$\omega_k = 0$
Reference frame fixed with rotor	k, l	$\omega_k = \omega$
Reference frame fixed with rotor magnetic flux linkage	d, q	$\omega_k = \omega_1$

Table 4.2. Reference frame overview [47]

In our model, the reference frame fixed with the rotor magnetic flux linkage is used. The circuit equations in the d, q reference frame are expressed in matrix form as shown in (4.117) and (4.118).

$$\begin{bmatrix} u_{sd} \\ u_{sq} \end{bmatrix} = R_s \begin{bmatrix} i_{sd} \\ i_{sq} \end{bmatrix} + \frac{d}{dt} \begin{bmatrix} \psi_{sd} \\ \psi_{sq} \end{bmatrix} + \omega_s \begin{bmatrix} 0 & -1 \\ 1 & 0 \end{bmatrix} \begin{bmatrix} \psi_{sd} \\ \psi_{sq} \end{bmatrix} \tag{4.117}$$

$$\begin{bmatrix} u_{rd} \\ u_{rq} \end{bmatrix} = R_r \begin{bmatrix} i_{rd} \\ i_{rq} \end{bmatrix} + \frac{d}{dt} \begin{bmatrix} \psi_{rd} \\ \psi_{rq} \end{bmatrix} + \omega_r \begin{bmatrix} 0 & -1 \\ 1 & 0 \end{bmatrix} \begin{bmatrix} \psi_{rd} \\ \psi_{rq} \end{bmatrix} \tag{4.118}$$

Where the indexes d and q represent projections of the space vector to the d and q axis of the reference frame. The stator and rotor magnetic flux linkage equations in d, q reference frame are expressed in matrix form as shown in (4.119).

$$[\,\psi_{dq}\,] = [\,M\,]\,[\,i_{dq}\,] \tag{4.119}$$

Where the $[\,\psi_{dq}\,]$ is the vector of stator and rotor magnetic flux linkage (4.120),

$$[\,\psi_{dq}\,] = \begin{bmatrix} \psi_{sd} \\ \psi_{sq} \\ \psi_{rd} \\ \psi_{rq} \end{bmatrix} \tag{4.120}$$

$[\,M\,]$ is the matrix of Self and Mutual inductances defined in (4.121)

$$[\,M\,] = \begin{bmatrix} L_s & 0 & L_m & 0 \\ 0 & L_s & 0 & L_m \\ L_m & 0 & L_r & 0 \\ 0 & L_m & 0 & L_r \end{bmatrix} \tag{4.121}$$

and $[\, i_{dq} \,]$ is the vector of stator and rotor currents as described in (4.122).

$$[\, i_{dq} \,] = \begin{bmatrix} i_{sd} \\ i_{sq} \\ i_{rd} \\ i_{rq} \end{bmatrix} \tag{4.122}$$

Stator and rotor currents are expressed from the equation (4.119) by left multiplication of the equation by inverse matrix of Self and Mutual inductances. This results in equation (4.123).

$$[\, i_{dq} \,] = [\, M \,]^{-1} [\, \psi_{dq} \,] \tag{4.123}$$

If the rotor is a squirrel-cage type, then rotor voltage is equal to zero as described in (4.124).

$$\begin{bmatrix} u_{rd} \\ u_{rq} \end{bmatrix} = \begin{bmatrix} 0 \\ 0 \end{bmatrix} \tag{4.124}$$

As space vector of rotor magnetic flux linkage is aligned with d axis of d, q reference frame, ψ_{rq} is considered as $\psi_{rq} = 0$ and $\frac{d\psi_{rq}}{dt} = 0$. The torque of the induction motor is the sum of torques produced by windings of both axis d and q. The torque produced by d-axis winding is applied in counter-clockwise direction and is considered as positive value. This torque is expressed in equation (4.125).

$$M_{rd} = \frac{3}{2} \cdot p \cdot \psi_{rq} \cdot i_{rd} \tag{4.125}$$

Similarly, the torque produced by q-axis winding is applied in clockwise direction and is considered as negative. This torque is expressed in equation (4.126).

$$M_{rq} = -\frac{3}{2} \cdot p \cdot \psi_{rd} \cdot i_{rq} \tag{4.126}$$

The resulting torque is the sum of these two torques as described in equation (4.127).

$$M_{em} = M_{rd} + M_{rq} \tag{4.127}$$

By substitution of equations (4.125) and (4.126) into (4.127) we get equation (4.128).

$$M_{em} = \frac{3}{2} \cdot p(\psi_{rq} \cdot i_{rd} - \psi_{rd} \cdot i_{rq}) \tag{4.128}$$

By another substitution of equation (4.119) into equation (4.128) for ψ_{rd} and ψ_{rq} we get equation (4.129).

$$M_{em} = \frac{3}{2} \cdot p \cdot L_m(i_{sq} \cdot i_{rd} - i_{sd} \cdot i_{rq}) \tag{4.129}$$

The relation between electrical and mechanical angular velocity is shown in equation (4.130).

$$\omega_{el} = p \cdot \omega_{mech} \tag{4.130}$$

The last equation of the equation system is the equation of motion (4.131) [49][50][51].

$$M_{el} - M_{load} = J \cdot \frac{d\omega_{mech}}{dt} \tag{4.131}$$

4.5.3 Power Electronics

A power converter from SEVCON company is used in Škoda Rapid EV and also in the laboratory in Roztoky. The type of the power converter is Gen4 size 8. The main function of Gen4 size 8 is to control the power to 3-phase squirrel-cage AC induction or PMSM motors in electric vehicles. Four-quadrant control of motor torque and speed (driving and braking torque in the forward and reverse directions) is allowed without the need for directional contactors. Regenerative braking is used to recover kinetic energy which is converted into electrical energy for storage in the battery.

In a traction application control commands are made by the driver using a combination of digital controls (direction, foot switch, seat switch, etc.) and analog controls (throttle and foot brake). The controller provides all the functions necessary to validate the driver's commands and to profile the demand for speed and torque according to stored parameters.

Throttle inputs can be configured as speed or torque demands with throttle-dependent speed limits: in either case, a torque demand is continually calculated to take account of preset limits on the level and rate-of-change of torque. The torque demand is used to calculate current demands; that is, the controller calculates what currents will be required within the motor to generate the required torque. There are two distinct components of the current,d, q axis currents, which control current flow in the motor.

Measured phase currents and current demands i_d and i_q, the $d-q$ axis currents, are used as part of a closed-loop control system to calculate the necessary voltage demands for each phase of the motor. Voltage demands are then turned into PWM demands for each phase using the Space Vector Modulation (SVM) technique. SVM ensures optimum use of the power semiconductors [52].

The power converter is using Field Oriented Control (FOC) for control currents i_d and i_q. The principle of this control is to measure and decompose of the instantaneous stator current into two components:

- flux current i_d
- torque producing current i_q

This decomposition guarentees correct orientation of the stator current vector with respect to flux linkage. The control algorithm can oriente on control of flux in stator or in rotor. Based on this the control strategy can be divided into:

- Rotor Flux Oriented Control (R-FOC)
- Stator Flux Oriented Control (S-FOC)

The next division is into direct and indirect control. Based on the number of control strategy options is not possible to detect which version is used in the SEVCON Gen4 power converter. Each producer has also own developed modifications of the possible control algorithm and this know-how is not public. Based on this is necessary to simplify a model into measured efficiency maps of power converter and induction motor. This simplification is deeply explained in the next section.

4.5.4 Powertrain model simplification

The dynamic model of the powertrain described in the previous sections so far is useful to observe certain operation states and transition between these states. The accuracy of the dynamic model goes hand in hand with its complexity, so it cannot be used in mathematical iterative methods. These methods are used in optimizing. To minimize

the calculation time of an iteration, the model of the powertrain has to be simplified. An efficiency map is a model describing efficiency of energy conversion in all operation states of the powertrain. The efficiency map is used in optimizing method, where energy consumption is observed and minimized. It fulfils the requirement of low calculation time, however, it only describes efficiency of energy conversion in steady-state. Energy conversion process in powertrain is displayed in figure 4.21.

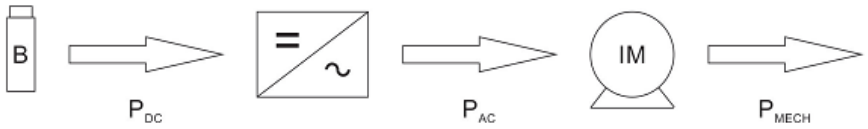

Figure 4.21. Power conversion in powertrain [40]

The efficiency of the induction motor is calculated as

$$\eta_{im} = \frac{P_{mech}}{P_{AC}} \tag{4.132}$$

the efficiency of the power converter is calculated as

$$\eta_{pc} = \frac{P_{AC}}{P_{DC}} \tag{4.133}$$

and the efficiency of the powertrain is calculated as:

$$\eta_{sys} = \eta_{im} \cdot \eta_{pc} = \frac{P_{mech}}{P_{DC}} \tag{4.134}$$

The result measured on the laboratory test bench with TEM112 induction motor and SEVCON Gen4 power converter is shown in the Fig. 4.22. Up to 1000 rpm is the efficiency in range 40% - 60%. For the higher speed increases the efficiency up to approx. 90% with the peak of 93%. The measurement limits are on the limits of power converter and induction motor. The maximal torque is approx. 170 Nm and the maximal speed 4500 rpm.

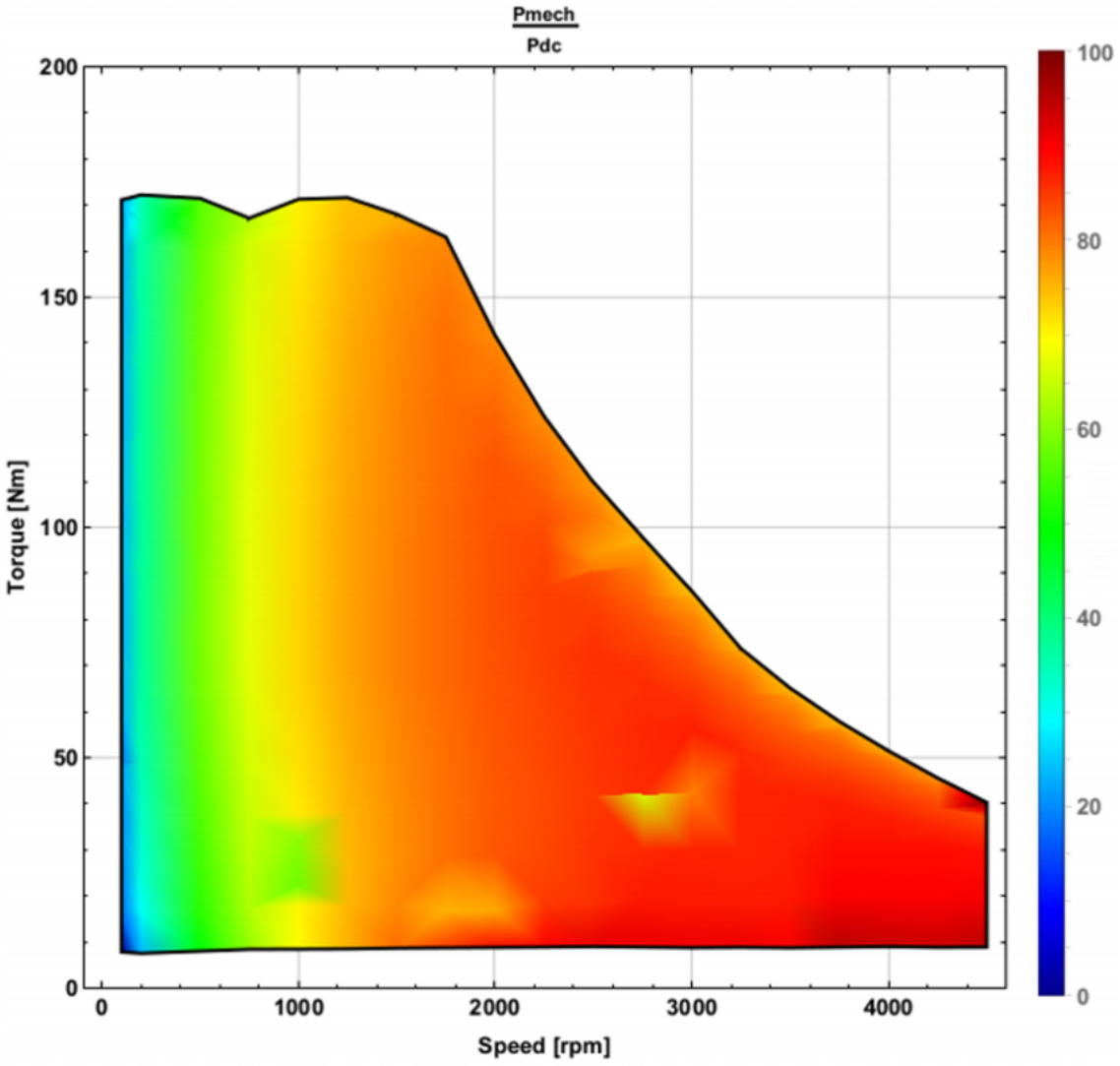

Figure 4.22. Powertrain efficiency map

Chapter 5
Simulation System

This chapter deals with a description of the hardware laboratory and about software and hardware equipment used for automated driving cycle simulation and measurement.

5.1 Hardware Laboratory in VTP Roztoky

Science and Technology Park in Roztoky town has been founded in the year 2012. The place is situated on the Nord-west of Prague 5.1. Main field of research works is focused onto the automotive techniques based on advanced internal combustion engines (ICE) and progressive electric (ED) and hybrid drives (HD) technology. One of the special laboratories is focused on electric and hybrid-electric drives measurement and development. For this purposes is laboratory equipped by electric power supplies and by dynamometric testing bench [53].

Figure 5.1. View of the Science and Technology Park in Roztoky

Testing bench is designated for AC and DC supplied powertrains. For induction motor measurement special power source with secondary tap-changing transformer is used. This transformer enable to supply very spread spectrum of induction motors designated for automotive applications. Similarly for other types of motors, like synchronous permanent magnets motor or brush-less DC motors, supplied via DC/AC inverter, battery simulator for supplying of this assembly is designated. Like frequency converter supplying dynamometer so battery simulator operates in „active front-end“mode. Such arrangement enables bi-directional energy transmission (from mains to the machine and from the machine to the mains in case of recuperation regime). Dynamometer from VUES company is equipped by asynchronous machine with rotary stator. Mechanical torque is measured by means of strain-gauge-bridge.

Block diagram of the whole testing bench is shown in the figure. 5.2. Dynamometer control system is equipped by basic controlling PC. This PC via RS 485 lines controls converters supplying dynamometer and testing induction motor. Torque and revolutions are measured on the dynamometer by means of separated sensors. Electrical parameters – tested motor supply voltages, currents and powers are measured and calculated by YOKOGAWA precision power analyser. Measured and calculated data are transmitted via Ethernet line to the control computer. For data collecting, calculating and plotting ASMOT programme is used. Application programme ASMOT is firmware specialized for routine measurement of broad spectrum of induction motors characteristics. The main parameters of the dynamometer are in a table 5.1.

Parameter	Value	Unit
Maximal AC voltage	400	V
Maximal AC current	147	A
Maximal AC power	85	kW
Maximal speed	6000	rpm

Table 5.1. VUES dynamometer - parameters

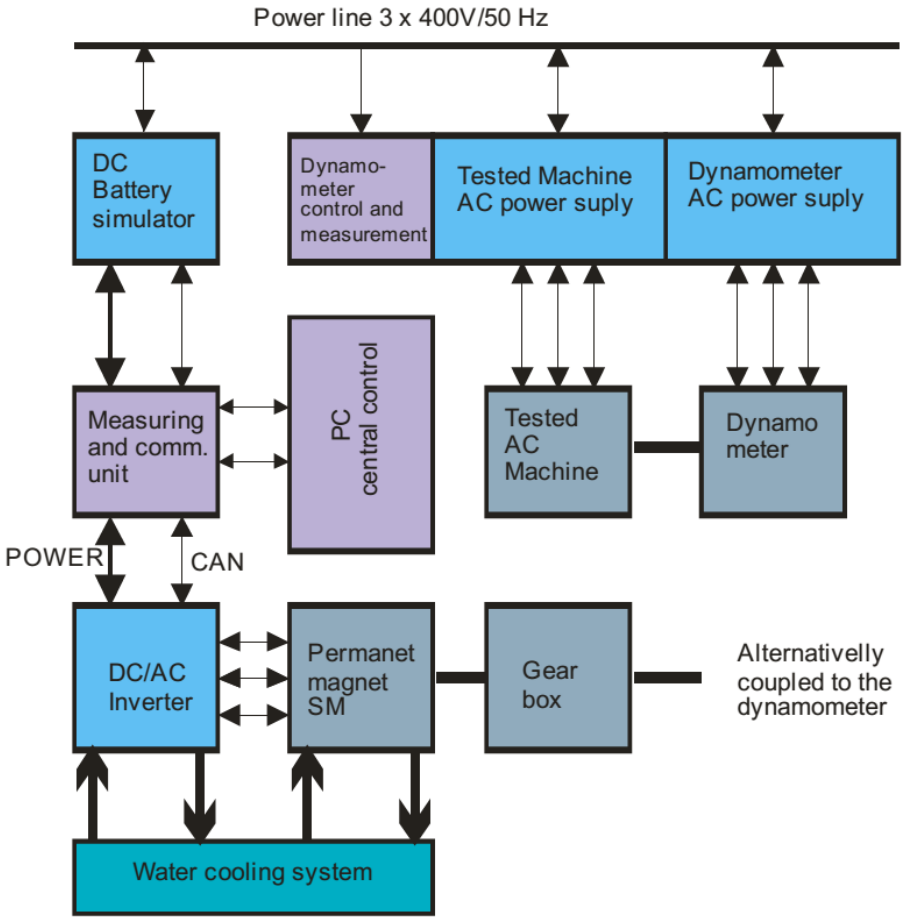

Figure 5.2. Block diagram of automotive electric powertrain testing bench

The picture of the YOKOGAWA and the PC with ASMOT is shown in the figure 5.3

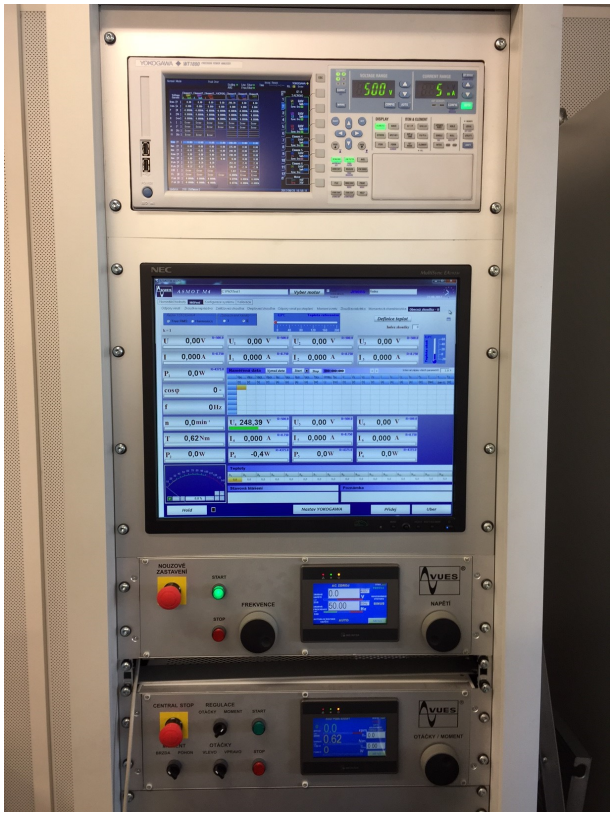

Figure 5.3. YOKOGAWA and PC with ASMOT

5.2 Battery Simulator

The battery simulator used in the laboratory in Roztoky is a product of AVL company. Basically it is a DC source with the calculation of a battery model and setting of the output voltage. The parameters of the battery simulator are presented in the table 5.2.

The block diagram is shown in the Fig. 5.4. The 3-phase supply voltage is connected to AC/DC rectifier. The output voltage of this rectifier is 810 V. This voltage is connected to the chopper. The chopper can operate in two modes:

- Step-Down (IGBT1 is used)
- Step-Up (IGBT2 is used)

Parameter	Value	Unit
Maximal DC output voltage	800	V
Maximal DC output current	600	A
Maximal DC output power	160	kW

Table 5.2. AVL battery simulator - parameters

The control algorithm controls the voltage on the output in accordance with the output of the included battery model. Step-Down mode is used when the energy from the 'battery' is needed and the Step-Up mode is used during recuperation of the energy back into the 3-phase network. The both converters are not direct in the laboratory but in a separate room. PDSB/PDU unit is located direct in the laboratory (see figure 5.5) and the output from chopper is conneted to this unit.

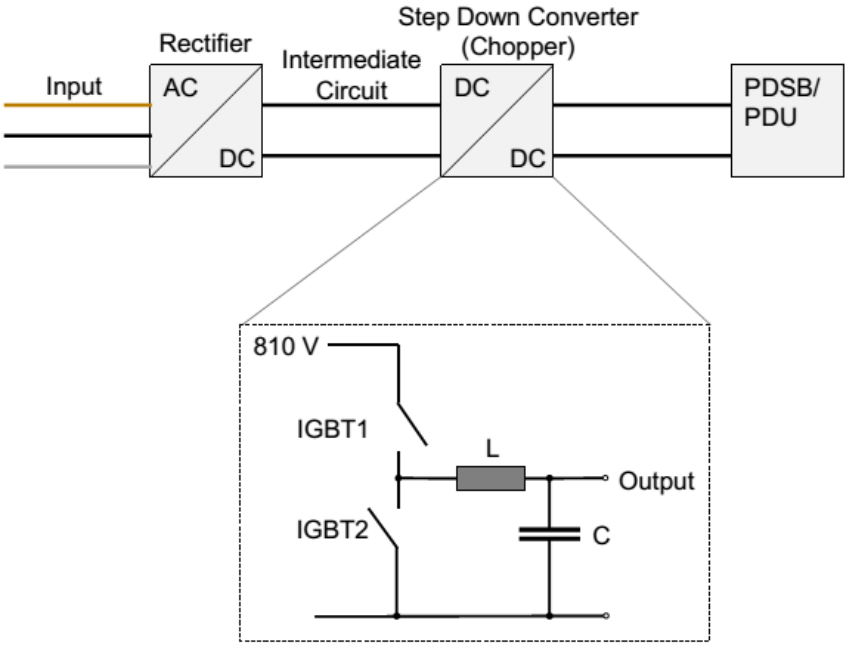

Figure 5.4. Block diagram of battery simulator [54]

Figure 5.5. PDU unit of the battery simulator

For the control and parametrization of the battery simulator a AVL Workstation PC is used. This PC comunicates with the battery simulator via TCP/IP protocol. In this PC is installed an application which enables:

- Battery model selection
- Battery model parametrization
- Control of battery simulator
- Energy consumption calculation

The battery simulator can use 5 possible battery models. The models are explained bellow.

U-Ramp model It is a constant voltage source independent on the current. Normally used only for commisioning and testing. The schematic is shown in the Fig. 5.6.

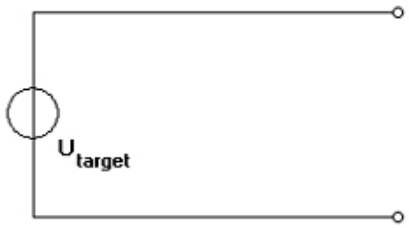

Figure 5.6. U-Ramp model [54]

Simple model Only internal resistance is simulated. There is R_0 and U_0 configurable. This model allows temperature and battery state-of-charge (SOC) calculation. The schematic is shown in the Fig. 5.7.

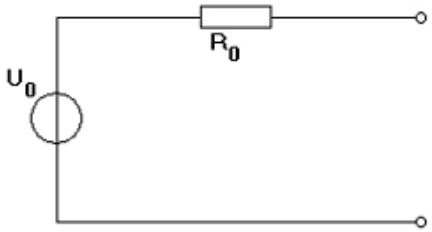

Figure 5.7. Simple model [54]

Advanced model It is a second order battery model with resistances and capacitances. It is much more complex model. Basically all battery models can be converted into this type of model. This model is used for the testing in the laboratory. The parameters of the model are from the chapter Battery Pack. The schematic is shown in the Fig. 5.8.

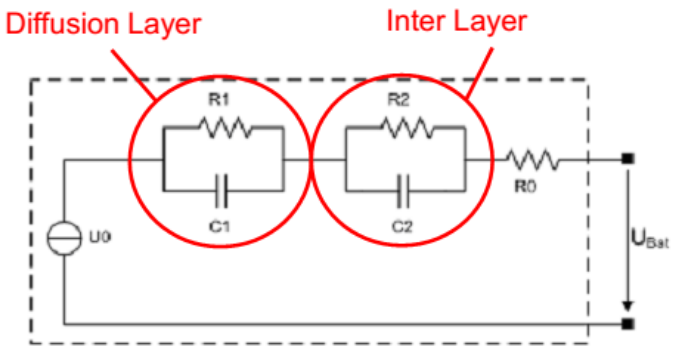

Figure 5.8. Advanced model [54]

External model It is a battery model from external source (via CAN bus). The battery simulator supports only U-Ramp and Simple model types. Temperature and state-of-charge (SOC) is calculated only by external source. If the communication is broken, then the battery simulator takes a default value. The schematic is shown in the Fig. 5.9.

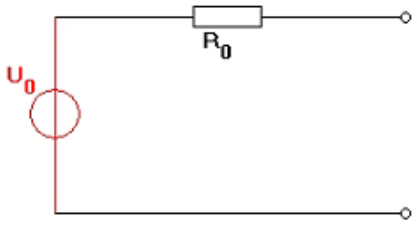

Figure 5.9. External model [54]

I-Ramp model It is a constant current source. It is used only for commisioning, there is no direct U control. There is a danger of excessive voltage. The schematic is shown in the Fig. 5.10.

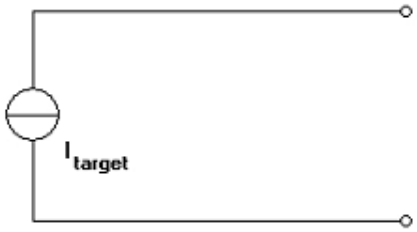

Figure 5.10. I-Ramp model [54]

5.3 Electric Drive

As was presented in the section 4.5 the electric powertrain has the same configuration as in Škoda Rapid EV prototype. Škoda Rapid EV is using an water cooled induction motor (IM) TEM112 from EM Brno s.r.o. company. The main parameters are in a table bellow. The picture of the test bench with induction motor is shown in the figure 5.11.

Parameter	Value	Unit
Nominal voltage	180 Y	V
Nominal torque	90	Nm
Nominal speed	2900	rpm
Nominal power	28	kW
Weight	68	kg

Table 5.3. TEM112 - parameters

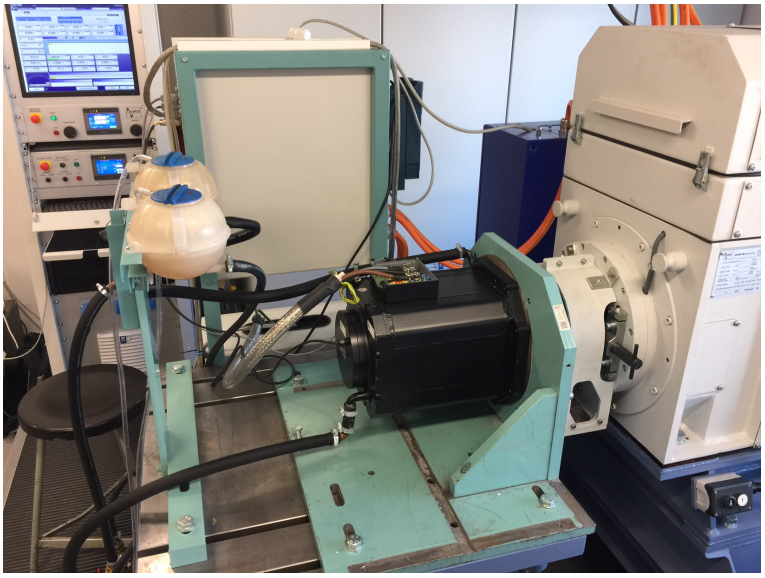

Figure 5.11. Test bench with TEM112 motor

The other part is an electric power converter (EPC) SEVCON Gen4 size 8 (see figure 5.12) from SEVCON company. The main parameters are in a table 5.4.

Figure 5.12. Sevcon power converter with control and measurement unit

The EPC and IM are watter cooled with a cooling system in the laboratory. The cooling circuit is connected via a heat exchanger to the common bulding cooling system.

Parameter	Value	Unit
Maximal DC voltage	400	V
Peak power output	100	kW
Continuous power output	60	kW

Table 5.4. SEVCON Gen4 size 8 - parameters

5.4 Control System

The simulation system has to simulate EV drive along a track with a known altitude according to a predefined speed of the vehicle. The vehicle speed profile and the profile of the angle of inclination are the main inputs for the control system. There has to be also a vehicle dynamic model which produces a load for the electric drive. As the control platform dSpace single board DS1103 was selected. The dSpace DS1103 (see Fig. 5.13) is a controller board used for rapid control prototyping. The control model is developed in MATLAB/Simulink programmable environment. Based on the developed model generates Simulink C code which is compiled and uploaded into the dSpace. A part of the control system was created by my student Jan Kacetl as a part of his diploma thesis [40].

Figure 5.13. dSpace DS1103 [55]

dSpace DS1103 is a part of the dSpace AutoBox system with Ethernet interface for the comunication with PC. AutoBox needs only 12 V power supply and can be mounted direct in a vehicle if a testing in vehicle is needed. The AutoBox is shown in the Fig. 5.14.

Figure 5.14. dSpace AutoBox

The communication schematic is shown in the Fig. 5.15. The main part is dSpace DS1103 which controls SEVCON via CAN bus and dynamometer via RS-232. On the

CAN bus is connected also a PC using USB/CAN interface. The CAN bus is using a CANOpen protocol and RS-232 is using own developed protocol.

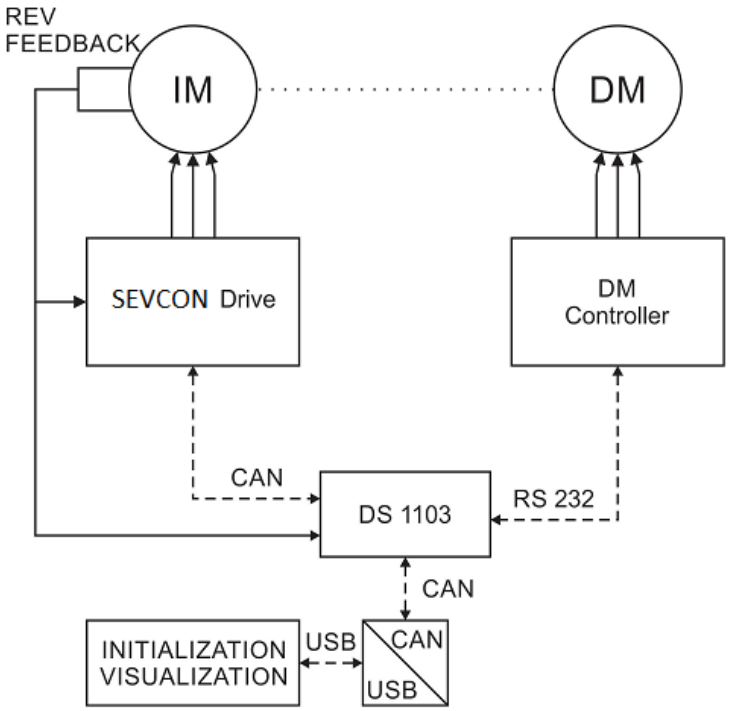

Figure 5.15. Schematic of communication

5.4.1 Communication Protocols

CANOpen is a CAN-based higher-layer protocol and device profile which simplifies the development of control system by standardized communication objects and device structure. CANOpen supports direct access to device parameters and transmission of time-critical process data. Every communication object is associated with one or more identifiers called Communication Object Identifier (COB-ID) which defines implicitly its priority on bus. CANOpen defines all communication objects and information of their properties and functions. These objects are stored in Object Dictionary (OD). The OD is used as an interface between application and device. The messages and their properties are presented in a table 5.5.

RS-232 is an asynchronous serial bus. The RS-232 standard defines how to transmit certain bit sequence, however, it does not define higher communication layers. The data length is not limited. The data bits are transmitted in order from the LSB to the MSB. As the communication is asynchronous, a synchronization of the slave must be done before data transmission begins. It is done by synchronization message sent by master.

Parameter	Value
Speed	19200 bit/s
Data length	8 bits
Parity bit	No
Number of stop bits	1 bits

Table 5.6. RS-232 communication settings

Message	ID	Signal	Start bit	Length	Factor	Offset
sevcon_NMT	0x0	NMT_Command	0	8	1	0
		Node_ID	8	8	1	0
sevcon_PDO1_R	0x202	sevcon_ControlWord	0	16	1	0
		sevcon_TargetTorque	16	16	1	0
sevcon_PDO1_T	0x291	sevcon_StatusWord	0	16	1	0
		sevcon_ActualTorque	16	16	1	0
vis_PDO1_T	0x202	vis_act_position	0	19	0.1	0
		vis_act_speed	19	9	0.1	0
		vis_dm_torque_dem	28	13	0.1	409.6
		vis_status_word	41	8	1	0
vis_PDO1_R	0x182	wt_status	0	8	1	0
		vis_lut_data_length	8	13	1	0
vis_PDO6_T	0x302	vis_lut_index	0	16	1	0
vis_PDO6_R	0x282	vis_lut_bp	0	19	0.1	0
		vis_lut_speed	19	9	0.1	0
		vis_lut_alpha	28	19	1e-5	1.5
		vis_lut_index	44	16	1	0
		vis_lut_upl_compl	60	1	1	0

Table 5.5. CANOpen communication protocol

The RS-232 communication protocol between dSpace as a master and the dynamometer as a slave is defined in a table 5.6. The master sends every 100 ms a message and the slave answers. The message is encrypted as follows. The first character is a star (0x2A in ASCII table), each of the following words is divided into two nibbles in HEX format. The nibble characters are represented by the corresponding ASCII code in HEX format. The message is supplemented with a control sum of all ASCII codes except the star, and coded in the same way as the rest of the message. The message types are defined in table 5.7.

Message name	Message composition
Synchronization message	[02][FF]
Switch to manual control	[02][01]
Switch to remote control	[02][02]
Switch to drive mode	[02][03]
Switch to brake mode	[02][04]
Set rampl	[03][05][Ramp]
Set torque reference	[04][06][T HB][T LB]
Status	[08][80][Control mode][DM mode][T HB][T LB][Ramp][Error]

Table 5.7. RS-232 communication protocol

The Control mode is 0 for manual control and 1 for remote control. The DM mode is 0 for drive mode and 1 for brake mode. The Error signal does not equal 0 in an error state. The torque reference signal is multiplied by 100 to increase the precision.

5.4.2 Control Algorithm of the Test Bench

The control algorithm is developed in MATLAB/Simulink programmable environment. The control system is using Stateflow toolbox which enables a development of the state

machines in a graphical way. The schematic of the control system is show in the Fig. 5.16. Then main part is the Main Logic block. This block reads the statuses from other blocks and send the commands for these blocks. The other blocks are responsible for sub-coordination of SEVCON power converter, Dynamometer and Visualization. These blocks are also directly connected to the Interface block. These block is responsible for communication on the CAN bus and on the RS-232. Each block except interface block consists of a state machine and a sequence. All block functionality is described later.

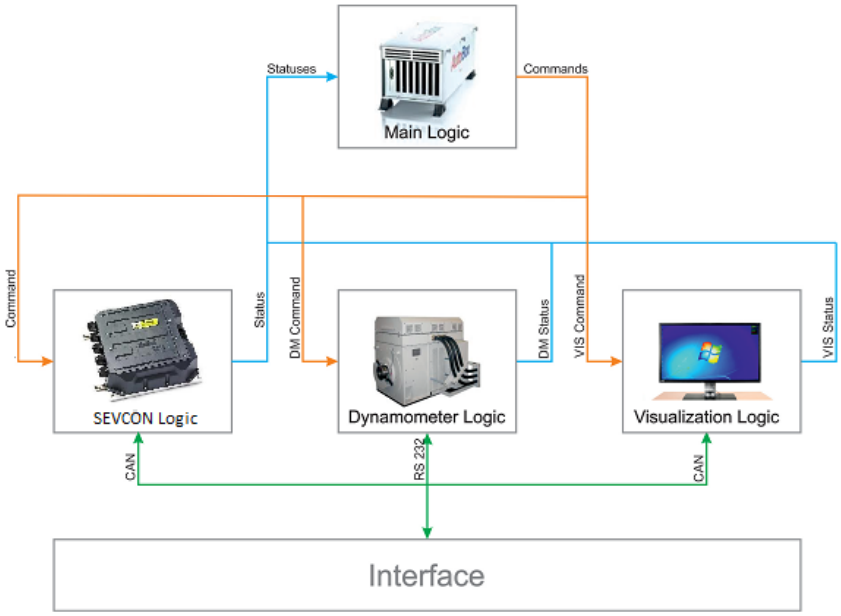

Figure 5.16. Schematic of control algorithm in dSpace

Main Logic

The Main Logic is the top layer control logic. This block reads the statuses from the other blocks (Sevcon, Dynamometer and Visualization) and sends the commands to these blocks. In the figure 5.17 is shown the structure the Main Logic. The structure includes 3 main sub-blocks:

- Logic
- Measu_Sequence
- Driver_Controller

The block Logic is a state machine which based on the status signals controls Sevcon, Dynamometer and Visualization blocks. The structure of the state machine is shown in the figure 5.18. The state machine starts in INIT state. In this state the block Measu_Sequence is disabled and the state machine waits until it receives *Initialized* status from all sub-coordinate blocks. If receives then goes to the MEASPREPAR state where sends the command to the block Visualization to initialize data. When the data are initialized, it continues to READY state. In this state waits the state machine on the *VisReadyToMeasure* status. If the state machine receives the status then it goes to the MEASUREMENT state. In this state the block Measu_Sequence is enabled and it sends the commands to all sub-coordinate blocks to start the driving cycle. After the driving cycle is finished (measu_complete flag is 1) and the electric machine speed is less than 30 rpm, the state machine goes to the STOPPED state where sends the commands for the stopping of electric machine and dynamometer rotating. After 2 seconds the state machine goes to DISABLE state and disables the

block Measu_Sequence and the Sevcon power converter. After 1 second continues the state machine back to MEASPREPAR state.

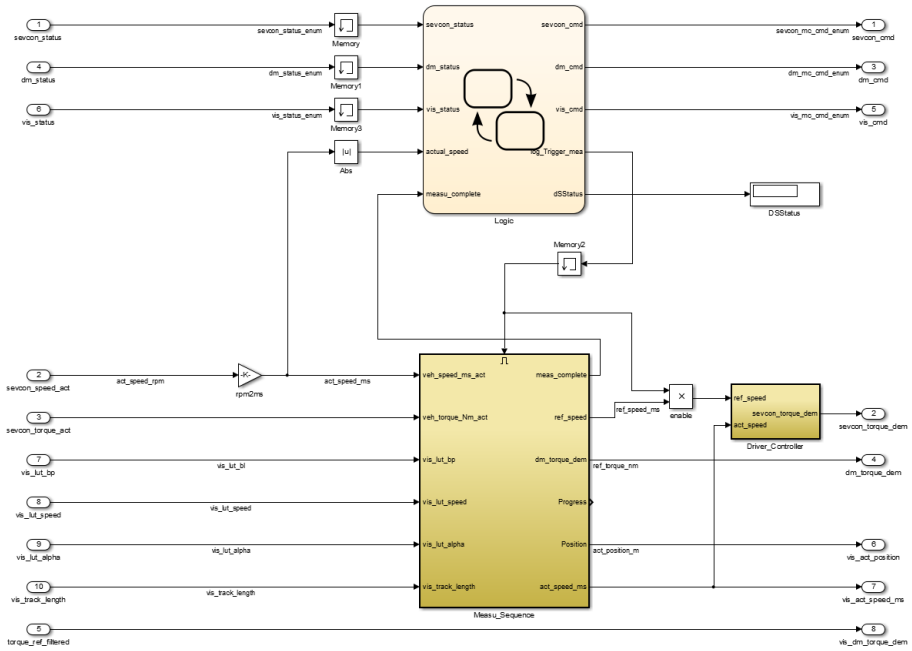

Figure 5.17. Main Logic block: structure

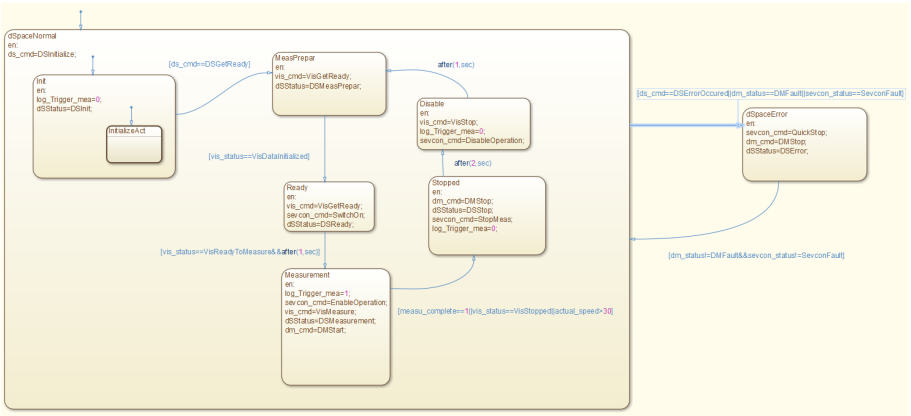

Figure 5.18. Main Logic block: state machine

The block Measu_Sequence is responsible for the calculation of the load torque which is sent to dynamometer and for the generation of the speed profile based on the received data. The structure of this block is shown in the figure 5.19. The block Torque_dem_calc includes a mathematical model of the vehicle. The mathematical model calculates from the actual speed of the vehicle, actual torque and the road angle alpha the load torque which is sent to the dynamometer. The block Driver_Controller includes a controller which simulates a driver of the vehicle. Based on the reference and actual vehicle speed generates the block a needed torque which is sent to Sevcon power converter.

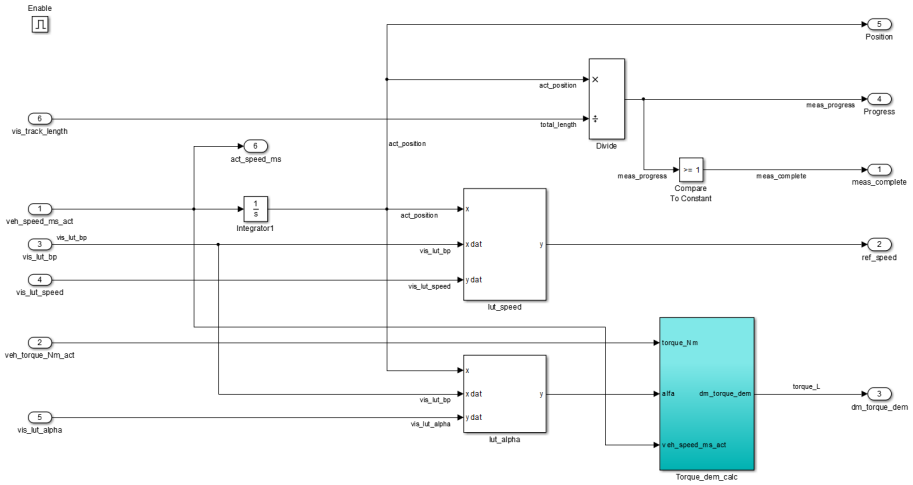

Figure 5.19. Main Logic block: measurement sequence

Sevcon Logic

The block Sevcon Logic is responsible for the control of the Sevcon power converter. The Sevcon power converter is controlled by a Control Word signal and a Target Torque signal. The both signals are a part of the sevcon_PDO1_R message. The structure of the block Sevcon Logic is shown in the figure 5.20. The block has 3 sub-blocks:

- Sevcon_Logic
- Sevcon_Sequence
- Sevcon_Torque_Calc

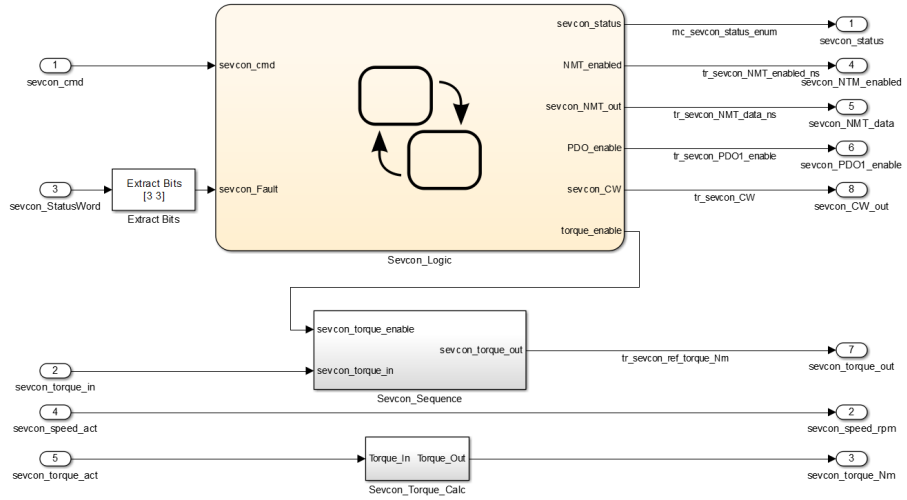

Figure 5.20. Sevcon Logic block: structure

The main part of the Sevcon Logic block is the sub-block Sevcon_Logic which contains a state machine. The state machine is shown in the figure 5.21. The state machine starts in the state INIT. After 1 second goes the state machine to the state PREOPERATIONAL and waits on the command *GoToOper* from the Main Logic. After receiving of this command goes the state machine to the state GOTOOPER and then to the OPERATIONAL state. This state includes other state machine which is responsible for the starting sequence of the Sevcon power converter. The first step is to send ControlWord = 6. After sending of this ControlWord the Sevcon goes to the READYTOSWITCHON state. In this state waits the state machine on the command from

Main Logic called *SwitchOn*. After receiveng of this command sends the state machine the ControlWord = 7 and waits on the command from Main Logic called *EnableOperation*. After receiving of the command EnableOperation sends the state machine the ControlWord = 15 and enables the Sevcon_Sequence block which enables the torque sending to the Sevcon power converter. The safe state of the Sevcon power convertor is the SWITCHONDISABLED state where the IGBT transistors in the Sevcon's brigde are closed (no current to the electric machine stator winding is applied).

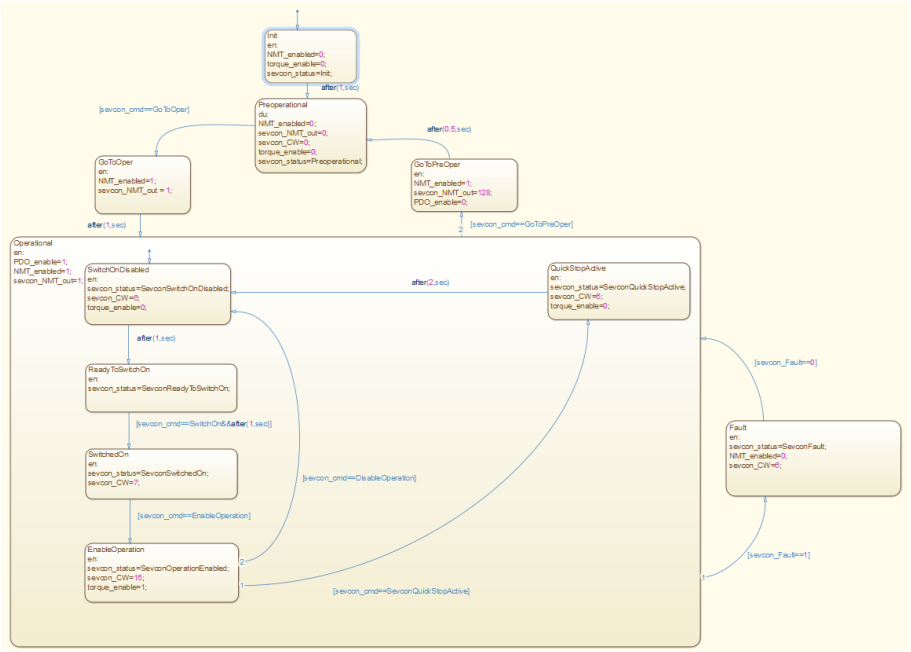

Figure 5.21. Sevcon Logic block: state machine

Dynamometer Logic

The block Dynamometer Logic is responsible for the control of the dynamometer. The dynamometer can be controlled on a panel via PLC or remotely using RS-232. The communication protocol is shown in the table 5.7. The structure of the block is shown in the figure 5.22.

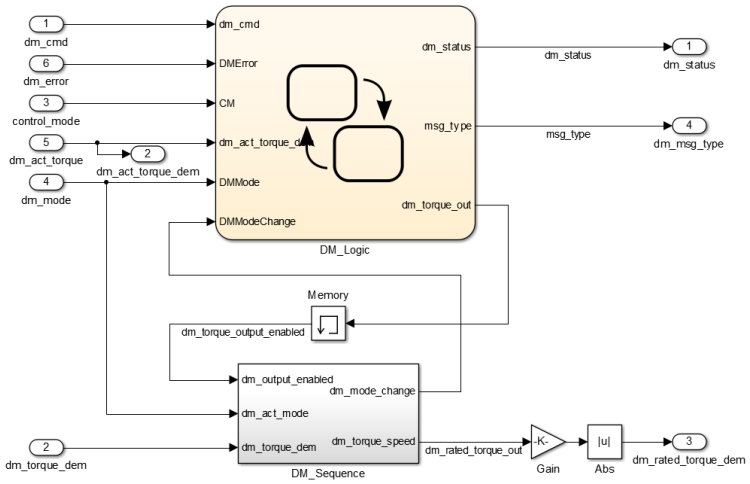

Figure 5.22. Dynamometer Logic block: structure

The block includes two main sub-blocks:

- DM_Logic
- DM_Sequence

The block DM_Logic includes a state machine which controls the dynamometer. The structure of the state machine in shown in the figure 5.23. The initial state is DMOFF state. In this state waits the state machine on the command DMStart from the Main Logic. After receiving the command *DMStart* sends the state machine to dynamometer a command for setting of a ramp and turns on the remote control. After reveiving of the confirmation from dynamometer goes the state machine to the DMON state. In this state is necessary to check the *DMModeChange* signal from DM_Sequence block and based on this signal generates the state machine a message for changing of the dynamometer mode. The dynamometer receives the reference torque as a absolute value and sending of the command *ChangeMode* generates positive or negative torque. From the safety reasons is necessary to push the button START on the dynamometer control panel. For the emergency case is there also a button STOP which turns off a power converter which controls the dynamometer. The normal turning off procedure is via a command *DMStop* received from the Main Logic.

The DM_Sequence block generates a torque value for dynamometer, detects negative or positive torque value and based on this generates a signal*dm_mode_change* (true or false).

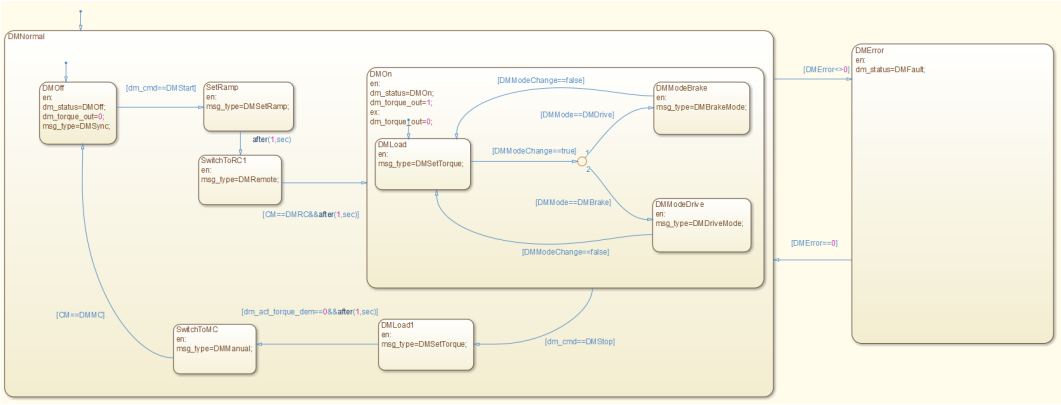

Figure 5.23. Dynamometer Logic block: state machine

Visualization Logic

The Visualization Logic block communicates with a PC and receives the data and the commands from PC. In the PC there is an MATLAB application where is possible to generate a driving cycle and upload via USB/CAN interface into the dSpace. The application is explained bellow in the next section. The structure of the Visualization Logic block is shown in the figure 5.24. The block contains the two sub-blocks:

- Vis_Logic
- Vis_Sequence

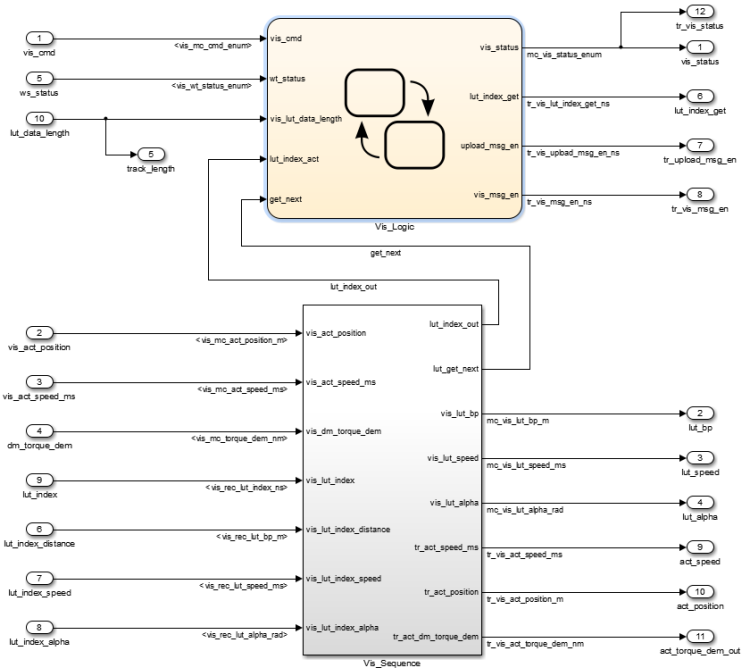

Figure 5.24. Visualization Logic block: structure

The block Vis_Logic contains as in the previous cases a state machine which is responsible for the data upload and visualization logic. The structure of the state machine is shown in the figure 5.25.

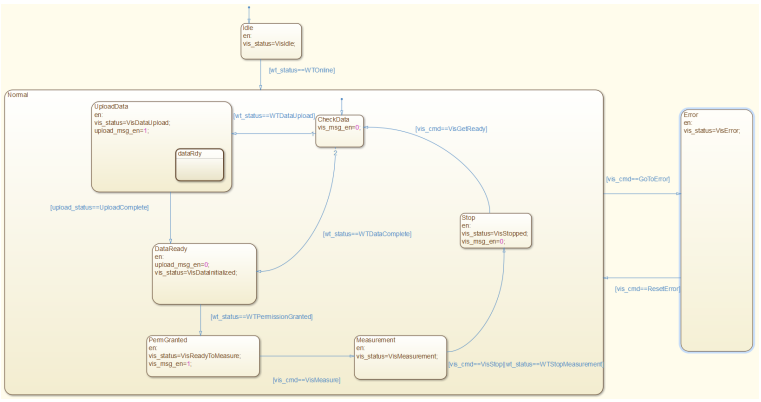

Figure 5.25. Visualization Logic block: state machine

The initial state is IDLE state. In this state waits the state machine on the command *WTOnline* from a PC where is an Electric Vehicle Optimizer Application (description of this application is in the next section). If the *WTOnline* command is received then goes the state machine to NORMAL state. This state includes a sub-state machine which starts in CHECKDATA state. The state machine disables the the visualization messages and waits for the command deciding whether to upload new data (*WTDataUpload* command) or to continue without upload (*WTDataComplete* command). If the command is *WTDataUpload*, then it goes to the UPLOADDATA state where is other sub-state machine responsible for the control and indexing of the data sent by the PC via CAN bus. If the data are uploaded then the sub-state machine continues with the state DATAREADY. In this state the sub-state machine waits on the user action. If the user enables the start of the measurement it continues with the PERMGRANTED

state and waits on the command *VisMeasure* from the Main_Logic. If the command *VisMeasure* is received then the sub-state machine continues with the MEASUREMENT state where is a driving cycle measured. After the driving cycle measurement is finished or the user cancel the measurement then it continues with the STOP state where the status of the Vis_Logic state machine is *VisStop*.

5.4.3 Electric Vehicle Optimizer Application

The Electric Vehicle Optimizer Application (EVO application) is an application developed in MATLAB envirenment. The application is divided into three main parts:

- Computer Part
- Graphical User Interface
- Data Gathering Part

The application is responsible for the track planning via Google maps or GPX measured data, for the vehicle parameters settings, for the optimization of the energy consumption calculation and for the visualization of the speed and position on the track during the driving cycle measurement of the test bench. This application was developed by my student Tomas Kacetl in his diploma thesis [40].

Computer Part

The computer part is responsible for all calculation on a given track and a vehicle. The computer part of the project has the following classes:

- @Drive: superclass defines the project and associates the other classes
- @Vehicle: defines the vehicle parameters and environment parameters
- @Track: gathers all data of the given track
- @Speed: specifying the speed profile and implements driver simulation controller
- @Energy: provides all calculation of the energy and time
- @Optim: implements an algorithm which is the main part of this thesis

As mentioned, the @Drive is the superclass of all computer classes, which represent the properties of this superclass. The vehicle, speed and track classes are defined as handle class, in order to have direct access to the vehicle, speed and track information in every class and keep the only instance of these objects. Handle represents a reference to an object and it is simply passed to every single class as a property to provide direct access and keep the object as unique.

Graphical User Interface

The issues of graphical user interface (GUI) in Matlab is described in many publications, however, almost all of them use a built-in graphic editor GUIDE, which is not optimal for larger-scale pro jects. Hence, advanced GUI technique is introduced to create a well-arranged and easily expandable GUI. These two demands lead to the use of object oriented programming, as in the case of computer classes. In the GUI, each of the classes represents one window with its graphical objects. To explain the technique, the simplest window of the object is selected. The window in figure 5.26 welcomes the user when the application is started up. There are only four graphical objects in the window, three buttons and a title. This window represents class @startup of the project in interface package folder +interface.

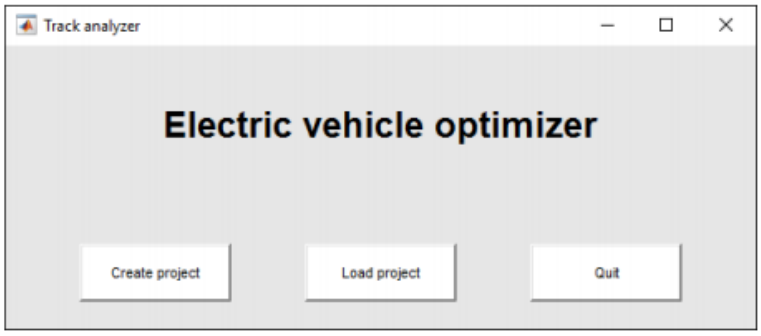

Figure 5.26. Start-up EVO application window

Each of the classes of GUI includes a set of typical properties to simplify the handling of the window:

- The **EVO** property specifies the project where the window belong. This superclass connects the interface to the computer classes.
- **position** determines where the windows appears when opened. Value of the position is either normalized or in pixels.
- **handles** is a structure with handles of every graphical object of the window and their children. The handle structure allows the developer comfortable changes of any object or property.
- **isOpened** represents open flag to determine whether the window is opened or not.

As in the case of properties, the classes of GUI have also characteristic methods. The input of the class method is always the handle of the object to allow the method to manipulate and access properties and to call other methods. The most important method is the constructor of the class, where the object is assigned to the project. The class also includes callbacks of the graphical objects.

As we can see in figure 5.27, the web page includes a few objects, and the HTML script is simple as well, however, the JS code is far more complicated. Google maps service distinguishes several interfaces to obtain different geographical data. To gather data sufficient for the calculation, the application uses Google Maps Directions API to design the track and collect GPS coordinates, and Google Maps Elevation API to collect elevation level of the track. Both of these interfaces use JavaScript Object Notation (JSON) for input and output, and the use of the interface is quite comfortable. Moreover, complete documentation is provided, including examples of use. The use of Google Maps API is, for free users, limited in number and length of the request. Therefore, the JS must split the data obtained from Direction API to more requests for Elevation API and compose the result back.

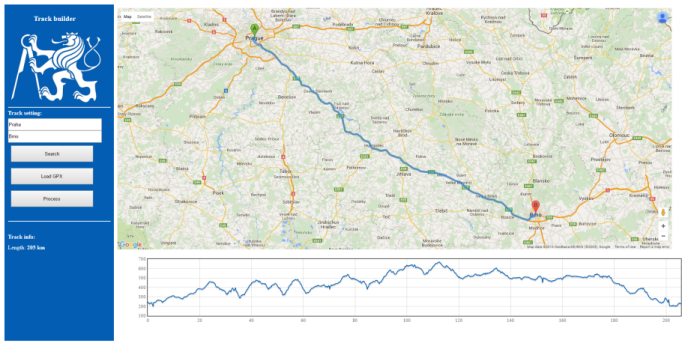

Figure 5.27. Implemented web application for track design

EVO Application Structure

The application is designed regularly to fit the character of the given task and the used solution. It provides creation of a project with a design of a track and a setting of parameters, optimization of a speed profile along the track, and simulation of a drive with direct visualization. Export of results and import of data is naturally included.

The project is created in 4 steps by classical wizard:

1. The name of the project and location is selected. In this step, the type of the project is also selected to determine the regular speed limit (city, countryside, highway). The speed limits are not a part of the data provided by Google for free.
2. The track is designed in the implemented web page including Google maps. This step also provides importing GPS coordinates of a track from gpx file in a standard form.

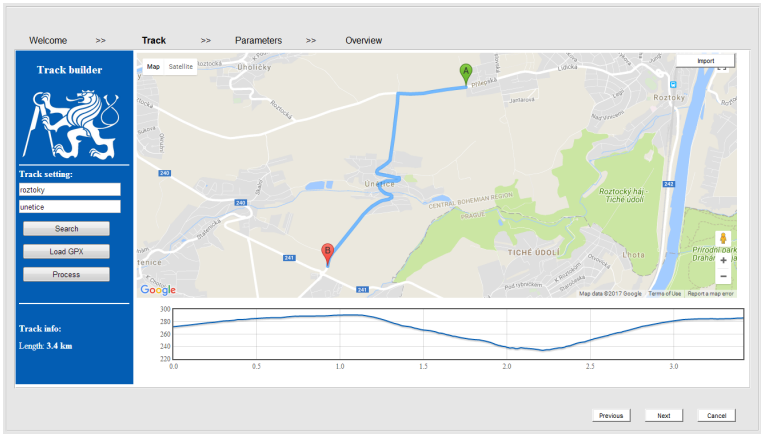

Figure 5.28. EVO application wizzard: Track

3. The complete parameters of vehicle and enviromental conditions are specified in this step, including the import of the efficiency map from Excel document.

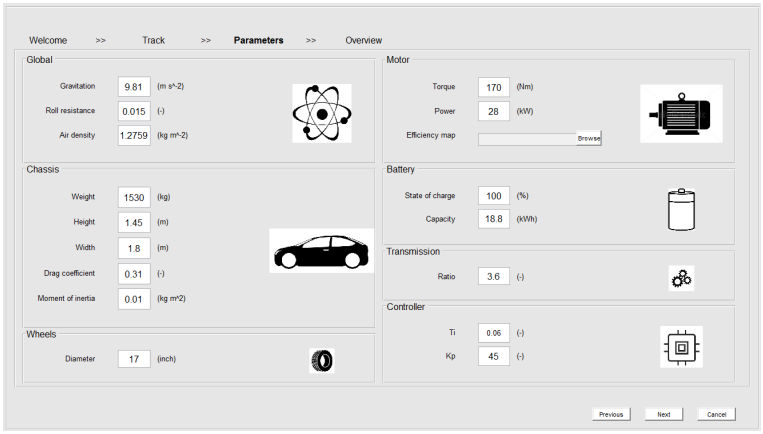

Figure 5.29. EVO application wizzard: Parameters

4. The last step shows the track, and the calculated speed limits. The limits can be imported from an Excel file. After clicking on the button Finish, the project file is created with the designed track and given parameters. The project is now opened in the project viewer window.

Figure 5.30. EVO application: Project viewer

The **project viewer** is the main part of the application. The figure 5.30 allows us to view the given track, run the desktop real-time simulation of the drive and observe the current track and motor values. The real-time simulation runs in the background in Simulink model based on introduced dynamic model calculation. Different speed profiles are chosen in the control panel on the left side of the viewer, in order to evaluate the results of different drive strategies obtained from the optimization algorithm, driver simulation or imported from file. The menu in the left upper corner provides common project operations as save, load and create new project. Moreover, the results of the simulation may be exported to csv. The option to change track, or parameters of the vehicle and environment is available only during the creation of the project for very simple reason. Once any of the project parameters is changed, the results given by optimization of the algorithm are invalid. This is apparent in the case of motor torque change. If the calculation of the optimal speed profile consider a value of torque, which would be subsequently reduced, the vehicle may no longer manage to pass the track with the prescribed speed profile. Therefore, changing any parameter makes the project worthless and it is recommended to create a new project, instead.

Interface

The data upload and visualization is provided by a real-time Simulink model running in the background. The real-time model allows two options:

- To run a real-time simulation of the vehicle motion without a possibility to connect to the test bench
- To run a real simulation on the test bench. Before the start of the simulation is necessary to upload the data into the dSpace.

The real-time is provided by a Real-Time Synchronization block from the Real-Time Windows Target library. The communication between EVO application and dSpace is provided by a CAN-USB interface and the Vehicle Network Toolbox. The CAN configuration block supports the interfaces from Kvaser and Vector companies. In this project a Kvaser Leaf Light device is used. The CAN message is received by CAN Receive block and unpacked by CAN Unpack block from the toolbox. The CAN Unpack block also supports the message specification by CAN database. The CAN message transmission is done by CAN pack and CAN Transmit blocks. In figure 5.31, the real-time Simulink model is displayed. In the left part, there are arrays to be uploaded. These arrays enter the function called subsystem. The subsystem is called

by CAN Receive block if a message is received. The subsystem unpacks the messages vis_PDO6_R and the vis_PDO1_R. An index of the arrays to be uploaded is obtained from the vis_PDO6_R. The data from the vis_PDO1_R is visualized. The data to be uploaded is then packed as vis_PDO6_T and sent. The *WTStatus* and data length are packed and sent as vis_PDO1_T.

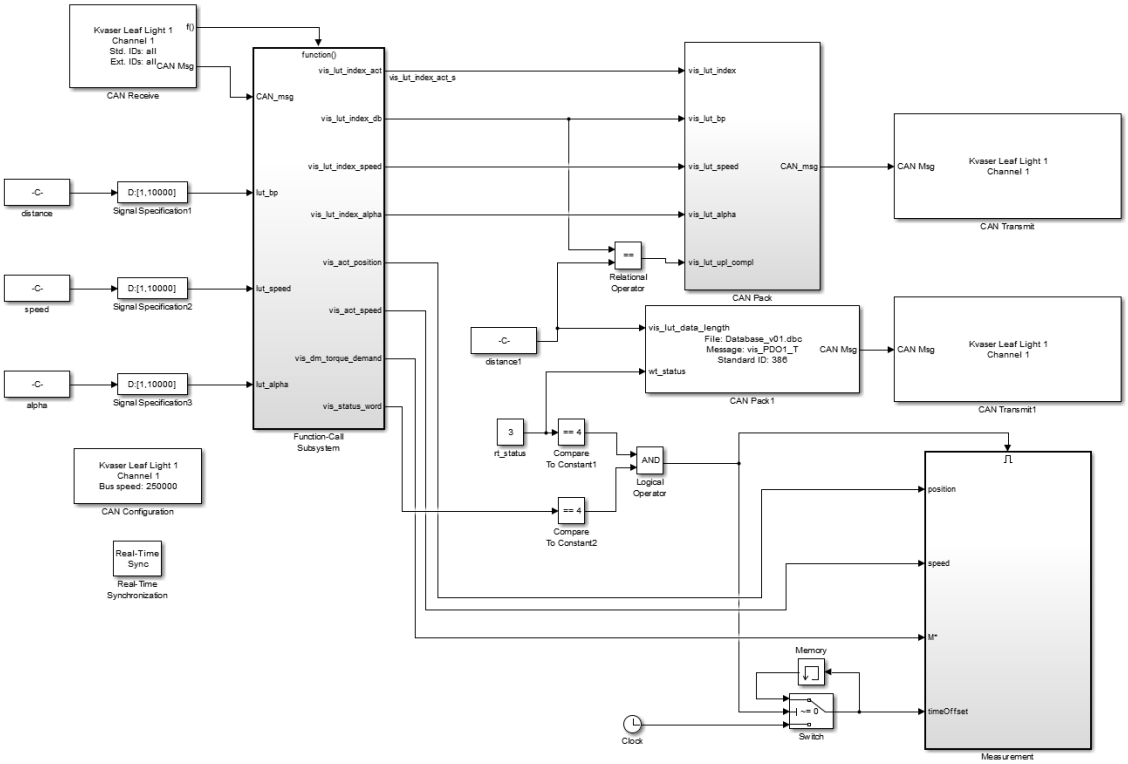

Figure 5.31. EVO application: Real-time interface

Chapter 6
Optimization

This chapter deals with the main part of this thesis which is optimization focusing on the energy consumption reduction during drive. First it is necessary to think about important facts, which can help us to determine the optimization problem. It is clear that slower vehicle needs less energy than faster vehicle. But based on the established model, this fact is not always true. The powertrain is represented by an electric motor and a power inverter. This powertrain operates for example in the low revolution with low efficiency. Once the saved energy from decreasing velocity falls under the increase of consumption. That means the slower motion is no longer efficient. However, the optimal efficiency map is the subject of motor design and we will therefore omit these marginal cases. Still, from what was said, we must add a very important constraint, which will assign each speed profile to a group of equivalent solutions. This constraint is arrival time and we would like to find optimal speed profile from set of profiles with the same arrival time and the lowest value of consumed energy.

6.1 Optimization Problem

The objective function is the function of the consumed energy calculation over the trajectory subject to constrains by powertrain limits. The limits of the powertrain were introduced earlier in this thesis as power P_{max}, torque T_{max} and revolutions. We can consider that the vehicle has constant motor revolution vs. vehicle speed ratio. Thus we can use maximal vehicle speed v_{max} as a constraint. In addition, the acceleration applied on the passengers is not limited only in lateral, but also in forward direction. The value of maximum forward acceleration is, as in the case of lateral acceleration, completely subjective and is based on demands on the comfort of drive. For energy model, the optimization problem can be formed as:

$$\begin{aligned} \min_{v(k)} \quad & E(v) \\ \text{subject to} \quad & v(k) \leq v_{max}(k) \\ & M(k) \leq M_{max} \\ & P(k) \leq P_{max} \\ & a(k) \leq a_{max} \\ & T \leq T_{max} \end{aligned}$$

The variable k refers to the index of track section. Optimization methods routinely solves quadratic problems, which would be exactly the objective function of energy on wheels [56]. However, as is introduced earlier, the energy drained from the battery is adjusted by the power dissipation in the powertrain obtained from the efficiency map. This efficiency map represents huge non-linearity, apparent in figure 6.1.

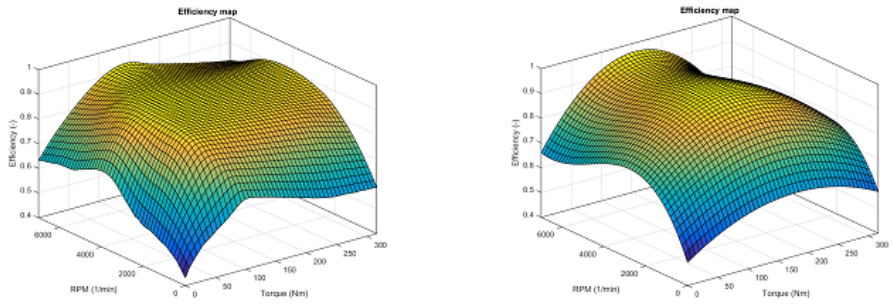

Figure 6.1. Example of the measured (left) and surfaced (right) efficiency map

The standardized procedure is to map the optimization problem to the standard optimization algorithm, for example linear or quadratic programming, and to use the standard solvers for the solving of the optimization problem. The optimization problem introduced earlier uses a nonlinear mathematical model and if we want to guarantee accuracy and correctness of the solution then is not possible to map the optimization problem to the standard optimization algorithm. The other option is to create an own algorithm based on the knowledge of the optimization problem inspired by a heuristic algorithm. The disadvantage of this option is that the algorithm might easily find local minimum where it could get stuck and there is no possibility to determine whether the minimum is local or global.

6.2 Reference Drive Algorithm

The Reference drive algorithm is the first developed algorithm which is used for comparing and validating of optimized data. The goal is to develop an algorithm which has at least the same results in consumption as a real driver. The algorithm is based on the set of rules established from experience. The control algorithm uses the energy model presented earlier. That means the trajectory is divided into sections with constant length. The algorithm defines four operation modes of the vehicle:

- A – accelerate
- B – brake
- C – constant velocity
- G - glide

6.2.1 Accelerate

The first mode Accelerate represents an acceleration of the vehicle by the highest possible rate. The rate of acceleration is limited by the maximum torque and power of the motor and also by the maximum acceleration given by demands of the comfort of the drive. The algorithm calculates the velocity of the section endpoint as result of acceleration. The velocity (as a result of the acceleration) is calculated separately as a result of maximal torque, maximal power and comfort acceleration. From these three velocity values selects the algorithm the lowest. The lowest value represents the acceleration which is applied to the vehicle.

6.2.2 Brake

The second mode Brake is an inverse to the Accelerate mode. This mode is used if a velocity limit by for example a curve is coming. For the calculation of this mode is necessary to use a prediction in control. The prediction always calculates a few next points of the track in case of using brake mode. The result of this calculation is used for the determination of the current action. For example the vehicle has a velocity of the k-th section. The velocity of the next section $v(k+1)$ has to be calculated in respect to the velocity limit of the following sections. The desired velocity $v(k+1)$ has to be validated by simulation of braking from this velocity value on the following section until the vehicle is stopped. If the vehicle stops on the n-th section, it is obvious that changing velocity on (k+1)-th section to the value $v(k+1)$ affects only sections of band $< k+1, n >$. The figure 6.2 represents an example of a test for brake mode calculation.

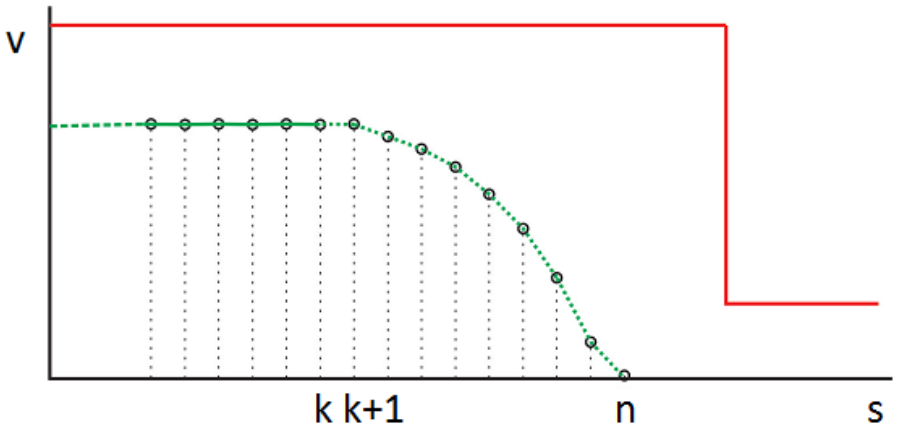

Figure 6.2. Brake mode: test to validate velocity of the point $k+1$

The violation of the speed limit of any section in the band brings about restriction of the velocity value $v(k+1)$. If the violation of the velocity limit occurs on the l-th section, then the velocity of the vehicle is set to the value of the limit on this section and the braking is reversely simulated from this point back to point $k+1$. By this process, the value of the velocity $v(k+1)$ is calculated and there is a guarantee that the speed limit on the l-th section is not violated. The vehicle has the velocity $v(l)$ equal to the speed limit in this point. The explanation is shown in the figure 6.3.

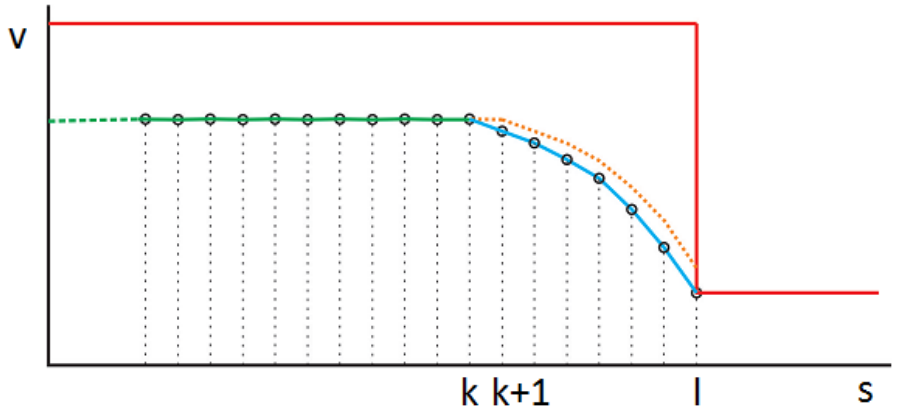

Figure 6.3. Brake mode: inverse velocity profile construction

6.2.3 Constant Velocity

In this mode the velocity on the start point is the same as on the end point of a section. The value is only validated by the maximal torque and maximal power of the motor. If one of the limit is exceeded, the velocity value is recalculated regarding this limit.

6.2.4 Glide

The Glide mode represents a drive with no power of the motor. The value of the end point of calucated in respect to the energy which represents losses.

6.2.5 Implementation

Implementation of the algorithm is based on the idea where slower vehicle needs less consumed energy and a move with constant velocity over the track. At the first we have to calculate the average velocity $\bar{v}$ which is determined by the arrival time t_{arr} and total length of the track s as

$$\bar{v} = \frac{s}{t_{arr}} \tag{6.1}$$

Traveling slower than the average velocity in some sections requires increasing of the velocity in other sections of the track to have to same arrival time. The energy consumption is non-linearly proportional to the traveling velocity, one can determine the saved energy on the part of the track where the velocity is lower than average as lower than spent energy on the part of the track where the velocity must be higher than average. The most efficient mode in this algorithm is to travel with the average velocity. When the vehicle moves slower than the established average velocity, the command is to accelerate. If the average velocity is reached, then the velocity is constant. If the track is downhill or the velocity is higher than the average, the vehicle glides. In each point is calculated the brake test introduced earlier. The brake command has the biggest priority in order not to violate the speed limit. The figure 6.4 represents an example of a short driving cycle.

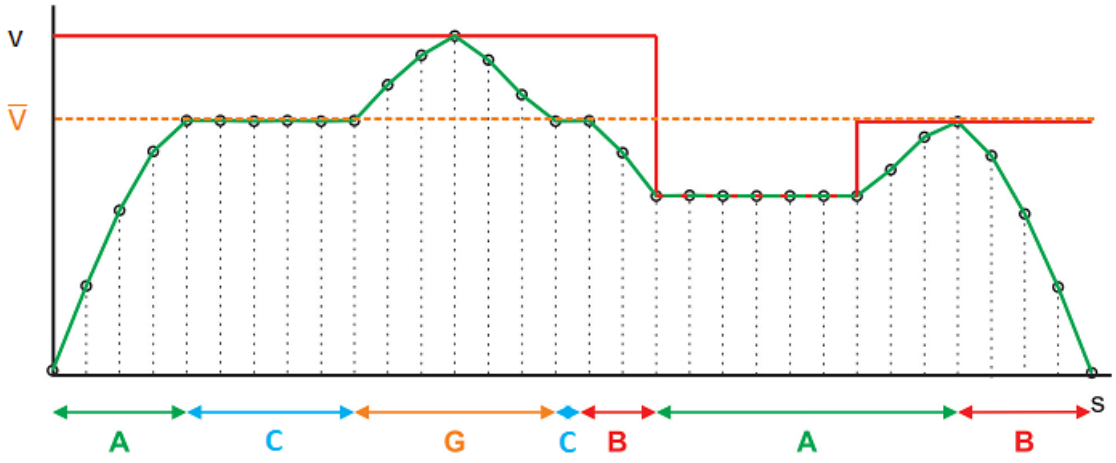

Figure 6.4. Reference drive: Example of driving cycle

As the resultant velocity is not equal to the established average velocity on every section, due to acceleration and braking, the arrival time related to the resultant speed profile differs from the desired time. The average velocity value must be properly recalculated and the speed profile is, therefore, built up in more iterative steps of

the algorithm. The algorithm provides speed profile with exact arrival time without violating any constraints formed earlier.

6.3 Optimization Algorithm

Heuristic algorithms are based on various ways of searching for the best result of possible solutions. The algorithms start with initial solution trying to improve the result in interactive steps. The new solution is chosen by a logic based on the knowledge of previous solutions. The logic which chooses the next step determines the optimization (solution) method. Approaches to the optimization problem therefore involve some kind of compromise, such as very long computation time or the possibility of not finding the best solution [56].

The heuristic methods do not have strict procedure and they can be easily modified for an improvement of the algorithm performance. In the next section is presented an algorithm based on the existing methods.

6.3.1 General Scheme

The idea of the algorithm is to evaluate each point of the track in the domain of the objective function, in our case energy. We need for the evaluation to calculate the demands of the track points as a result of velocity changes in these points. The changes in the velocity are not constant, and they are calculated to bring about constant change in arrival time ΔT, for each track point. The algorithm calculates in the next points:

1. Determine time step

The time step ΔT is a constant because it is needed keep the same demand in all points and the time step represents a change in the velocity on the section. Hence, speed in each point is recalculated for ΔT and $-\Delta T$ in respect to the fact that changing of k-th velocity $v(k)$ changes section time $t(k)$ and $t(k-1)$. An example of the calculation is shown in the figure 6.5.

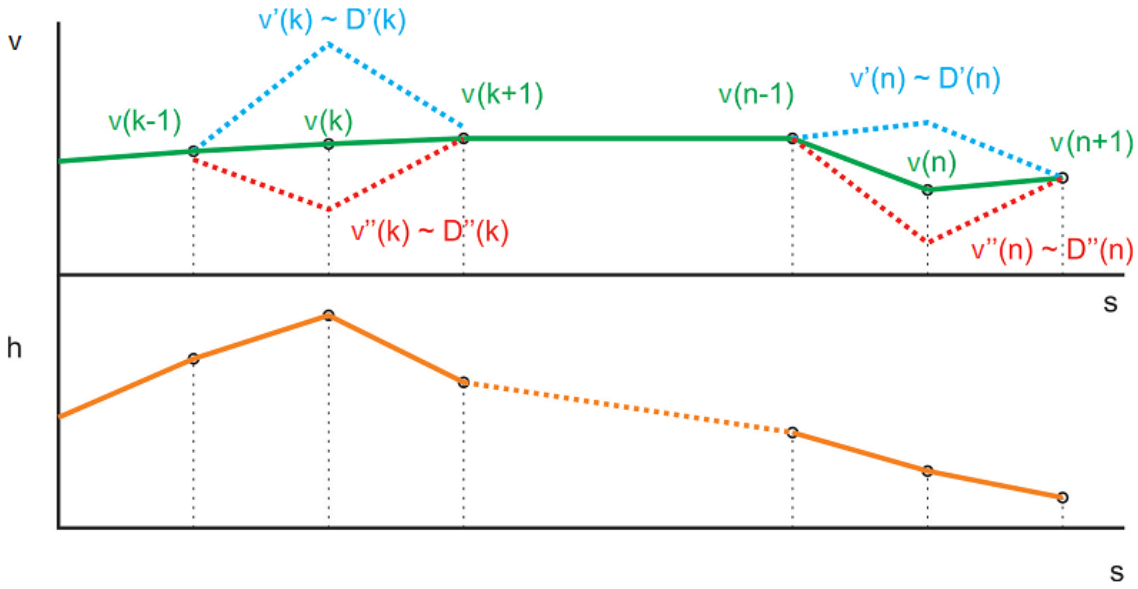

Figure 6.5. Optimization algorithm: recalculation

It is clear for the figure 6.5 that the value of the velocity $v'(k)$ and $v''(k)$ is calculated in respect to validity of the following equations:

$$t(k-1) + t(k) - \Delta T = t'(k-1) + t'(k) \tag{6.2}$$

$$t(k-1) + t(k) + \Delta T = t''(k-1) + t''(k) \tag{6.3}$$

Where time $t(k)$ refers to the velocity $v(k)$, time $t'(k)$ referes to the velocity $v'(k)$ and the time $t''(k)$ refers to the velocity $v''(k)$.

2. Evaluate points of the track by energy demands

Energy demand $D'(k)$ of k-th point is calculated as the difference between energy for the velocity $v(k)$ and energy for the velocity $v'(k)$ as follows

$$D'(k) = (E(k) + E(k-1)) - (E'(k) + E'(k-1)) \tag{6.4}$$

The energy demand $D'(k)$ would be enough to evaluate the k-th point when we consider the slope of the tangent:

$$\frac{D'(k)}{\Delta T} = \frac{D''(k)}{-\Delta T} \tag{6.5}$$

3. Variation of the most demanding and least demanding point

If the energy demands are calculated then the most demanding and the least demanding poist are chosen. We can consider for example that the most demanding point is the k-th point and the least demanding point is the n-th demanding point. If we change the velocity in these points then we can determine whether this change brings any improvement in total energy consumptions:

$$D''(k) + D'(n) > 0 \tag{6.6}$$

If the equation (6.6) is valid, the velocity variation brings a better solution of the optimization problem. The velocity has to be changed in accordance with constraints introduced in the optimization problem specification. That means it is necessary to calculate the torque, power and acceleration needed for velocity change from the point $v(k)$ to the point $v''(k)$ and from the point $v(n)$ to the point $v'(n)$. The new power in k-th point is calculated as:

$$P''(k) = \frac{D''(k)}{t(k)} \tag{6.7}$$

the new torque as:

$$M''(k) = \frac{P''(k)}{N''(k)} \tag{6.8}$$

where $N''(k)$ is motor revolution calculated as:

$$N''(k) = \frac{v(k-1) + v''(k)}{2} \cdot \frac{2\pi}{60} \cdot c_{tr} \tag{6.9}$$

where c_{tr} is the transmission ratio.

The new acceleration is calculated as:

$$a''(k-1) = \frac{v''(k) - v(k-1)}{t''(k-1)} \tag{6.10}$$

$$a''(k) = \frac{v(k+1) - v''(k)}{t''(k)} \tag{6.11}$$

If one of the variables exceeds the constraint, the velocity change $v''(k)$ is forbidden.

6.3.2 Local Miminum Prevention

A disadvantage of heuristic algorithms is getting stuck in a local minimum. The optimization problem introduced at begin of this chapter is nonlinear problem where are local minimums. Based on this fact is necessary to consider the local minimum prevention. The track data and speed profile are sampled with a dense grid and if we consider the constraints, the speed profile change in one interaction step of the algorithm is marginal. Therefore the algorithm tends to get stuck in the local minimum. The solution of this problem is to admit temporary violation of the constraints or to reduce speed profile sampling grid to cause major changes without violations any constraints. That means we still have to make all calculations, primarily verification of constraints. The altitude profile and maximal speed profile has always the same dense grid, only speed profile grid is changed. The method is apparent in figure 6.6.

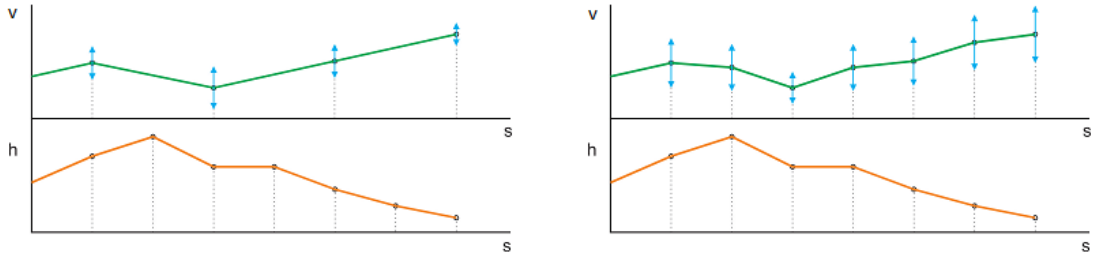

Figure 6.6. Reduced grid (left) - Soft grid (right)

The method of grid reduction is rather chosen as each iteration provides valid solution and major changes improve the approach to the global minimum. Unfortunately, this method does not allow us to start with any previously achieved solution and the speed profile has to be built up from the beginning. The speed profile is preferably built up gradually by setting intermediate time constraint. The algorithm can be then described by the following scheme, starting with few points of speed profile grid and considering energy demand evaluation associated to the time step ΔT in each of these points:

1. **Set intermediate time**

   Strategy of the intermediate time setting determines how fast the algorithm will reach the original time constraint, or how dense the grid is when the original time constraint is reached. In each iteration of the scheme, the intermediate time is reduced.

2. **Speed up until intermediate time reached**

   Velocity of the least demanding sections is repeatedly increased in a cycle until the intermediate time is reached. Each iteration of this inner cycle decreases the arrival time by the time step ΔT, and all constraints are treated as in the case of section variation.

3. **Find intermediate solution**

   After the intermediate time is reached, the optimization algorithm finds, for the current grid, the least demanding solution according to the scheme introduced in the section 6.3.1.

4. **Soften the grid**

   The grid is softened by splitting each section in half. This step requires recalculation of the demands of all the newly established sections. This operation decreases the ability of making major changes, however, the closer to the final solution we are, the less this ability is required.
5. **Find intermediate solution**

   After the grid is softened, the previously established solution is no longer considered as the least demanding, therefore, the least demanding solution must be found by the same algorithm as in the third point of this scheme.

6.3.3 Implementation

The optimization algorithm is implemented in MATLAB as a part of the EVO application (see the chapter 5) in the class @Optim. The algorithm starts in the function RUN where is implemented a state machine based on the steps introduced in the previous section. The algorithm starts in INIT state where is the algorithm initiated. The other states are:

1. speedUp
2. slowDown
3. combine
4. split
5. changeDt

The algorithm runs in a cycle where one from these states is selected. The first iteration starts for the grid made by three points (start point, end point and middle point). The algorithm continues to SPEEDUP state to try to change the middle point accordance with the constraints. If there is no possibility to change the speed and the arrival time is not reached then the algorithm continues with CHANGEDT state where change the grid in a half and continues with SPEEDUP or COMBINE state. The COMBINE state tries to change speed profile based on the point number 3 from previous section.

6.3.4 Computation Time Improvment

The calculation time is highly watched indicator and it is clear that an optimization algorithm with very high calculation time is not an algorithm for online using in vehicle. The target is to reduce the calculation time to the same or better value than arrival time. The algorithm is designed in accordance to the previous rule and the result is not optimal solution but it is on 95% of this solution. One method how to improve the computation time is to skip COMBINE state until the arrival time calculated from the speed profile is not to close to the arrival time selected by a user.

Chapter 7
Results

This chapter presents the results of the thesis. The first result is an experimental result on the DC/DC power converter for super-capacitor and comparsion of simulation and converter prototype. The second result deals with the comparing of dynamic and enery models. The other results deals with the comparing of optimization algorithm, reference drive algorithm and measured driving cycle in Škoda Rapid.

7.1 DC/DC Power Converter

It was created the model in MATLAB/Simulink and the same algorithm was implemented to the Freescale processor 56F8257. The converter prototype was created for validation of simulated data. For comparing simulation and prototype the next experiment was designed. The initial condition is the voltage 35 V on super-capacitor and 200 V on DC bus. In time 1 s it is started the discharging of super-capacitor by the power 0.1 kW. The super-capacitor reference voltage is 20 V. In time 320 s is started the charging by power 0.15 kW with voltage reference 25 V. In time 450 s is started again charging by power 0.15 kW with voltage reference 38 V. The results are shown in Fig. 7.1 and in Fig. 7.2 . From 1 s to 300 s super-capacitor is discharged by power 0.1 kW. The source in model is simulated like ideal part with zero internal resistance. The discharging is stopped after the voltage on super-capacitor is 20 V. The next is buck mode with overcurrent protection. The controller limits the current, if the voltage is lower than minimal value 120 V. In time 420 s the source voltage was lower than minimal value, charging was stopped and the charging was started in time 465 s, where the voltage was greater than minimal value.

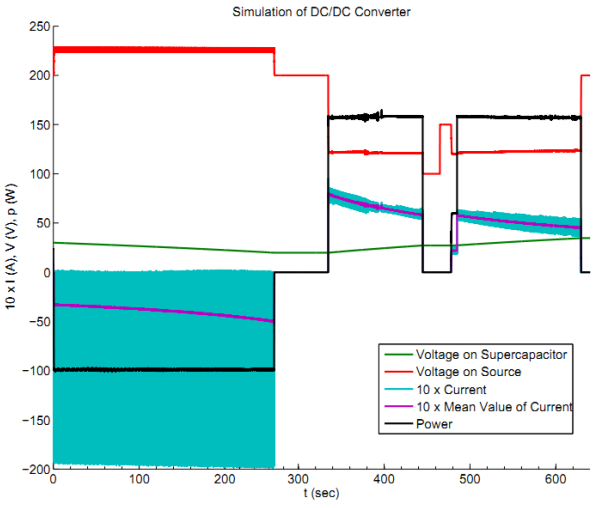

Figure 7.1. Experimental Results: Simulation

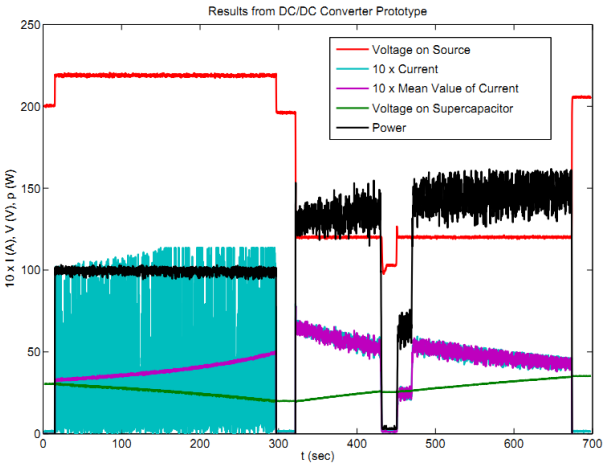

Figure 7.2. Experimental Results: Converter Prototype

7.2 Energy and Dynamic Model Comparsion

The principle of simplification introduced in energy models brings about the difference between results produced by dynamical and energy model. Divergence of operating values is apparent in sample of drive in figure 7.3.

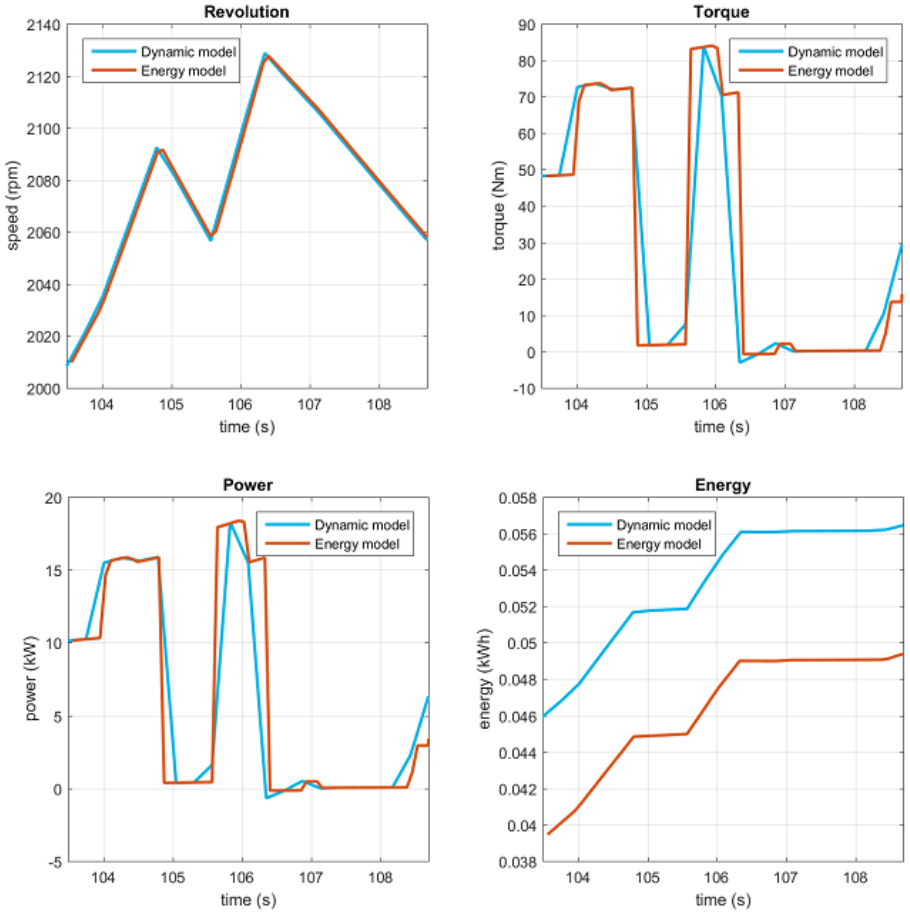

Figure 7.3. Energy and dynamic model comparsion

The speed profile suggested by the using of energy model represents prescribed speed for the dynamic model, thus, the divergence is given by the quality of controller tuning. Power and torque are considered as constants by sections, which makes the difference, as their dynamic behavior is omitted. Therefore, the operational point of the motor is not accurately determined continuously during the drive, but as a constant by sections, although the value in dynamic drive continuously changes. These facts cause slightly different results between total energy of dynamic model and energy model. Nevertheless, the character of the vehicle of dynamical model is satisfactorily reflected by the energy model, and the result of the optimization algorithm can be considered as valid.

7.3 Long Track

The first result on the test bench in Roztoky is called long track. This result presents a comparing of driving cycle near Roztoky. The driving cycle starts in front of the building where is located the laboratory. Then it continues in direction to Velké Přílepy up to the small hill. After about 700 meter the track turns right in direction to Únětice. It goes a little bit up the hill and down the hill to Únětice village. The track continues straight on the main street. At the end of Únětice there is again up the hill and the track finishes about 100 m before roundabout where is a Lidl supermarket located. The map of this track together with altitude profile is shown in the figure 7.4. The figure is a screenshot from the EVO application.

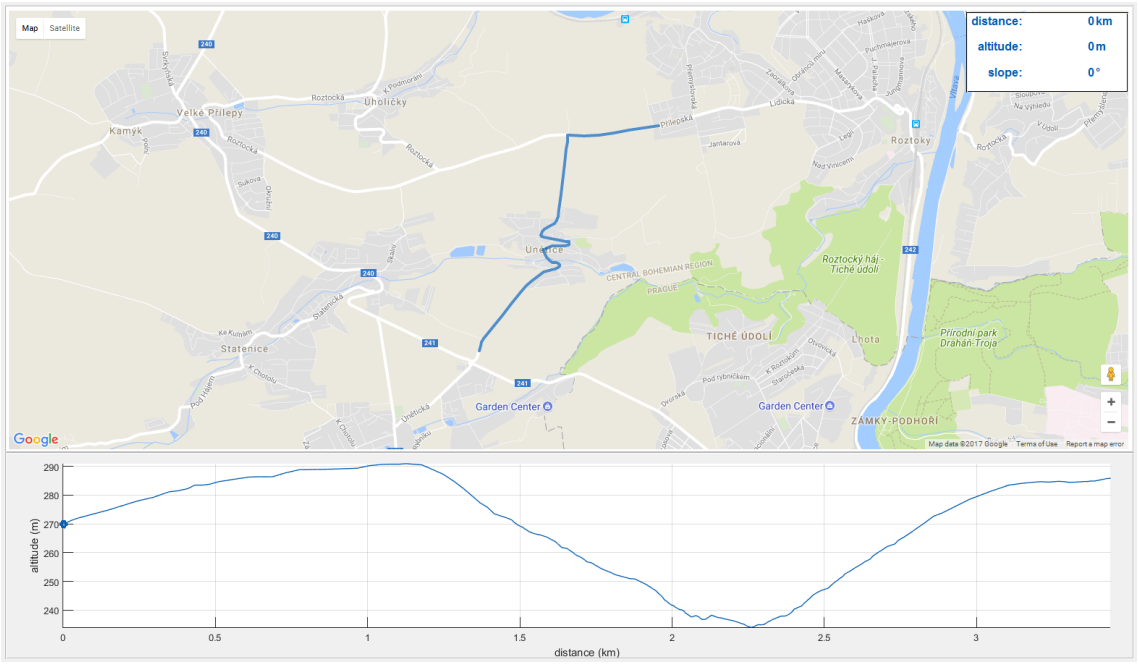

Figure 7.4. Long track: map and altitude profile

Based on the coordinates provided by Google and manually added speed limits is calculated the maximal speed on the track. The maximal speed profile is shown in the figure 7.5.

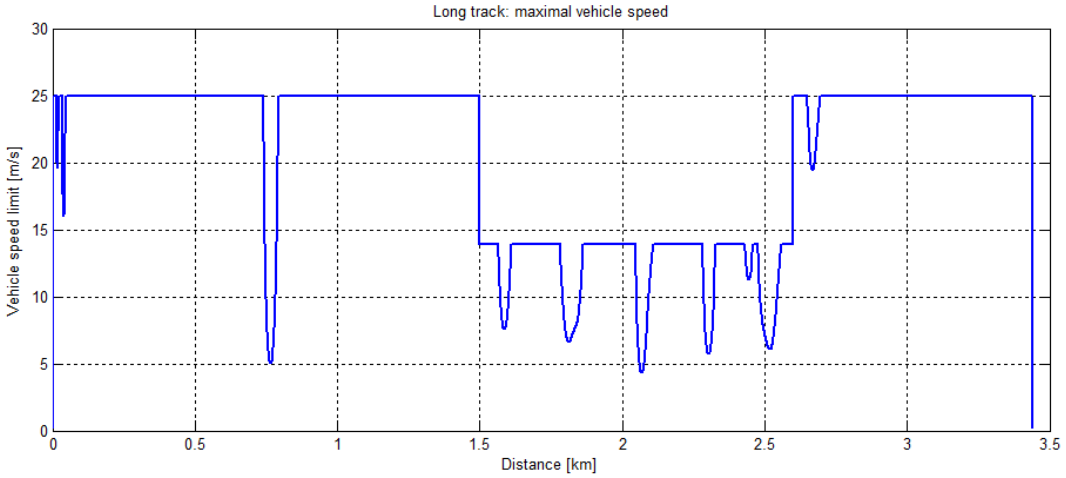

Figure 7.5. Long track: maximal speed profile

The first drive was performed by Škoda Rapid EV prototype provided by Škoda auto a.s. The vehicle is shown in the figure 7.6. The vehicle parameters were introduced in the chapter 4.

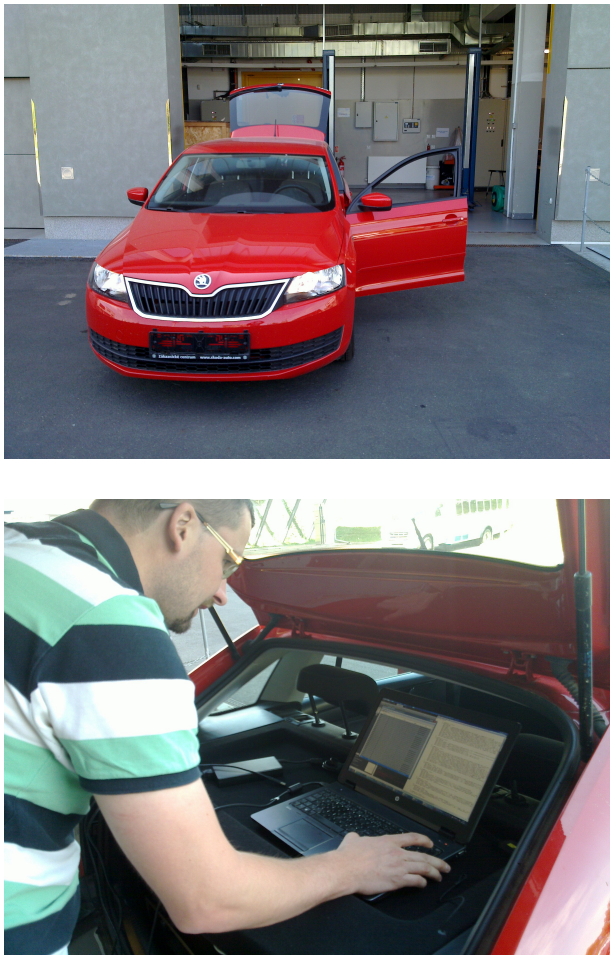

Figure 7.6. Škoda Rapid EV prototype

The driving cycle data from CAN bus was logged via USB/CAN converter from Vector by Vehicle Network Toolbox included in MATLAB. The data from GPS was

logged from bult-in GPS receiver via serial interface. The most important information was the vehicle speed, which came from ESP unit of the vehicle. The driver was asked for a drive oriented to low energy consumption. The speed profile of the track is shown in the figure 7.7.

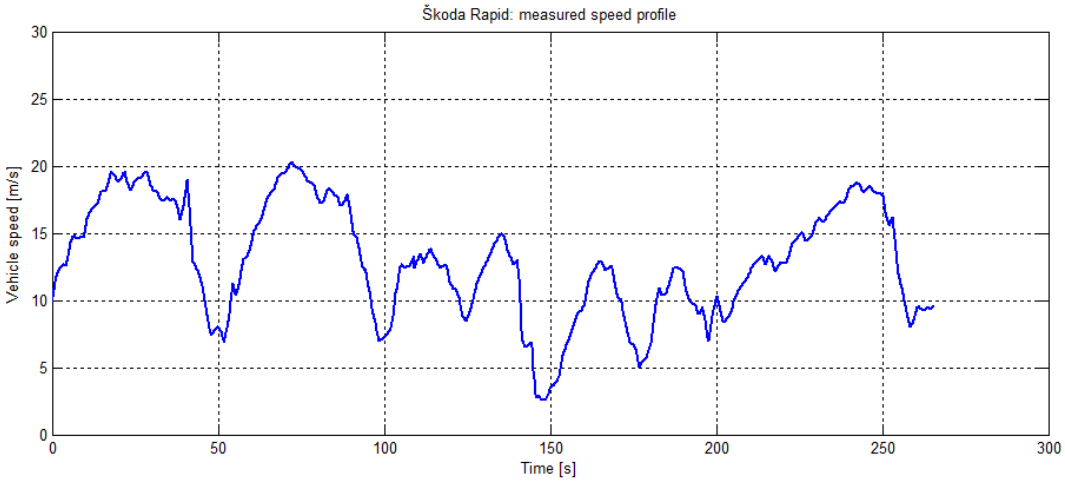

Figure 7.7. Škoda Rapid EV: measured speed profile

On the test bench is the same electric motor and power converter, but different battery model operating with different voltage and different vehicle model. The pure comparing of logged data from vehicle and from test bench would not be correct. I used the measured speed profile as the input to the test bench and used the same arrival time and the same track as the input to the optimization algorithm. I made three measurements:

1. The first measurement uses as the input the measured speed profile in Škoda Rapid EV
2. The second measurement uses the calculated speed profile from optimization algorithm
3. The third measurement uses the calculated speed profile from reference drive algorithm

The all measurements use the same test bench with the same initial values, because we need the direct comparing of total energy consumption.

7.3.1 Results

The speed profiles were uploaded one by one into the dSpace. After uploading and starting the speed profile simulation is only the dSpace responsible for the simulation control. The PC with EVO application is using only for showing the actual state of simulation. A video from the measurement is on DVD which is a part of this thesis or it is possible to download from the website https://www.dropbox.com/s/y6wzozcdwf4jcid/LongTrack.MOV?dl=0 where will be located until May 2018. The all results of the simulations were logged via ASMOT software.

Škoda Rapid

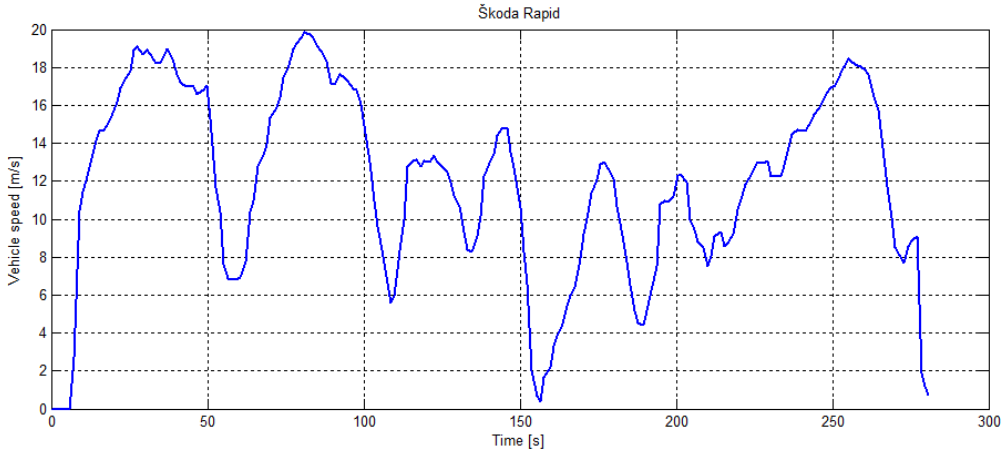

Figure 7.8. Škoda Rapid EV: speed profile

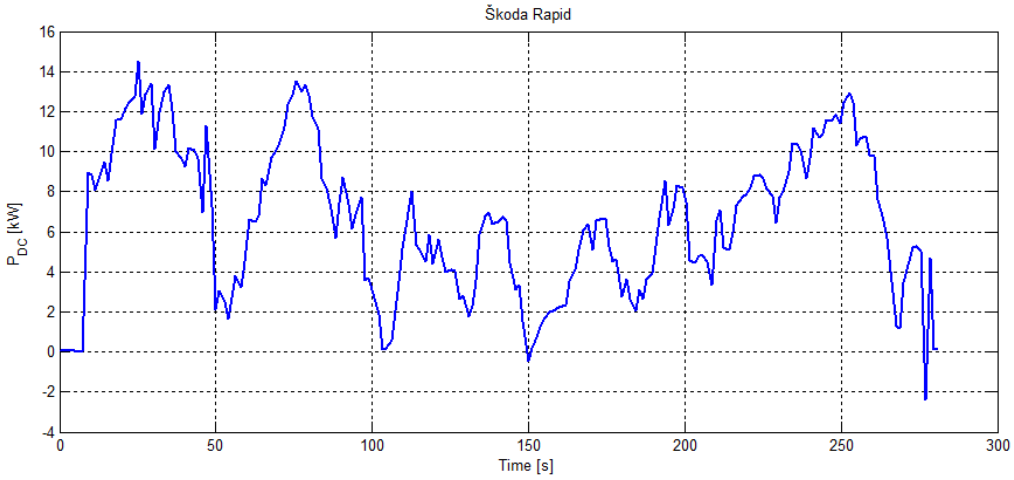

Figure 7.9. Škoda Rapid EV: DC power calculated from battery voltage and current

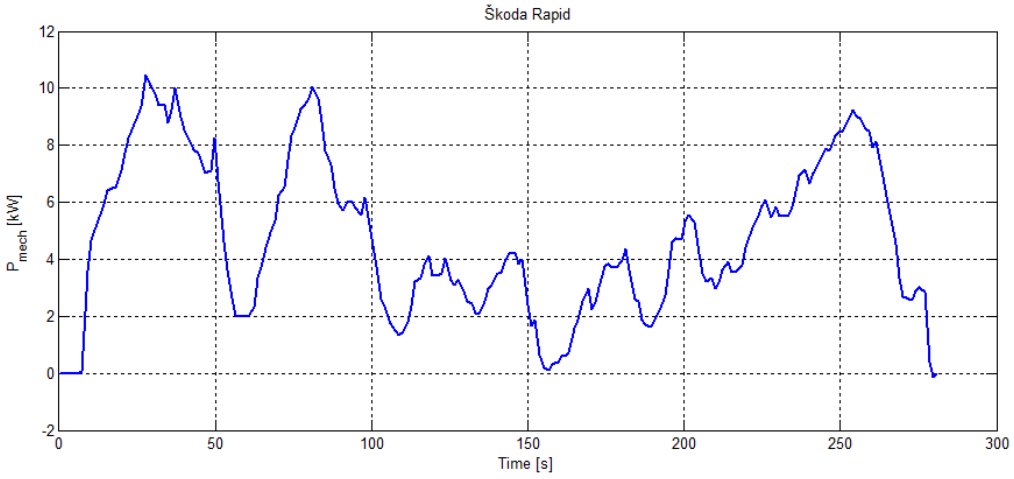

Figure 7.10. Škoda Rapid EV: Mechanical power calculated from torque and speed

Optimization algorithm

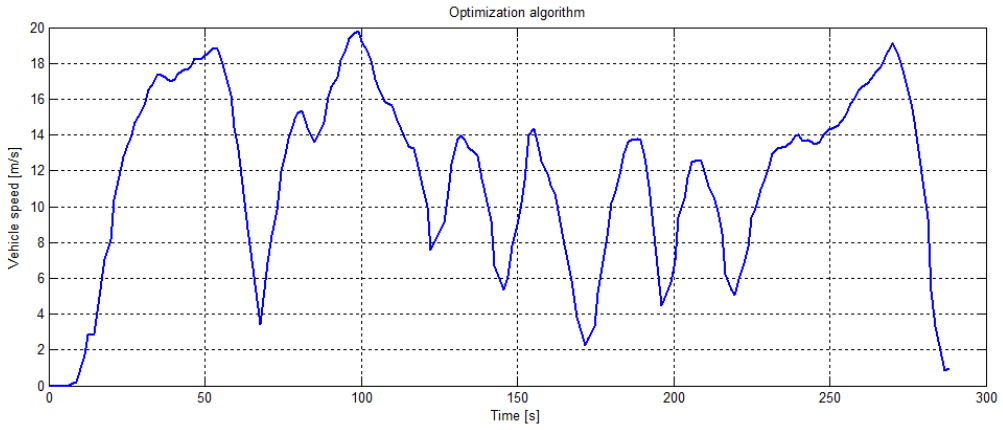

Figure 7.11. Optimization algorithm: speed profile

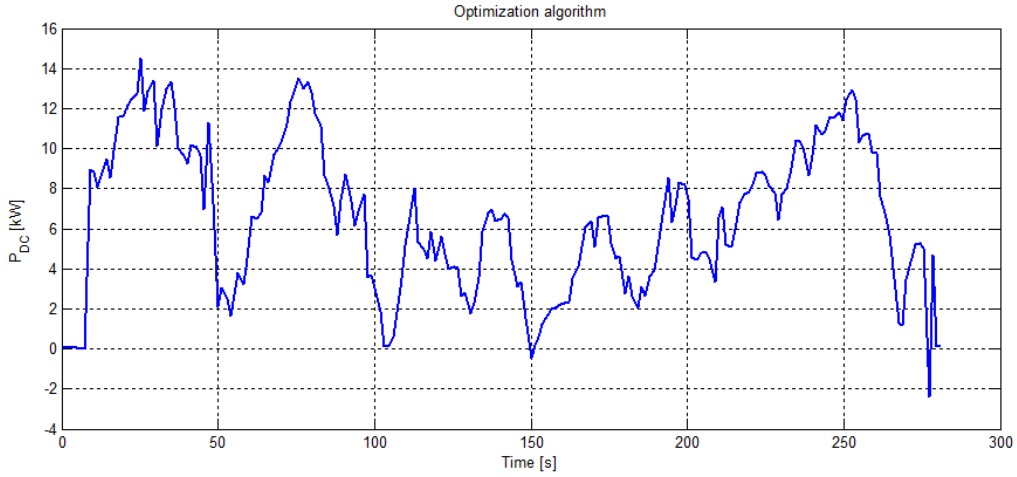

Figure 7.12. Optimization algorithm: DC power calculated from battery voltage and current

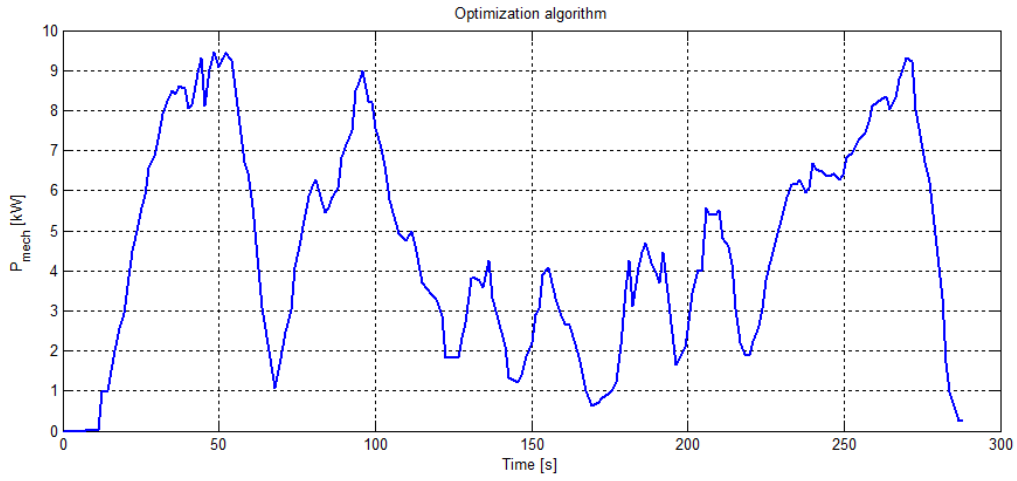

Figure 7.13. Optimization algorithm: Mechanical power calculated from torque and speed

Reference drive algorithm

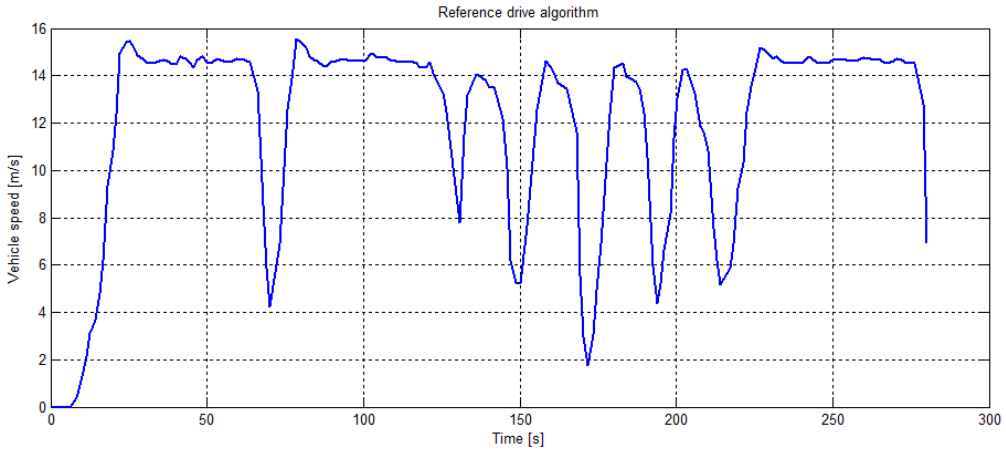

Figure 7.14. Reference drive algorithm: speed profile

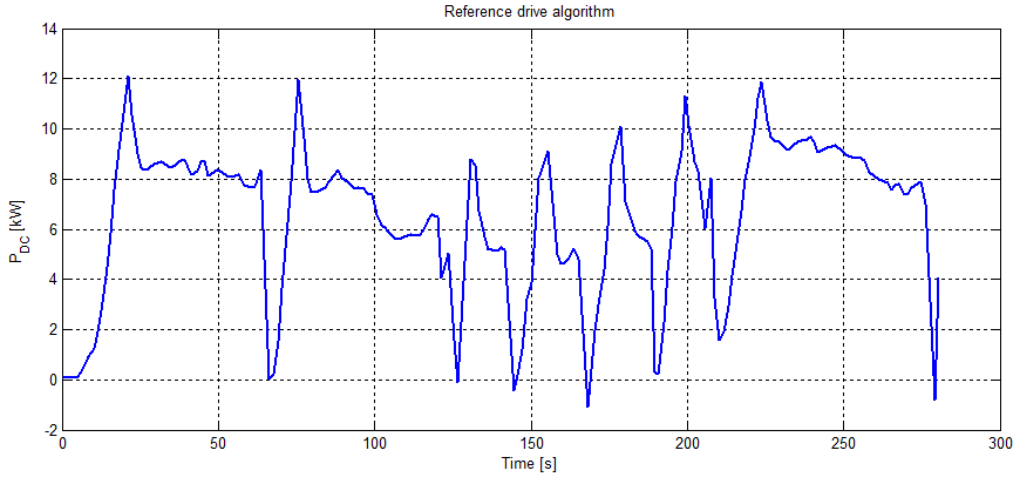

Figure 7.15. Reference drive algorithm: DC power calculated from battery voltage and current

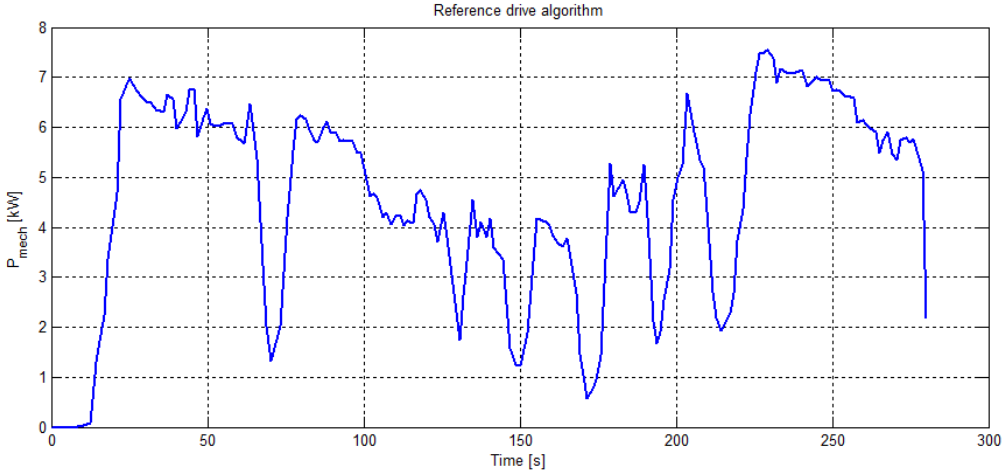

Figure 7.16. Reference drive algorithm: Mechanical power calculated from torque and speed

7.3.2 Comparing

The total energy consumption was calculated from the battery simulator control software which calculates the total energy consumed and recuperated. The total energy consumption is shown in the table and in the figure bellow.

Drive	Energy consumption	Saved energy
Škoda Rapid	0.54 kWh	3.4 %
Optimization algorithm	0.52 kWh	5.8 %
Reference drive algorithm	0.56 kWh	

Table 7.1. Long track: Energy consumption comparing

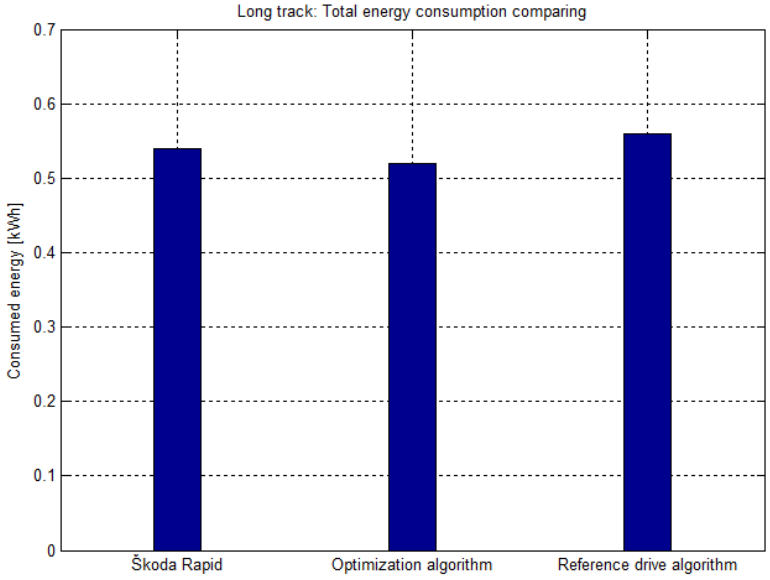

Figure 7.17. Long track: Total energy consumption comparing

7.4 Short Track

The second result on the test bench in Roztoky is called short track. This result presents a comparing of short driving cycle near Roztoky. The driving cycle is a part of the long track. The goal is to use only Optimization algorithm for speed profile calculation. Only arrival time was changed. The speed profile was calculated for these arrival times:

- 150 s
- 160 s
- 175 s

The map of this track together with altitude profile is shown in the figure 7.18. The figure is a screenshot from the EVO application.

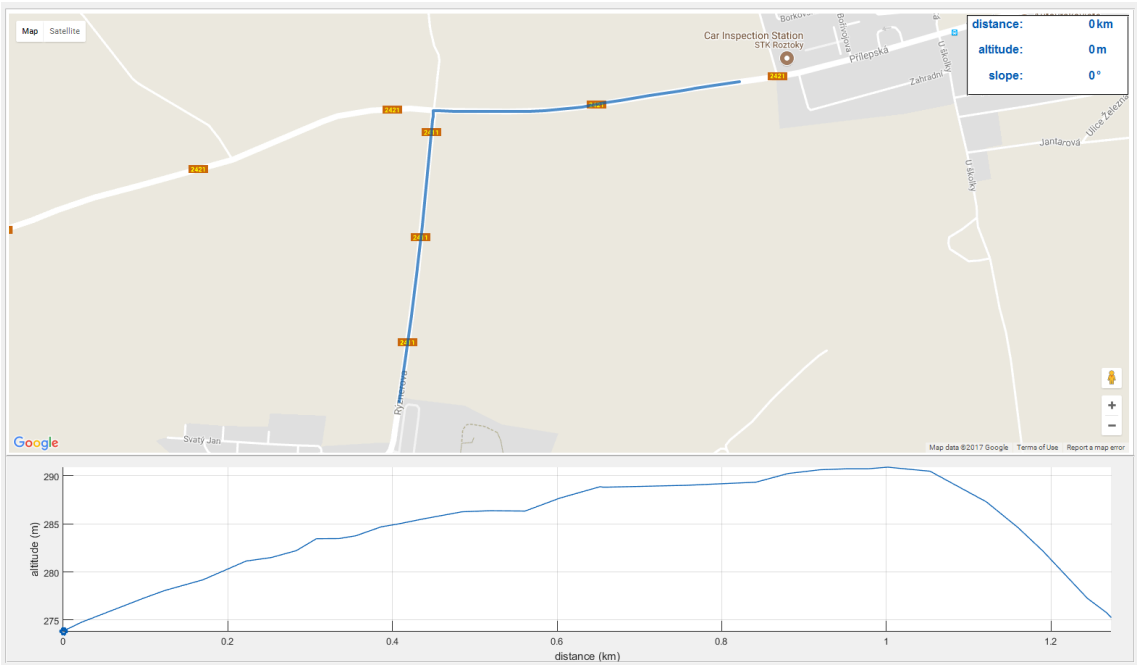

Figure 7.18. Long track: map and altitude profile

Based on the coordinates provided by Google and manually added speed limits is calculated the maximal speed on the track. The maximal speed profile is shown in the figure 7.19.

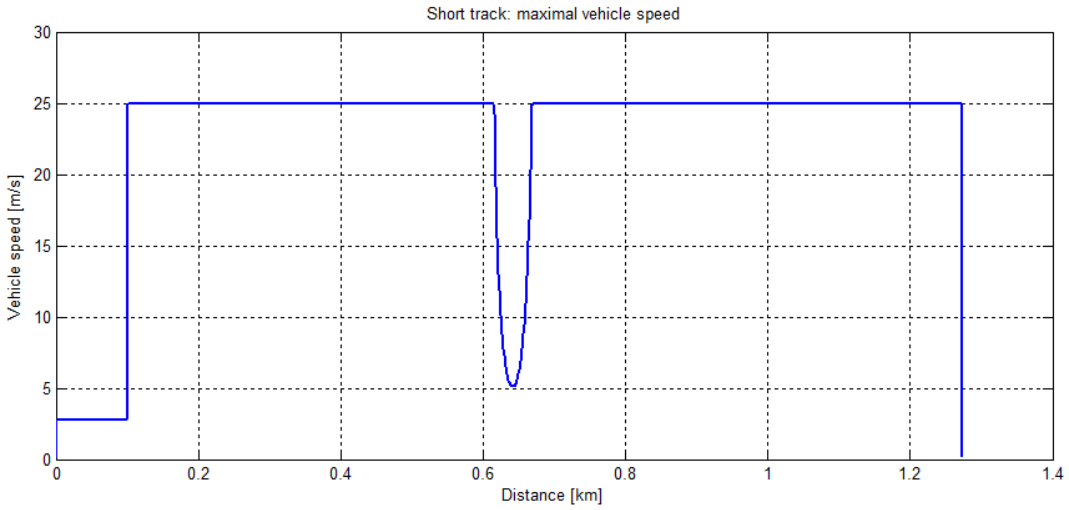

Figure 7.19. Short track: maximal speed profile

7.4.1 Results

The speed profiles were uploaded one by one into the dSpace as in the previous case. As the consumed energy was used a value calculated by the battery simulator.

Arrival time 150s

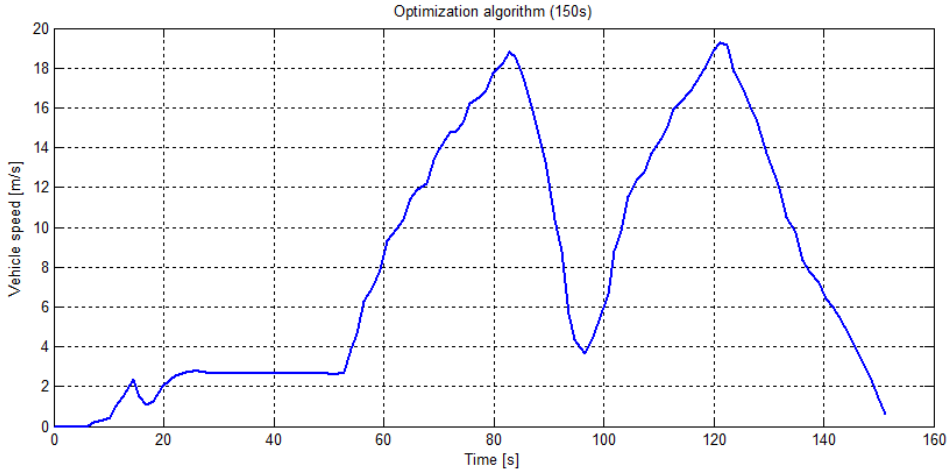

Figure 7.20. Optimization algorithm (150 s): speed profile

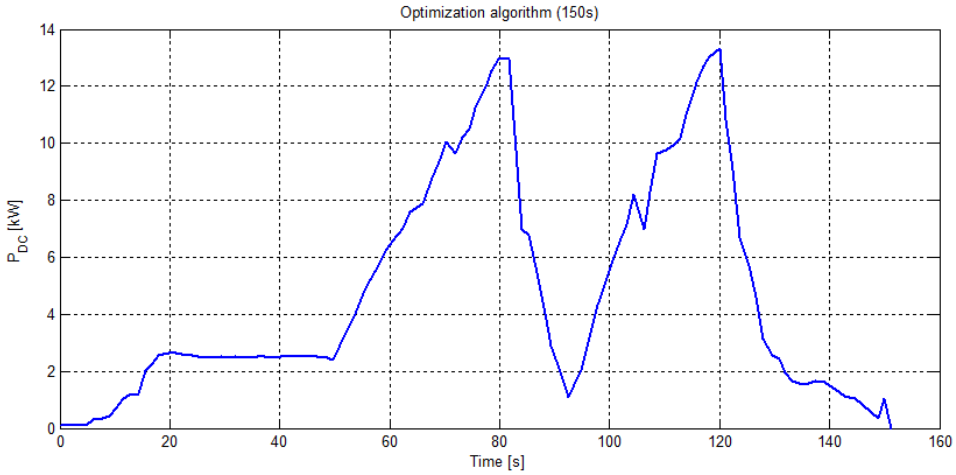

Figure 7.21. Optimization algorithm (150 s): DC power calculated from battery voltage and current

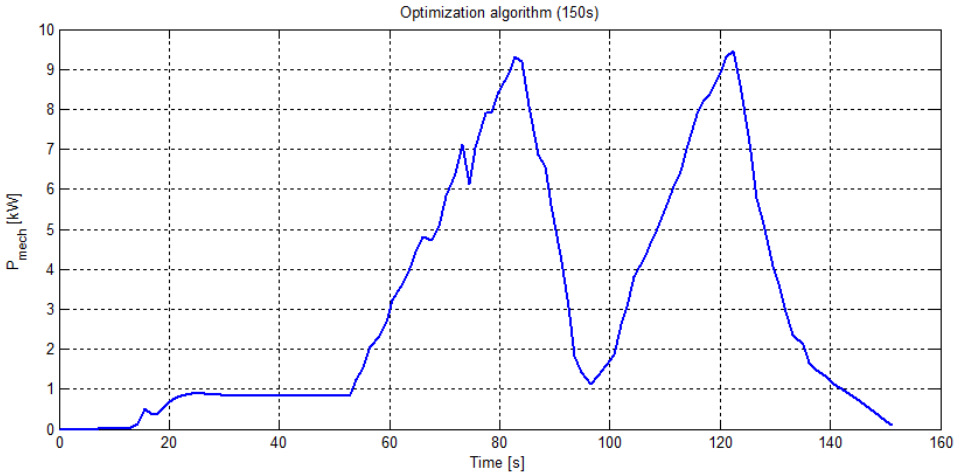

Figure 7.22. Optimization algorithm (150 s): Mechanical power calculated from torque and speed

Arrival time 160s

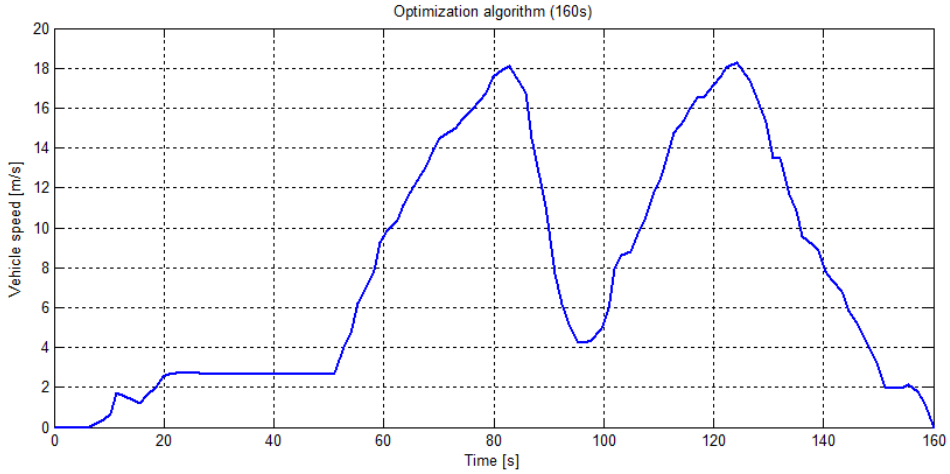

Figure 7.23. Optimization algorithm (150 s): speed profile

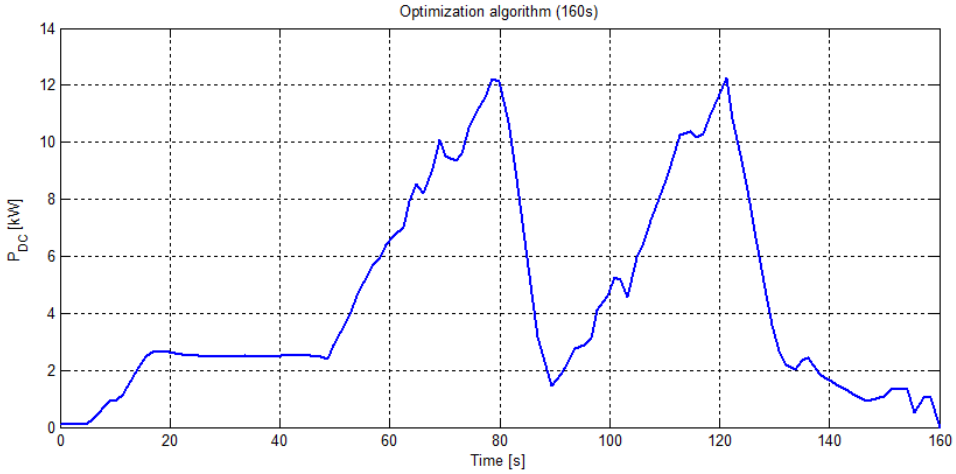

Figure 7.24. Optimization algorithm (160 s): DC power calculated from battery voltage and current

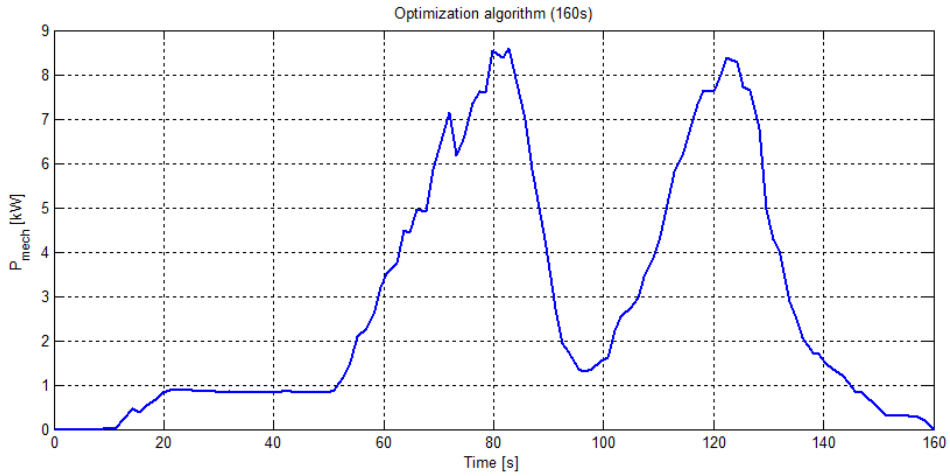

Figure 7.25. Optimization algorithm (160 s): Mechanical power calculated from torque and speed

Arrival time 175s

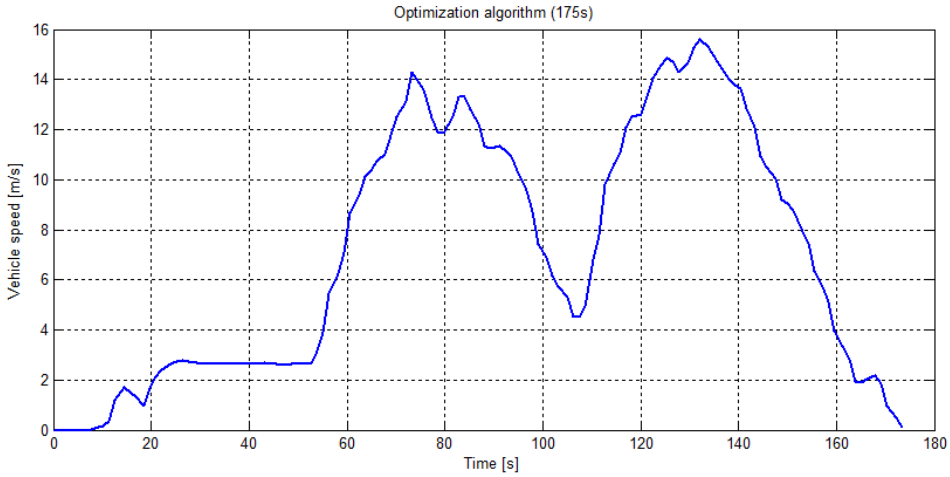

Figure 7.26. Optimization algorithm (175 s): speed profile

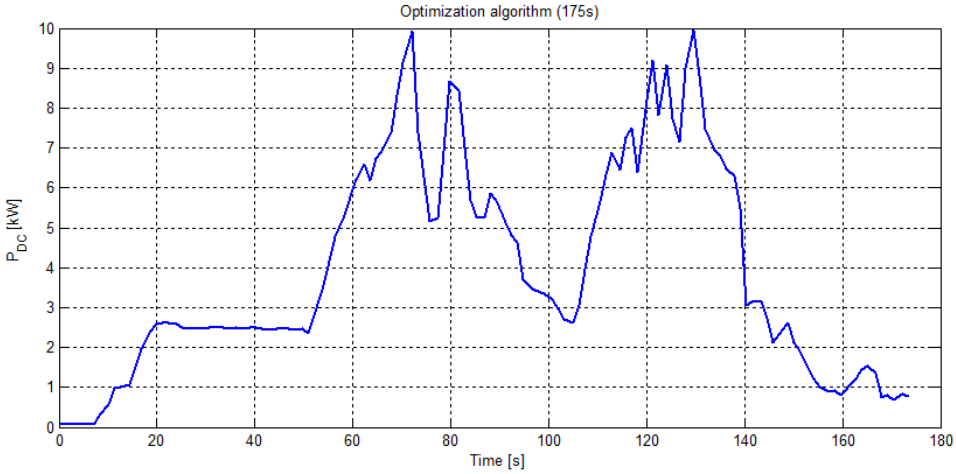

Figure 7.27. Optimization algorithm (175 s): DC power calculated from battery voltage and current

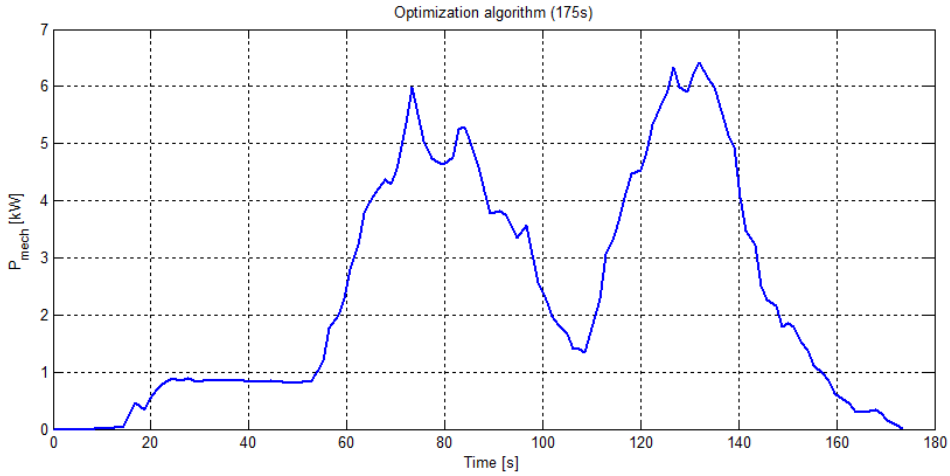

Figure 7.28. Optimization algorithm (175 s): Mechanical power calculated from torque and speed

7.4.2 Comparing

The total energy consumption was calculated from the battery simulator control software which calculates the total energy consumed and recuperated. The total energy consumption is shown in the table 7.2.

Arrival time	Energy consumption
150 s	0.24 kWh
160 s	0.21 kWh
175 s	0.20 kWh

Table 7.2. Short track: Energy consumption comparing

The goal of this result is to find a dependence consumed energy vs. arrival time for the same driver's style. The results presented in the table 7.2 are results of the real consumption measured on the test bench. The shorter time is not possible to drive on the test bench, because we are limited by the maximal torque and power of the electric motor. If we want to decrease the arrival time, it is necessary to use a motor with better performance. This motor not allow the test and we have to simulate the results only on the mathematical model which is a part of the EVO application. By the using of electric motor with nominal power 80 kW and 330 Nm we can simulate the shorter arrival times. The figure 7.29 presents an extension of the table 7.2. The time interval between 140 and 160 s presents a compromise between the consumed energy and duration of the drive.

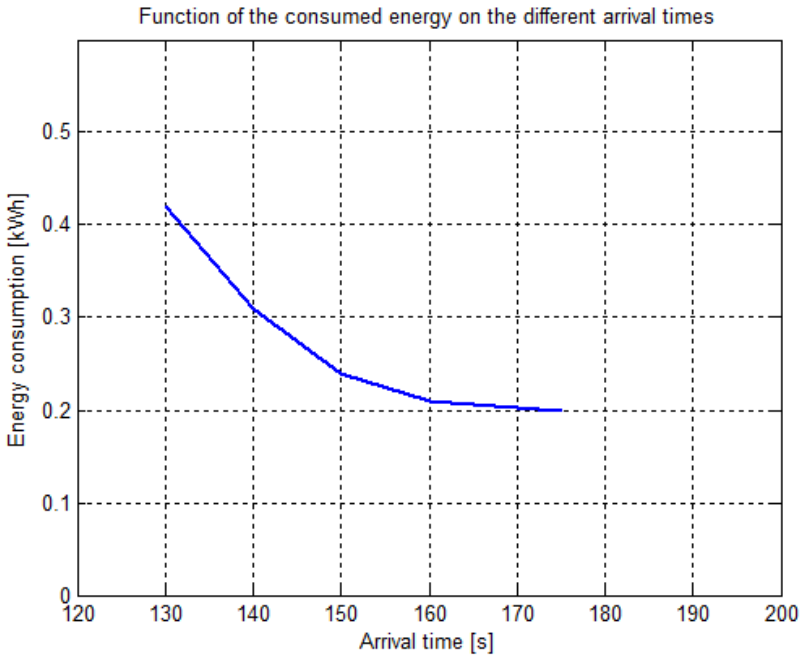

Figure 7.29. Short track: funtion of the consumed energy for the different arrival times

Chapter 8
Conclusion

The main goal of this thesis was to design and to verify the optimization algorithm for the optimal speed profile design and to design the DC/DC controller for super-capacitor charging and discharging. The optimization algorithm is a part of control system in the laboratory in VTP Roztoky. The control system was designed as an open platform with possibility to use different electric drives or different storages.

8.1 Overview of the Results

Chapter 2 provides an overview through powertrain types of hybrid electric vehicles and electric drives used in hybrid and electric vehicles. The last section of this chapter provides a market overview where three producers (BMW, Volkswagen and Tesla) are presented.

Chapter 3 deals with the design of controller for DC/DC power converter for super-capacitor charging and discharging. The first part brings an overview of the experimental stand of hybrid drive. The second part deals with the design of mathematical model. Based on the DC/DC power converter functionality the two models were designed. The first for charging (buck mode) and the second for discharging (boost mode). The next sections deal with the switching losses and switching frequency analysis. The main goal was to create a dependency of the power on the time where the transistor is switched ON. The last section deals with the design of controller for the DC/DC power converter.

Chapter 4 provides an overview of mathematical models of the track, vehicle dynamics, energy model and powertrain model. The models are simplified in order to using in the optimization methods. The main part is the energy model which is directly used in own developed optimization algorithm.

Chapter 5 presents the equipment in the laboratory in VTP Roztoky and the design of the control system for automated driving cycles simulation and measurement. The control system is implemented in dSpace system and communicates with electric drive, dynamometer and own developed application for data loading and analyzing. The input of this application is a map of the track provided by Google and the vehicle parameters. A part of this application is the optimization method presented in chapter 6.

Chapter 6 deals with the optimization algorithm design. The first part deals with the optimization problem description with using of nonlinear energy model of the vehicle. The second part presents the reference drive algorithm designed for the comparing of optimization algorithm results. The last part of this chapter deals with the optimization algorithm description. The main challenge was to using of the nonlinear model of the vehicle and the time calculation reduction. The new approach to the optimization algorithm is based on the division of the track into the sections, calculation of the energies for each section and changing the vehicle speed based on the calculated energies. There is also discussed a method for local minimum prevention based on the changing of the grid.

Chapter 7 presents the results of the DC/DC power converter and optimization algorithm. The first result is the measurement and comparing of the DC/DC power converter mathematical model and prototype. The main strategy is to calculate the charging and discharging power in accordance with the high voltage level limits. Based on the calculated power to change the switching frequency value. The other results are from the test bench in the laboratory in Roztoky. The first test bench measurement was to compare the speed profile made by the Škoda Rapid EV with the speed profile designed by the optimization algorithm. The saved energy is approximately 3%. The other result called short track presents the dependence of the consumed energy on the arrival times. The main result is the function of the consumed energy on the different arrival times where is possible to find optimal arrival time as a compromise between consumed energy and duration of the drive.

8.2 Suggestions for the Future Work

The idea is to implement the designed optimization algorithm into dSpace system which will be built up into real vehicle and online to calculte the optimal speed profile with a prediction horizon about 1 – 2 km. The algorithm can be a part of the adaptive cruise control (ACC) system, which controls the longitudinal vehicle dynamics. The ACC is a normal cruise control, which keeps the constant vehicle speed, extended by a radar in front of vehicle which detects other vehicles. If another vehicle is detected, then the ACC starts to follow this vehicle. The automotive producers are developing similarly systems, for example Porsche with ACC InnoDrive.

The other idea can be to use a super-capacitor as a temporary storage of the electric energy and to use this for recuperation instead of batteries. The recuperation efficiency of the super-capacitor is much bigger than the efficiency of the batteries. It could be possible to extend the test bench in Roztoky by the super-capacitor and the designed DC/DC power converter and verify the cooperation with batteries.

8.3 Fullfillment of the Objectives Defined in Goals

I consider all objectives of this thesis to be satisfied.

- The design of the DC/DC power converter is presented in the section 3.5. Before the design was necessary to create an analysis of the switching frequency. Based on this analysis was created an innovative structure of the control where PWM frequency is not a constant, but it is changed in accordance to the required power.
- The prototype based on the processor Freescale 56F type was presented in the section 3.6. It was necessary for the verification to design an interface board for connection to the universal high power bridge module and measurement module. The results are presented in the section 7.1. The verification of the DC/DC power converter was made in the experimental stand of hybrid electric vehicle.
- The design of control concept is described in the section 5.4. The main part is dSpace DS1103 board where the presented control algorithm is included. The control algorithm is designed according to the rules for automotive software design.
- The optimization algorithm was designed based on the knowledge of vehicle energy model introduced in section 4.3. The design of the oprimization algorithm is explained in the chapter 6.

- The verification and comparing of the optimization algorithm was made on the test bench in the laboratory in VTP Roztoky together with cooperation with Škoda auto a.s. For this purpose we had available Škoda Rapid EV prototype. The results of the comparing is presented in the section 7.3.

References

[1] M. Chis; S. Jayaram; R. Ramshaw; K. Rajashekara. *Efficiency optimization of EV drive using fuzzy logic.* In: *Industry Applications Conference, Thirty-Second IAS Annual Meeting, IAS '97.*. 1997.

[2] M. Chis; S. Jayaram; K. Rajashekara. *Neural network-based efficiency optimization of EV drive.* In: *Electrical and Computer Engineering, Engineering Innovation: Voyage of Discovery.* 1997.

[3] S. E. Lyshevski. *Diesel-electric drivetrains for hybrid-electric vehicles: new challenging problems in multivariable analysis and control.* In: *Proceedings of the 1999 IEEE International Conference on Control Applications (Cat. No.99CH36328).* 1999.

[4] L. Wang; X. Wen. *Dynamic match and optimizing design of electric vehicle powertrain.* In: *Vehicle Electronics Conference, 1999. (IVEC '99) Proceedings of the IEEE International.* 1999.

[5] A. Brahma; Y. Guezennec; G. Rizzoni. *Optimal energy management in series hybrid electric vehicles.* In: *Proceedings of the 2000 American Control Conference. ACC (IEEE Cat. No.00CH36334).* 2000.

[6] R. Zhang; Y. Chen. *Control of hybrid dynamical systems for electric vehicles.* In: *Proceedings of the 2001 American Control Conference. (Cat. No.01CH37148).* 2001.

[7] A. Piccolo; L. Ippolito; V. zo Galdi; A.Vaccaro. *Optimisation of energy flow management in hybrid electric vehicles via genetic algorithms.* In: *2001 IEEE/ASME International Conference on Advanced Intelligent Mechatronics.* 2001.

[8] S. Delprat; T. M. Guerra; J. Rimaux. *Control strategies for hybrid vehicles: optimal control.* In: *Proceedings IEEE 56th Vehicular Technology Conference.* 2002.

[9] J. G. Supina; S. Awad. *Optimization of the fuel economy of a hybrid electric vehicle.* In: *46th Midwest Symposium on Circuits and Systems.* 2003.

[10] A. Kleimaier; D. Schroeder. *Hybrid cars, optimization and control.* In: *IEEE International Conference on Industrial Technology.* 2004.

[11] M. Huang; H. Yu. *Optimal Multilevel Hierarchical Control Strategy for Parallel Hybrid Electric Vehicle.* In: *IEEE Vehicle Power and Propulsion Conference.* 2006.

[12] A. Sciarretta; L. Guzzella. Control of hybrid electric vehicles. *IEEE Control Systems.* 2007,

[13] Ali M. Bazzi; Philip T. Krein. Review of Methods for Real-Time Loss Minimization in Induction Machines. *IEEE Transactions on Industry Applications.* 2010,

[14] Sara Deilami; Amir S. Masoum; Paul S. Moses; Mohammad A. S. Masoum. Real-Time Coordination of Plug-In Electric Vehicle Charging in Smart Grids to Minimize Power Losses and Improve Voltage Profile. *IEEE Transactions on Smart Grid.* 2011,

[15] Eric Sortomme; Mohamed A. El-Sharkawi. Optimal Charging Strategies for Unidirectional Vehicle-to-Grid. *IEEE Transactions on Smart Grid*. 2011,

[16] P. Richardson; D. Flynn; A. Keane. Optimal Charging of Electric Vehicles in Low-Voltage Distribution Systems. *IEEE Transactions on Power Systems*. 2012,

[17] Gang Lei; Tianshi Wang; Youguang Guo; Jianguo Zhu; Shuhong Wang. System-Level Design Optimization Methods for Electrical Drive Systems: Deterministic Approach. *IEEE Transactions on Industrial Electronics*. 2014,

[18] Stefano Di Cairano; Daniele Bernardini; Alberto Bemporad; Ilya V. Kolmanovsky. Stochastic MPC With Learning for Driver-Predictive Vehicle Control and its Application to HEV Energy Management. *IEEE Transactions on Control Systems Technology*. 2014,

[19] Hai Yu; Ming Kuang; Ryan McGee. Trip-Oriented Energy Management Control Strategy for Plug-In Hybrid Electric Vehicles. *IEEE Transactions on Control Systems Technology*. 2014,

[20] Andreas A. Malikopoulos. Supervisory Power Management Control Algorithms for Hybrid Electric Vehicles: A Survey. *IEEE Transactions on Intelligent Transportation Systems*. 2014,

[21] Rui Wang; Srdjan M. Lukic. *Dynamic programming technique in hybrid electric vehicle optimization.* In: *2012 IEEE International Electric Vehicle Conference*. 2012.

[22] Heeyun Lee; Yeong-il Park; Suk Won Cha. *Power management strategy of hybrid electric vehicle using power split ratio line control strategy based on dynamic programming.* In: *15th International Conference on Control, Automation and Systems (ICCAS)*. 2015.

[23] D. Maamria; K. Gillet; G. Colin; Y. Chamaillard; C. Nouillant. *On the use of Dynamic Programming in eco-driving cycle computation for electric vehicles.* In: *IEEE Conference on Control Applications (CCA)*. 2016.

[24] Song Juanjuan; Yang Xinhao; Li Ze; Wang Fudong. *Smooth control for hybrid electric vehicle based on the Pontryagin's Minimum Principle and the observer.* In: *32nd Youth Academic Annual Conference of Chinese Association of Automation (YAC)*. 2017.

[25] Namwook Kim; Sukwon Cha; Huei Peng. Optimal Control of Hybrid Electric Vehicles Based on Pontryagin's Minimum Principle. *IEEE Transactions on Control Systems Technology*. 2011,

[26] Teng Liu; Yuan Zou; De-xing Liu; Feng-chun Sun. *Real-time control for a parallel hybrid electric vehicle based on Pontryagin's Minimum Principle.* In: *IEEE Conference and Expo Transportation Electrification Asia-Pacific (ITEC Asia-Pacific)*. 2014.

[27] V. Pavelka. *Rekuperační systém se superkondenzátorem pro hybridní pohon*. Ph.D. Thesis, Czech Technical University in Prague. 2006.

[28] D. Cundev. *CONTROL STRATEGY OF CAR HYBRID SYSTEM AND ITS EXPERIMENTAL CONFIRMATION*. Ph.D. Thesis, Czech Technical University in Prague. 2009.

[29] J. Kučka. *Návrh DC/DC měniče pro nabíjení superkondenzátoru*. Master's Thesis, Czech Technical University in Prague. 2012.

[30] T. Haubert, P. Mindl, and Z. Cerovsky. Design of Control and Switching Frequency Optimization of DC/DC Power Converter for Super-capacitor. *AUTOMATIKA*. 2016,

[31] Rajashekara K. Present Status and Future Trends in Electric Vehicle Propulsion Technologies. *IEEE JOURNAL OF EMERGING AND SELECTED TOPICS IN POWER ELECTRONICS*. 2013, 1 (1),

[32] *Toyota Prius*.
`https://en.wikipedia.org/wiki/Toyota_Prius`.

[33] J. Bauer, S. Flígl, and A. Steimel. Design and dimensioning of essential passive components for the matrix converter prototype. *AUTOMATIKA*. 2012, 53 (3),

[34] M. Kanechika, T. Uesugi, and T. Kachi. *Advanced SiC and GaN power electronics for automotive systems.* In: *Proc. IEEE Int. Electron Devices Meeting*. 2010. 1-4.

[35] D. Cundev, and P. Mindl. *European driving schedule of hybrid electric vehicle with electric power splitter and supercapacitor as electric storage unit.* In: *Proceedings of the 2008 International Conference on Electrical Machines, Portugal: Vilamoura*. 2008.

[36] D. Cundev, Z. Cerovsky, and P. Mindl. *Modelling of the hybrid electric drive with an electric power splitter and simulation of the fuel efficiency.* In: *EPE '09, Spain: Barcelona*. 2009.

[37] M. Camara, H. Gualous, F. Gustin, A. Berthon, and B. Dakyo. Dc/dc converter design for supercapacitor and battery power management in hybrid vehicle applications polynomial control strategy. *IEEE Transactions on Industrial Electronics*. 2009, 57 587-597.

[38] M. Camara, H. Gualous, F. Gustin, and A. Berthon. *Control strategy of hybrid sources for transport applications using supercapacitors and batteries.* In: *Power Electronics and Motion Control Conference - IPEMC 2006, China: Harbi*. 2006.

[39] Y. G., and M. Ehsani. Design and control methodology of plug-in hybrid electric vehicles. *IEEE Transactions on Industrial Electronics*. 2010, 57 633-640.

[40] Tomáš Kacetl. *Optimization of Energy Consumption for Electric Vehicle Driving Cycle*. Master's Thesis, CTU in Prague, Faculty of Electrical Engineering. 2016.

[41] N. Chernov, and C. Lesort. Least squares fitting of circles. *Journal of Mathematical Imaging and Vision*. 2005,

[42] N. Chernov. *Circular and Linear Regression: Fitting Circles and Lines by Least Squares*. Taylor & Francis, 2010.

[43] M. Sands, R. P. Feynman, and R. B. Leighton. *The Feynman Lectures on Physics, Definitive Edition*. Addison Wesley, 2005.

[44] R. N. Jazar. *Vehicle Dynamics: Theory and Application*. Springer, 2014.

[45] J. F. Epperson. *An Introduction to Numerical Methods and Analysis*. Wiley, 2013.

[46] R. C. Kroeze, and P. T. Krein. *Electrical Battery Model for Use in Dynamic Electric Vehicle Simulations*. In: *Power Electronics Specialists Conference*. 2008.

[47] Jan Kacetl. *Mathematical Model and Validation of Powertrain*. Master's Thesis, CTU in Prague, Faculty of Electrical Engineering. 2016.

[48] M. Chen, and G. A. Rincon-Mora. Accurate electrical battery model capable of predicting runtime and I-V performance. *IEEE Transactions on Energy Conversion*. 2006, 21 (2), 504-511.

[49] N. Mohan. *Advanced electric drives: Analysis, Control, and Modeling Using MATLAB/Simulink*. John Wiley Sons, Inc., Hoboken, New Jersey, 2014.

[50] S. M. Gadoue, D. Giaouris, and J. Finch. *Tuning of PI speed controller in DTC of induction motor based on genetic algorithms and fuzzy logic schemes.* In: *Proceedings of the 5th International Conference on Technology and Automation.* 2005.

[51] W. Leonhard. *Control of eletrical drives.* Springer-Verlag, Berlin, Heidelberg, 1996. ISBN 3-540-59380-2.

[52] *SEVCON Gen4 size 8 Product Manual v3.2.*

[53] P. Mindl, P. Mňuk, Z. Čeřovský, and T. Haubert. *EV Drives Testing and Measurement System.* In: *2015 International Conference on Electrical Drives and Power Electronics (EDPE).* 2015.

[54] *AVL Battery Simulator Manual.*

[55] *dSpace DS1103 Product Manual.*

[56] Stephen Boyd. *Convex Optimization.* Cambridge University Press, New York, 2004.

Appendix A
List of author's publications

A.1 Publication Related to the Thesis

A.1.1 Publications in Journals with Impact Factor

1) Haubert, T.; Mindl, P.; Čeřovský, Z.: Design of Control and Switching Frequency Optimization of DC/DC Power Converter for Super-capacitor, Automatika. 2016, 57(1), 141-149. ISSN 0005-1144. Contribution **33%**

A.1.2 Publications in Reviewed Journals

1) Haubert, T.; Mindl, P.; Hlinovský, T.: Modelling of Electric Vehicle Dynamics using dSpace DS1103, Transaction on Electrical Engineering. 2014, 3(4), 106-110. ISSN 1805-3386. Contribution **33%**

A.1.3 Patents

—

A.1.4 Publications Excerpted in Web of Science

1) Mindl, P.; Mňuk, P.; Čeřovský, Z.; Haubert, T.: EV Drives Testing and Measurement System, In: Proceedings of the Electrical Drives and Power Electronics (EDPE 2015). Košice: TU Košice, FEI, 2015, pp. 328-332. ISBN 978-1-4673-9661-5. Contribution **25%**

A.1.5 Other Publications

1) Mindl, P.; Mňuk, P.; Čeřovský, Z.; Haubert, T.: Testing bench for measurement of electric cars powertrains characteristics, In: Sborník XXXIV. celostátní konferenci elektrické pohony. Plzeň: Západočeská univerzita v Plzni, 2015, pp. 94-99. ISBN 978-80-02-02592-4. Contribution **25%**
2) Haubert, T.; Hlinovský, T.; Mindl, P.: MATHEMATIC MODEL OF ELECTRIC VEHICLE OPTIMIZED FOR USING IN DSPACE DS1103, In: Technical Computing Bratislava 2014 Proceedings. Saarbrucken: LAP LAMBERT Academic Publishing, 2015, pp. 117-125. ISBN 978-3-659-40792-5. Contribution **33%**
3) Haubert, T.; Mindl, P.; Čeřovský, Z.; Mňuk, P.; Lettl, J.: Electric Vehicle Drive Control Based On GPS And GSM Path Parametres, In: Proceedings of PIERS 2015 in Prague. Cambridge: Electromagnetics Academy, 2015, pp. 2514-2517. ISSN 1559-9450. ISBN 978-1-934142-30-1. Contribution **20%**

4) Haubert, T.; Mindl, P.; Hlinovský, T.: Using of dSPACE DS1103 for Electric Vehicle Modeling, In: 22nd Annual Conference Proceedings Technical Computing Bratislava 2014. Praha: Humusoft, 2014, ISSN 2336-1662. ISBN 978-80-7080-898-6. Contribution **33%**
5) Bauer, J.; Haubert, T.; Flígl, S.; Lettl, J.: Mapa účinnosti asynchronního motoru – analytické odvození, In: XXXIII. celostátní konference o elektrických pohonech. 2013, ISBN 978-80-02-02457-6. Contribution **25%**
6) Haubert, T.; Mindl, P.; Čeřovský, Z.; Mňuk, P.: Control Strategy of Energy Flow in Hybrid Propulsion System with Super-capacitor, In: Proceedings of EVS27. Brussels: AVERE, 2013, ISBN 978-1-4799-3832-2. Contribution **25%**
7) Haubert, T.; Bauer, J.; Mindl, P.: Using of dSpace DS1103 for Electric Vehicle Power Consumption Modeling, In: 21th Annual Conference Proceedings Technical Computing Prague 2013. Praha: Humusoft, 2013, pp. 24. ISSN 2336-1662. ISBN 978-80-7080-863-4. Contribution **33%**
8) Haubert, T.; Mindl, P.: Optimization of DC/DC Power Converter for Super-capacitor Charging and Discharging, In: TRANSCOM 2013 - 10th European Conference of Young Researchers and Scientists - Section 4. Žilina: Žilinská univerzita, 2013, pp. 43-46. ISBN 978-80-554-0693-0. Contribution **50%**
9) Haubert, T.; Mindl, P.: DC/DC Power Converter for Super-capacitor supplied by Electric Power Splitter, In: Advances in Mechanisms Design. Heidelberg: Springer, 2012, pp. 509-515. Mechanisms and Machine Science. ISSN 2211-0984. ISBN 978-94-007-5124-8. Contribution **50%**
10) Haubert, T.; Kučka, J.: Design of Control for DC/DC Power Converter, In: POSTER 2012 - 16th International Student Conference on Electrical Engineering. Praha: Czech Technical University in Prague, 2012, pp. 10-14. ISBN 978-80-01-05043-9. Contribution **50%**
11) Haubert, T.: CAN-bus Communication for Hybrid Vehicle, In: XIX. International Symposium On Electric Machinery In Prague. Praha: ČVUT FEL, Katedra elektrických pohonů a trakce, 2011, pp. 33-36. ISBN 978-80-01-04890-0. Contribution **100%**
12) Haubert, T.: Design of CAN-BUS for Experimental Stand of Hybrid Drive, In: Proceedings of TRANSCOM 2011. Žilina: TU v Žilině, 2011, pp. 35-38. ISBN 978-80-554-0373-1. Contribution **100%**

A.2 Other Publications

A.2.1 Publications in Journals with Impact Factor

—

A.2.2 Publications in Reviewed Journals

—

A.2.3 Patents

—

A.2.4 Publications Excerpted in Web of Science

—

A.2.5 Other Publications

1) Hlinovský, V.; Haubert, T.; Bauer, J.: Automatizovaný PXI systém pro měření parametrů náhradního schématu asynchronního motoru použitelných v matematických modelech, In: XXXIII. celostátní konference o elektrických pohonech. 2013, ISBN 978-80-02-02457-6. Contribution **33%**
2) Bauer, J.; Haubert, T.; Lettl, J.: Torque Control of Matrix Converter Fed Induction Machine Employing Fuzzy Logic, In: TRANSCOM 2013 - 10th European Conference of Young Researchers and Scientists - Section 4. Žilina: Žilinská univerzita, 2013, pp. 5-8. ISBN 978-80-554-0693-0. Contribution **33%**
3) Haubert, T.; Hlinovský, T.; Vršínský, J.; Minko, Y.: Automated dynamometer based measuring system, In: POSTER 2013 - 17th International Student Conference on Electrical Engineering. Prague: Czech Technical University, 2013, ISBN 978-80-01-05242-6. Contribution **25%**
4) Pavelka, J.; Mindl, P.; Hlinovský, V.; Haubert, T.: Snížení transientního jevu při přechodu asynchronního motoru napájeného z měniče kmitočtu na napájecí síť, In: ELEN 2012. Praha: vydavatelství ČVUT v Praze, 2012, pp. 42. ISBN 978-80-01-05096-5. Contribution **25%**

A.3 Responses to Published Works

no responses yet

Appendix B
CV

Tomáš Haubert

Ždírec 39 • Havlíčkův Brod • 58001
TEL 603 118 371 • **E-MAIL** tomas@haubert.cz

BORN	**12. 5. 1986**
EDUCATION	**2010 – 2017 (expected) PhD.** Czech Technical University in Prague, Faculty of Electrical Engineering Electric Machines, Drives and Apparatus PhD. thesis: *Optimal Control Strategy of Hybrid Electric Vehicle* **2005 – 2010: Ing.** Czech Technical University in Prague, Faculty of Electrical Engineering Cybernetics and Measurement Master thesis: *Design and Realization of Control System pro Linear Combustion Engine*
EMPLOYMENT	**since 2012: Porsche Engineering Services, s.r.o.** 2012 – 2014: Development Engineer in Electric Drives Area since 2014: Project Manager **since 2012: CTU in Prague, Faculty of Electrical Engineering** Assistant of Professor
PROJECTS ON CTU	**2011 – ČKD Kompresory a.s.:** Mathematical Model of Synchronous Machine **2012 – BREMA s.r.o.:** Mathematical Model of Asynchronous Machine **2015 – DO-IT s.r.o.:** Development of Control System for 3D printer **2016 – Rieter s.r.o.:** Development of Controller for BLDC Motor
LANGUAGES	English: B2 active German: B1 active
HARD SKILLS	Programming languages: C, C#, Java, Visual Basic Databases: ORACLE, MySQL, Firebird

Programming languages: C, C#, Java, Visual Basic
MATLAB/Simulink: mathematical modelling, code generation, dSpace systems
Communication protocols: CAN, CANOpen, RS-485
Hardware development: EAGLE, OrCAD
PC: Windows, Mac OS X, MS Office

OTHER

Driver's licence B
2014 – 2015: Member of committee in ABB University Award